

Patterning of Surfaces by Locally Catalyzed Chemical Reactions

*A dissertation submitted to the
SWISS FEDERAL INSTITUTE OF TECHNOLOGY
LAUSANNE*

*for the degree of
Docteur ès Sciences*

*presented by
Hannes Kind
Dipl. Phys. UNI Freiburg (CH)*

*examining board:
Prof. Dr. K. Kern
Dr. E. Delamarche
Dr. S. Roth
Prof. Dr. H. Vogel*

December 8, 1999

Abstract

In this thesis, methods for the patterning of surfaces with different features (Pd and Co nanoislands, patterns of Cu, and patterns of multiwall carbon nanotubes) from a few nanometers to some tens of micrometers in size have been developed. All three systems studied have in common that a catalyst is required to start the chemical deposition of the corresponding material. Therefore, the central interest of this work is focused on the patterning of catalyst precursors on surfaces and the phenomena occurring before, during, and after their application to the substrate.

The first part deals with the patterning of self-assembled monolayers of aminothioliates on Au(111) with metal islands of a few nanometer diameter. For this purpose Pd²⁺ ions are covalently bound to amino groups on top of self-assembled monolayers. A solution containing a reducing agent serves to produce metallic islands of Pd of a monolayer height. In turn these Pd islands act as catalytic sites for the electroless deposition of Co islands which are a few monolayers thick. Mixed amino-/alkanethiolate monolayers are used to tune the density of the islands while a careful control of the O₂ concentration in the plating bath allows to vary their size. Our experimental results show that the final size of the metallic islands is governed by a radial diffusion phenomenon in the electrolyte which dominates the deposition processes at microelectrodes.

With the know-how obtained in the first part of the work a new variant of microcontact printing of catalyst precursors is developed in the second part and applied to two completely different systems. A patterned stamp is used to print a catalyst precursor from the stamp to the surface of the substrate. Electroless deposition of Cu at the solid/liquid interface and the growth of multiwall carbon nanotubes through pyrolysis of acetylene at the solid/gas interface are then chosen to show the potential of this technique to print patterns of catalysts down to feature size of ~ 200 nm. The rules for a successful combination of catalyst precursor, inking of the stamp, the choice of the substrate and its pretreatment, and finally the printing is elucidated for both systems.

Zusammenfassung

Im Verlauf dieser Arbeit wurden verschiedene Methoden zur Strukturierung von Oberflächen mit Objekten (Pd- und Co-Nano-Inseln, Cu-Strukturen, und strukturierte Filme von Kohlenstoff-Nanoröhrchen) im nm- bis zum μm -Bereich entwickelt. Sämtliche Systeme haben die Eigenschaft, dass ein Katalysator die entsprechende chemische Reaktion lokal aktiviert. Das zentrale Interesse der vorliegenden Studie ist die Erzeugung kleiner Strukturen anhand Modifikation von Oberflächen mit Katalysatoren und das Studium der dabei auftretenden chemischen und physikalischen Phänomene.

Der erste Teil beschäftigt sich mit der Strukturierung von selbstorganisierten Monolagen von Aminothiolaten auf Au(111) durch metallische Inseln von wenigen Nanometern im Durchmesser. Dazu werden Pd^{2+} -Ionen kovalent an die Aminogruppen der selbstorganisierten Monolagen angebunden. Mit einer reduzierenden Lösung können anschliessend metallische, monoatomar hohe Pd-Inseln hergestellt werden. Diese Pd-Inseln verhalten sich in der Folge als katalytische Zentren und erlauben die stromlose Abscheidung von Co-Inseln einer Grösse von wenigen Nanometern. Gemischte Monolagen aus Amino- und Alkanthiolaten ermöglichen die Inseldichte zu variieren, während die Sauerstoffkonzentration im Metallisierungsbad die Grösse der Co-Inseln bestimmt. Unsere Resultate zeigen, dass das Wachstum der Inseln durch ein radiales Diffusionsphänomen im Elektrolyten limitiert wird, welches die Abscheidungsprozesse an Mikroelektroden dominieren kann.

Basierend auf den Kenntnissen vom ersten Teil der Arbeit wird eine neue Variante von Mikro-Kontaktstempeln vorgestellt, die erlaubt katalytische Vorläufer auf Oberflächen zu stempeln. Dabei transferiert ein strukturierter Stempel verschiedene katalytische Vorläufer (Pd^{2+} , Fe^{3+}) durch mechanischen Kontakt auf Oberflächen. Elektrodenlose Stromabscheidung von Cu an der fest/flüssig-Grenzfläche und das Wachstum von Kohlenstoff-Nanoröhrchen durch Pyrolyse von Acetylen an der fest/gas-Grenzfläche zeigen die Möglichkeiten dieser lithographischen Technik zum Stempeln von Katalysatoren bis zu Strukturgrössen von ~ 200 nm. Die Regeln für eine erfolgreiche Kombination von katalytischem Vorläufer, Aktivierung des Stempels, Wahl und Vorbehandlung des Substrates, und schlussendlich der Prozess des Stempelns werden für die beiden sehr unterschiedlichen Systeme aufgestellt und diskutiert.

Contents

Abstract	i
Zusammenfassung	iii
1 Introduction	1
2 Background	5
2.1 Self-Assembled Monolayers	5
2.2 Electroless Deposition of Metals	7
2.3 Soft Lithography	9
2.4 Carbon Nanotubes	14
3 Electroless Deposition of Metals on Self-Assembled Monolayers	19
3.1 Introduction	19
3.2 Experimental	20
3.3 Activation of SAMs with Pd ²⁺ Catalyst	22
3.4 Electroless Deposition of Co	25
3.5 Discussion	30
3.6 Conclusions	33
4 Patterned Electroless Deposition of Cu	35
4.1 Introduction	35
4.2 Experimental	37
4.3 The Catalytic Ink	40
4.4 Printing the Catalyst onto Ti Films	41
4.5 The Role of the Stamp	45
4.6 High-Resolution Patterning	46
4.7 Conclusions	48
5 Patterned Growth of Carbon Nanotubes	49
5.1 Introduction	49
5.2 Experimental	50
5.3 Patterned Growth of Multiwall Carbon Nanotubes	52
5.4 The Catalytic Ink	53

5.4.1	Aqueous Inks	54
5.4.2	Ethanollic Inks	56
5.5	Morphology of the Carbon Nanotubes	59
5.6	Electron Emission Properties of Patterned Substrates	65
5.7	Conclusions	67
6	Conclusions and Outlook	69
	List of Publications	81
	Curriculum Vitae	83

Chapter 1

Introduction

Economy of space, energy, material, and cost is the immense driving force of all efforts to reduce the size of technological devices. For over 30 years the world market for semiconductors has grown approximately by 15% annually [1]. This growth has been maintained by the industry's ability to consistently provide higher device performance at lower cost and by the enormous demand for semiconducting devices in many areas. A true "nano-rush" started in the late eighties and early nineties when the combination of several important discoveries (and rediscoveries!) of techniques and experimental facilities stimulated an incredible research activity from fundamental physics and chemistry, to material and life science which have in common the goal to reach the limit of miniaturization of artificial structures¹ [2]. The commercialization of scanning probe techniques [3] in combination with an increasing acquaintance with self-assembly phenomena (for example, of atoms, molecules, and colloids) [4,5], the discovery of fullerenes and carbon nanotubes [6,7], and finally a broader availability of high-resolution lithographic methods (for example, electron-, x-ray-, ion-beam, and soft lithography) [1,8], probably triggered the nano-rush.

The collection of such techniques in combination with the unique behavior of nature to form highly ordered two- and three-dimensional structures through self-assembly (driven by the intrinsic kinetic and thermodynamic properties of atoms and molecules) provides an invaluable tool-box. The large number of possible combinations of these methods will have an unforeseeable outcome of results and applications in the future. The ultimate goal of research will be to define a set of tools and rules that provide the capability to construct nanoscale devices of arbitrary shape, at low cost and high speed, with the smallest features being less than 1 nm². Today, however, no approach exists that can meet all these criteria simultaneously.

The basic elements to build up laboratory-designed systems are nanometer-sized particles (atoms, molecules, and small aggregates of these). The fundamental interest in the physical and chemical phenomena of nanoobjects is obvious and is reflected in

¹The limit can be a single atom, single chemical functional groups of molecules, single molecules, or aggregates of a limited number of these units.

the large number of contributions during the last 10 years [9–19]. One selected issue relates to the fact that particles of this size can be used as catalysts for a large variety of chemical reactions. An especially surprising fact is that macroscopically non-catalytic materials can become catalytic active when their size is decreased below 10 nm. Gold, for example, is catalytically passive as bulk material but shows increasing activity when the particle size reaches the nanometer range. Even though the structure and chemistry of such particles have been examined for a long time, it often is partially unknown, how and why certain chemical reactions take place. In almost all cases, the only way to find the best catalyst for a reaction is to empirically try many different types of catalysts in a systematic way².

For the systems studied in this thesis we take advantage of some of the above mentioned techniques and materials to pattern substrates with different catalyst particles. The catalysts in turn are used to start chemical reactions for the growth of different structures (Co islands, Cu lines, and patterned films of carbon nanotubes) from a few nanometers up to a few micrometers in size. This work is not solely a study of fundamental physical and chemical phenomena of these systems, nor an exclusive development of patterning techniques. The outcome resulted from a strong “coupling” of these two approaches. An improved understanding of the fundamentals allowed new fabrication schemes and vice versa.

For all three systems studied here, *the central and common phenomenon was the application of a catalyst to a surface to produce small structures*. Therefore, the main goal was to answer the following two questions: (i) what combination of substrate, catalyst, method of patterning the catalyst, and chemical reaction is successful in achieving well-defined small structures and (ii) to understand why this combination is successful.

Chapter 2 describes the background of the methods: introduction to self-assembled monolayers (SAMs), electroless deposition (ELD), microcontact printing (μ CP), and a short review of the possibilities to pattern substrates with carbon nanotubes.

In Chapter 3, we use *wet chemical ligand exchange* to bind a molecular Pd²⁺ catalyst to aminothiolate SAMs on Au(111). After the reduction of the Pd²⁺ ions, the whole surface is decorated homogeneously, and hence unselectively, with nanometer sized islands of Pd which catalyze the ELD of Co. The behavior of such arrays of microelectrodes deviates from macroscopic electrodes for several reasons. It is known that the reactivity of catalysts depends on the size of the catalytic sites. Furthermore, mass transport to small electrodes is not controlled by planar diffusion but is strongly dominated by radial diffusion³ to the reaction sites [20, 21]. This radial contribution can force a change

²For the industrial synthesis of ammonia from N₂ and H₂, for example, several ten thousands of catalysts were tested before the basic requirements were covered. Even today new catalysts are developed.

³The expression *nonlinear diffusion* found in the literature is an unsuitable choice since the diffusion mechanism in question only depends on the geometry and not on a nonlinear diffusion behavior. We shall therefore use the term *radial diffusion* for this phenomenon.

of the dominant partial reaction⁴ occurring at the microelectrode when its size is decreased. The change from one dominant partial reaction towards another can lead to an inhibition of the overall chemical reaction or to a change of the reaction path.

In Chapters 4 and 5, we explore μ CP of catalytic patterns which in turn can catalyze different chemical reactions. The development of this non-photolithographic method to selectively decorate substrates with catalyst precursors⁵ allows the control of the geometry of the catalytic pattern and opens new exciting applications. ELD of Cu (Chapter 4) and the growth of carbon nanotubes through catalytic decomposition of acetylene (Chapter 5) are two interesting systems to check the potential of this procedure. On the basis of these examples problems such as the choice of the catalytic precursor, the loading of the stamp with the ink, the choice and pretreatment of the substrate, and finally the printing are discussed.

Patterned fixation of a Pd^{2+} catalyst for the ELD of Cu is described in Chapter 4. *Mechanical transfer* by μ CP is used to locally bind the catalyst by a *redox reaction* between the preconditioned substrate and the printed Pd^{2+} .

Chapter 5 deals with the production of substrates patterned with multiwall carbon nanotubes using μ CP. An Fe^{3+} catalyst is *microcontact printed* to a silicon wafer *mechanically, with no specific chemical reaction* occurring between the catalyst and the substrate. In particular, we outline the requirements on the catalyst to start the catalytic decomposition of acetylene for the growth of carbon nanotubes. Finally, we show that these micrometer sized devices can be used as electron field emitters.

⁴Usually, several different partial redox reactions take place at an electrode.

⁵We use the term *catalyst precursors* since the oxidation state and/or the morphology of the applied transition metal salts can (or even must) change during the growth process for a successful deposition.

Chapter 2

Background

This Chapter provides brief introductions to the techniques of self-assembled monolayers (Section 2.1), electroless deposition of metals (Section 2.2), and soft-lithography (Section 2.3). The patterning of substrates with carbon nanotubes is discussed in Section 2.4.

2.1 Self-Assembled Monolayers

It has been realized a long time ago that under certain circumstances organic species adsorb spontaneously on substrates so strongly that they are not noticeably removed by rinsing with an adsorbate free solvent. This has been one root for the development of the field of modified electrodes [22]. More recently, such irreversible adsorption processes have been the basis for modifying surfaces with supramolecular structures, for example, with surfactant molecules possessing a head group that binds to the substrate (Au, Ag, Pt, Cu etc.) and a specific chemical functionality as a tail group. In a systematic approach to the field, experimental and theoretical work has been conducted to characterize the stability and detailed structure of the so-called self-assembled monolayers (SAMs) [4, 23–28].

The most intensively studied systems are SAMs of organosulfur compounds (thi-

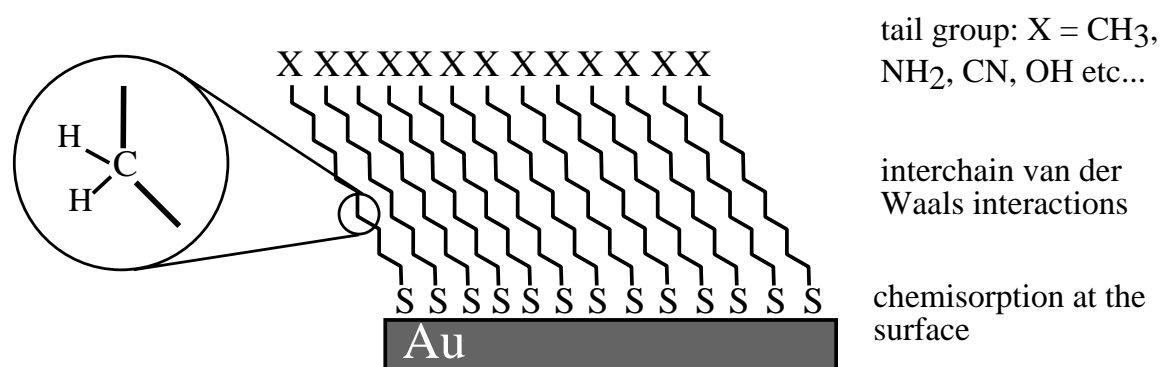


Figure 2.1: Representation of a self-assembled monolayer.

ols, disulfides etc.) on gold as shown in Figure 2.1 [24,25], and silanes (trichlorosilyl, trialkoxysilyl etc.) on silicon or glass [23]. SAMs of organosulfurs are known to be highly ordered and densely packed for $n > 9$ with properties comparable to crystalline polyethylene [25,26], where n is the number of CH_2 -units in the alkyl chain. The hydrocarbon chains tend to orient at an angle of about 30° to the surface normal to minimize their free energy [29–31]. The sulfur atoms form a strong, chemical bond with the gold and have a $(\sqrt{3} \times \sqrt{3})R30^\circ$ commensurate overlayer structure on Au(111) [32–35]. The binding energy of the S–Au bond is about 126 kJmol^{-1} , nearly independent of n [36].

During the last 15 years a large number of publications on the properties and use of SAMs has been conducted [4,37]. Many details of their growth behavior and of the properties of the resulting monolayers are now well understood. A few years ago, a second generation of experiments has started, where SAMs helped to build up more complicated structures than just one monolayer. Results have been published where SAMs were used as a covalent or electrostatic linker layer between the substrate and macromolecules. Much interest has been focused on the immobilization of biological molecules for the construction of functionalized supramolecular systems exhibiting molecular recognition sites [38–41]. Since in living organisms binding occurs in the proximity of surfaces, these systems may serve as sensing elements for the analytical detection of biomolecules. Another example of molecular architecture has been shown by Shon et al. who fabricated fullerene-terminated alkanethiolate SAMs on gold via an aziridine linkage between asymmetric disulfides and the fullerenes [42]. The production of self-assembled multilayer thin films with interesting photophysical properties stimulated several groups to develop different linker routes [43]. Such systems are of particular interest for their potential applications in nonlinear optics and molecular electronics, since complicated structures can be designed and prepared with molecular precision with many different molecules. A field of research which just started to attract interest is the grafting of polymers to SAMs to form brush-like layers [44]. The unique behavior of polymer brushes at solid interfaces results from the fact that they consist of end-grafted, strictly linear chains of the same length with a grafting density sufficiently high with respect to the radius of gyration of the grafted polymers. This can be used to prepare tailor-made intelligent materials to serve as functional devices on a nanometer scale. The grafting of a hydrophilic polymer film onto a hydrophobic solid could change the surface chemistry to a large extent while conserving the physical properties of the bulk. A hydrophobic poly(dimethyl)siloxane (PDMS) stamp, for example, could be modified with a sponge-like hydrophilic film to allow an improved loading of the stamp with polar transition metal catalysts¹.

An ideal system for creating reaction sites on surfaces are SAMs of organosulfurs on gold [24,25]. First, gold surfaces are chemically homogeneous, prepared in a simple way,

¹Hydrophobic PDMS stamps cannot be inked with transition metal catalysts directly. This is only possible after an O_2 plasma treatment of the stamp surface. The major drawback of the plasma treatment is that the stamp surface develops towards the original hydrophobic state when left in air for a few minutes. A stable film of a hydrophilic polymer would be an important improvement.

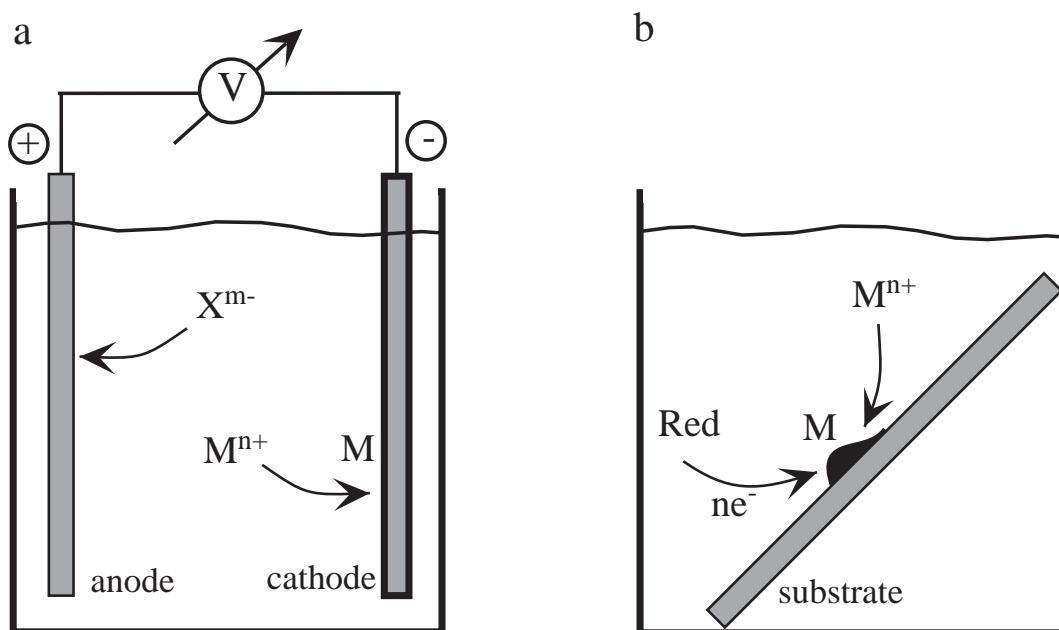


Figure 2.2: Experimental set-up for galvanic (a) and electroless (b) metallization (M^{n+} : cation, X^{m-} : anion, M: metal, Red: reductant).

and virtually free of contaminations. Second, a broad variety of analytical techniques can be used for the characterization of thin films [45–50]. Third, SAMs of different types of functionalized thiols enable the control of the reactivity or wetting, crucial to direct the specific desired chemistry to occur [25, 51, 52]. Fourth, mixed SAMs of organosulfurs allow the control of the lateral concentration of the different species, and hence the density of the reactions sites without losing order within the SAMs [53–55]. Finally, SAMs can be easily patterned with high homogeneity on substrates using UV light [56], electron beam [57], atom beam [58], or soft lithography [59–61]. All these properties highlight the advantages of SAMs to be studied as well-defined model systems but also as candidates for real technological applications.

2.2 Electroless Deposition of Metals

Metallization of surfaces can be achieved by two different methods. The first is based on the fact that a metal can be deposited on a surface by thermal evaporation or sputtering. Second, the metal can be grown on a substrate in a wet electrochemical environment. Metallization procedures through vacuum are always expensive. For this reason, wet electrochemical methods are mostly used in industry when they are compatible with the fabrication steps.

Electrochemical metallization involves the deposition of metals onto substrates by reduction of metal ions that are dissolved in an aqueous or organic electrolyte or in a molten salt. There are mainly three methods differing by their way of supplying electrons necessary for the reduction. In the *galvanic deposition (or electrodeposition)*,

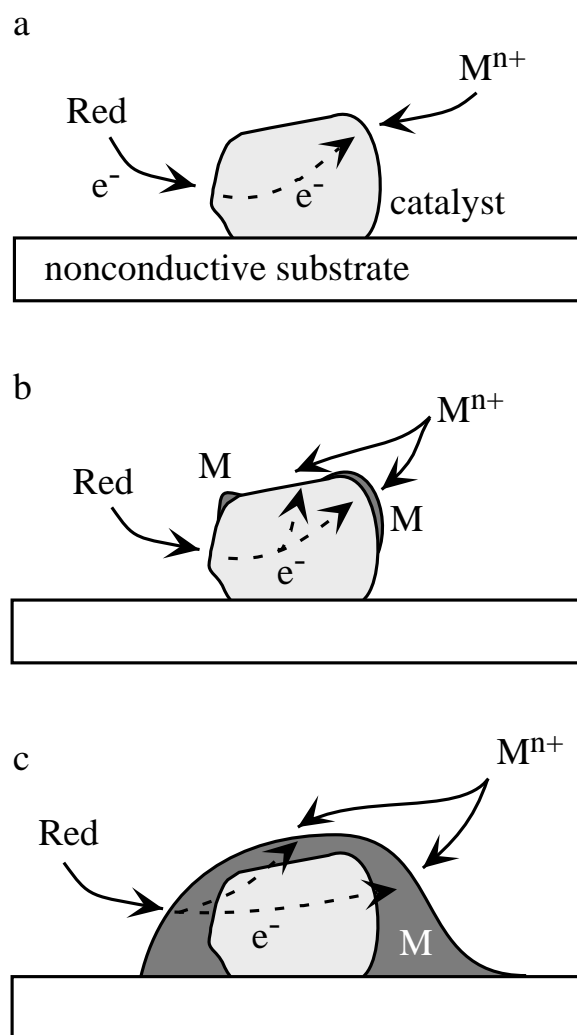


Figure 2.3: Schematic representation of the catalyzed electroless deposition. The oxidation of the reductant takes first place on the catalytic site (a) and later on the plated metal (c).

electrons are delivered by an external power supply, Figure 2.2(a). This simple technique is the most common method because of its easy control of the deposition by the applied potential or current. In *immersion plating*, electrons are provided by the basis metal as it dissolves in the bath through a displacement reaction. This often leads to a porous and poorly adhering deposit which has only little practical importance. Nonconductive substrates cannot be plated directly, neither by galvanic deposition nor by immersion plating. In this case one can use the method of *electroless deposition (ELD)*, in which the electrons are supplied by a chemical reducing agent present in the plating bath, Figure 2.2(b) [62–66].

ELD is an autocatalytic redox process in which metal ions are chemically reduced to metal at a surface in absence of any external current source (Figure 2.3) [64, 65, 67–69]. The reductant delivers electrons to the surface of a catalytic substrate or to a dielectric surface activated with a catalyst. In turn, a cation of the metal to be deposited can be

reduced by these electrons. When the catalytic sites are completely covered by metal, the metal ions themselves must continue to oxidize the reducing agent to further sustain deposition, Figure 2.3(c).

For the occurrence of any ELD reaction two requirements have to be fulfilled. First, the Nernst potential for the metal/metal ion half cell reaction has to be more positive than the Nernst potential for the reductant's half cell reaction. Second, the oxidation of the reductant has to be catalyzed by the surface of the substrate –which is often activated by a catalyst– and later by the plated metal itself. Basically, an ELD bath contains 3 species: the metal ion to be reduced at the substrate, the reducing agent (for example, formaldehyde, hypophosphite, or dimethylamine borane) as source of the electrons, and finally a chelator (for example, tartrate or EDTA) of the metal ions which inhibit the spontaneous reduction of the metal ions in the solution. Commercial plating baths, however, contain a selection of various ingredients in addition to the major bath constituents. They are added to retard the self decomposition of the bath (stabilizers), to maintain a constant pH (buffers), to change the deposition rate (inhibitors and accelerators), or to permit an anisotropic deposition [70]. Considering the complex composition of such baths highlights the difficulties to study the reaction paths in electroless deposition systems. Although several fundamental studies have been conducted many details of ELD remain unsolved yet [64–66, 69, 71].

ELD exhibits two major advantages over galvanic deposition: nonconductive substrates can be plated and the deposited material can follow complicated substrate shapes without building up at edges and kinks since the deposition takes place simultaneously on the whole surface. There exists, however, some disadvantages of electroless plating: it is difficult to control the plating rate, which, compared to typical rates in galvanic deposition, is relatively slow. Furthermore, the lifetime of the plating solution is short and waste solutions have to be treated.

The method of electroless plating is commercially important for the simple and low-cost deposition of metal coatings on a variety of substrates. Practical examples are corrosion-resistant electroless Ni coatings on steel, decorative coatings on plastics, or electroless Cu patterns for printed circuit boards. In order to minimize microchip design –which was based on Al circuitry up to now– Cu was found to be an ideal improvement with high electrical and thermal conductivity [72–75]. This change in microchip design had a breakthrough when IBM announced the fabrication of the first Cu circuitry-based microchip in 1997.

2.3 Soft Lithography

Soft lithography (SL) –introduced by Whitesides and coworkers at Harvard University in 1993– is the name of a set of non-photolithographic methods that share the common feature that they use a patterned elastomer which permits a spatially controlled delivery of material to a surface using printing, molding, and embossing [8].

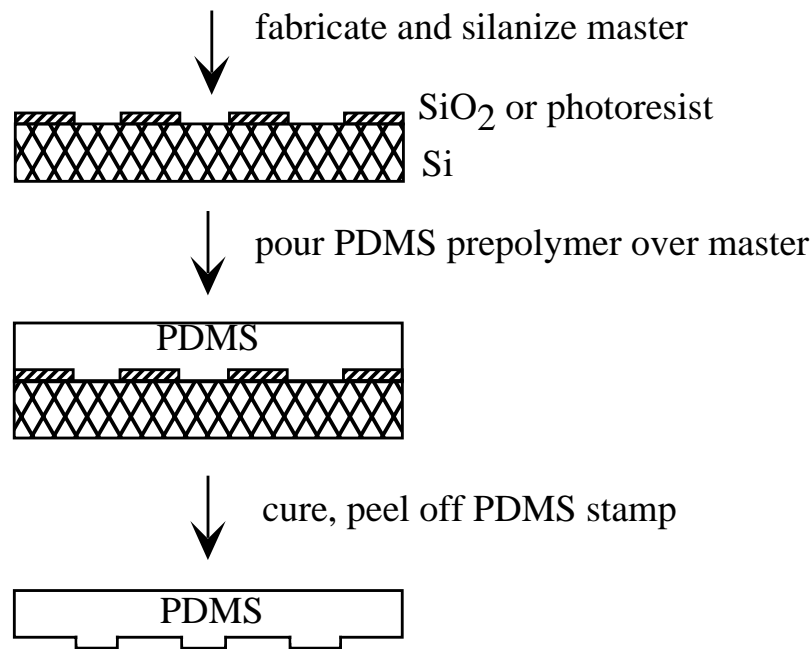


Figure 2.4: Illustration of the procedure for casting PDMS replicas from a master having relief structures on its surface.

The procedure of patterning by SL always consists of a sequence of 3 steps: fabrication of a master, replication of the pattern with an elastomer, and finally the patterning of the substrate. Masters used to cast the elastomer are usually fabricated using photolithography. Structuration is achieved by illumination of a photoresist through a chromium mask (which represents the most expensive part of SL). The master is then formed in photoresist, silicon, or some other materials. Replication of the pattern, shown in Figure 2.4, is obtained by pouring liquid poly(dimethyl)siloxane (PDMS) on top of the master which fills the crevices, forming a negative replica of the surface after curing. Finally, the elastomer is peeled off and used for the patterned delivery of material to a surface.

Figure 2.5 shows schematically the most important methods of SL namely micro-contact printing (μ CP) [59], replica molding (REM) [76], micromolding in capillaries (MIMIC) [77, 78], microtransfer molding (μ TM) [79], solvent assisted micromolding (SAMIM) [80], and masks as dry lift-off (MADLO) [81]. Depending on the chosen method, surfaces can be patterned directly or indirectly with organic or inorganic molecules, biomolecules, metals, semiconductors, polymers (conducting, nonconducting, or electroluminescent), or ceramics [8].

Most standard methods for microfabrication start by using photolithography to form a pattern in a photoresist on the substrate. This patterned resist can then be used in one of two ways: it either acts as a protection (for example, against dry or wet etching), or it serves as a removable mask for the deposition of material (for example, the evaporation of a metal) which is followed by a lift-off of the resist. Although these techniques are very widely used, they are often incompatible for solutions containing gels, polymers, organic

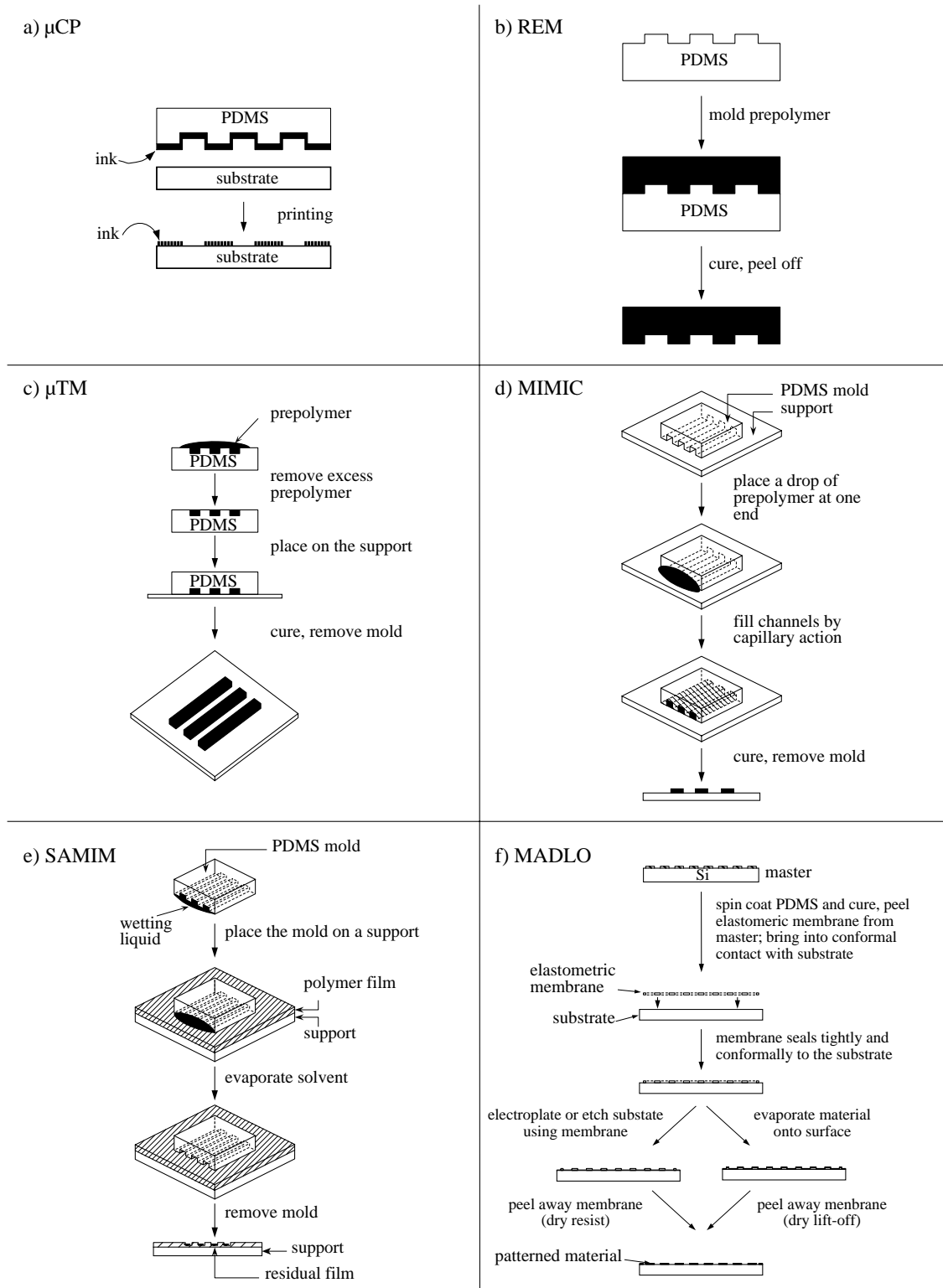


Figure 2.5: Strategies for (a) microcontact printing (CP), (b) replica molding (REM), (c) microtransfer molding (TM), (d) micromolding in capillaries (MIMIC), (e) solvent assisted micromolding (SAMIM), and (f) masks as dry lift-off (MADLO).

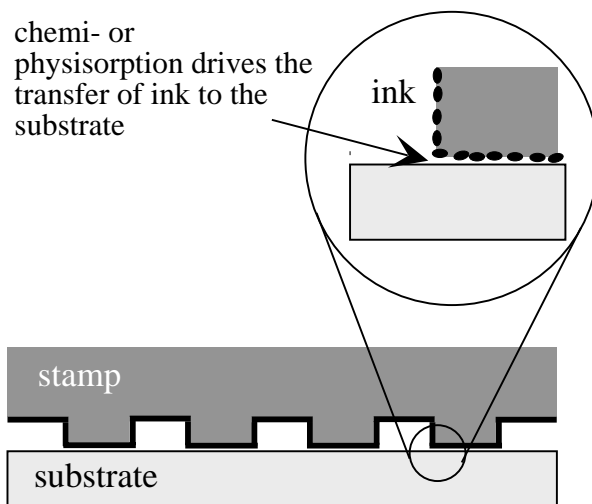


Figure 2.6: During the conformal contact the molecules are in proximal contact with the surface of the substrate and can either undergo a chemical reaction or only a physisorption.

and organometallic species, and biological molecules [82]. To pattern these materials successfully, the patterned photoresist must be impermeable to the reagents used and the deposited material should not be compromised by the solvents used for the lift-off. Other methods than photolithography involve a shadow mask formed from a rigid metal. The air gap between the mask and substrate, however, makes the use of rigid shadow masks to pattern materials from solution impossible.

Soft lithography can indeed circumvent some of these drawbacks since PDMS is a material which is (i) compatible with many of the above mentioned chemicals and (ii) can easily be used for additive or subtractive procedures [8, 59, 81, 83, 84]. The additional advantages of SL are diverse. Manufacturing steps should be of low cost. All process steps –which are completely parallel in nature– can easily be scaled up for large areas (planar and even nonplanar surfaces). The access of the technique to researchers in physics, chemistry, biochemistry and material sciences allows the adaption of the techniques to the specific tasks. Finally, the spatial resolution is mainly determined by van der Waals interactions, by wetting, by kinetic factors such as filling of the capillaries on the surface of the substrate, and by the properties of the materials, and not by optical diffraction.

We will now concentrate on microcontact printing (μ CP) since this method was exclusively used in the framework of this work.

Microcontact Printing

Microcontact printing (μ CP) is a flexible method that routinely forms patterned films of a variety of materials (for example, thiols, disulfides, silanes, protonic acids, biomolecules, colloids, catalytic precursors) [8, 59, 83, 85–87]. The procedure is remarkably simple, as shown in Figure 2.5(a). An elastomeric stamp is used to transfer particles

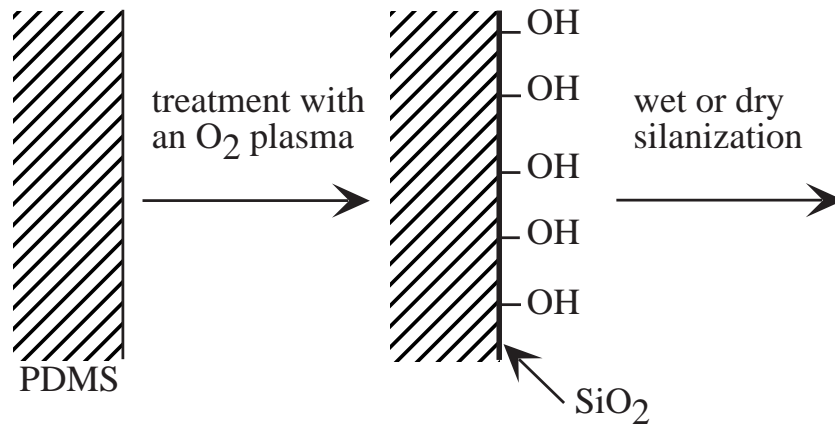


Figure 2.7: Schematic procedure for the modification of the PDMS surface. Different terminal groups give different interfacial properties [88, 89].

dissolved in an ink to the surface of the substrate. During the print a conformal contact² allows the particles to adsorb on the surface, Figure 2.6. This can be a chemi- or physisorption depending on the chemical nature of the surface and the ink-molecules.

The elastomeric stamp having a relief structure on its surface is the key element of μ CP and is usually formed by PDMS, for example Sylgard 184 from Dow Corning [90]. Several properties of PDMS are instrumental in the formation of high-quality patterns of structures in μ CP:

- PDMS is an elastomer and conforms to the surface of the substrate over large areas. Conformal contact can even be achieved on surfaces that are nonplanar on the micrometer scale.
- PDMS provides a surface that is low in surface free energy and chemically inert.
- PDMS is homogeneous, isotropic, and optically transparent down to at least 300 nm wavelength.
- PDMS is a durable and robust elastomer. Stamps can be reused for certain applications over a period of several months.
- The surface properties of PDMS can readily be modified by treatment with an O₂ plasma to give appropriate surface polarity (as represented in Figure 2.7).

Stamps for μ CP must have an affinity for the relevant molecules in the ink without being swollen or damaged by the ink. When alkanethiols diluted in ethanol form the ink, these molecules partition in and on the stamp so that stamps can easily be loaded with an excess of thiols before printing [84]. Inking a PDMS stamp with a catalyst

²The term *conformal contact* is used to describe the molecular-scale interactions that occur between the protruding regions in the elastomer and the substrate where the elastomer matches its contours on scales from nanometers to several tens of centimeters.

precursor (which was one of the main challenges of this work) represents a different paradigm for μ CP, however. The main factor responsible for this is the poor solubility of the catalytic precursors in the PDMS stamp due to their polarity. In contrast to inking a stamp with alkanethiols, no reserve of the polar catalyst precursor exists in the bulk of the stamp which could progressively release the precursor by diffusion during printing. We successfully introduce in this work a way for inking the stamp with a catalyst precursor: hydrophilization of the PDMS surface using an O_2 -based plasma increases the affinity between polar species and the stamp [89,91,92]. This treatment is simple and not detrimental to PDMS stamps because it oxidizes only a few nanometers of the surface of the stamp and preserves its elasticity and the accuracy of its pattern. Hydrophilization is a key step as it increases considerably the affinity between the stamp and a large variety of water- and ethanol-soluble catalytic precursors. Once hydrophilic, stamps are subsequently inked with a solution of catalyst or stored in deionized water to prevent the evolution of their surface towards a more hydrophobic-like state.

2.4 Carbon Nanotubes

A variety of graphite fibers and filaments have been known for more than two decades [93]. The interest in these structures comes from the inherent structural strength due to the covalent in-plane carbon bonds in graphite, which is considered to be one of the strongest in nature. The material is extremely light, highly electrically and thermally conducting, and corrosion resistant. Therefore, it is regarded as an ideal reinforcement in composite structures such as fiber-epoxy composites which are used for example as components in aircraft structures. The basic premise for this search to obtain structurally perfect single-crystalline fibers, however, was not achieved. Most of the produced fibers contain large amounts of structural defects.

It was in 1985 when the discovery of fullerenes (C_{60} , C_{70} , etc.) added an important milestone in carbon research [6]. The most prominent member of the fullerenes is the C_{60} which consists of a closed cage made of 60 carbon atoms arranged in pentagons and hexagons showing an exceptional high symmetry. A few years later, Iijima reported the production of nanometer-sized straight tubules by the arc discharge method³, the so-called carbon nanotubes [7, 94]. Nanotubes consisting of a single graphene layer are called singlewall nanotubes (Figure 2.8(a)) and tubes of multiple, concentric layers are called multiwall nanotubes (Figure 2.8(b)). Multiwall nanotubes have diameters ranging from 2–30 nm and lengths reaching up to several microns. Singlewall nanotubes show a narrow distribution in diameter from 1–2 nm.

The discovery of structurally perfect carbon nanostructures was now achieved. The production of macroscopic quantities of a single type of the nanostructures, however,

³In the arc discharge method, an arc is maintained between two cylindrical electrodes (sometimes containing a transition metal catalyst) for several minutes in an inert atmosphere. The tubes are found in the soot on the cathode.

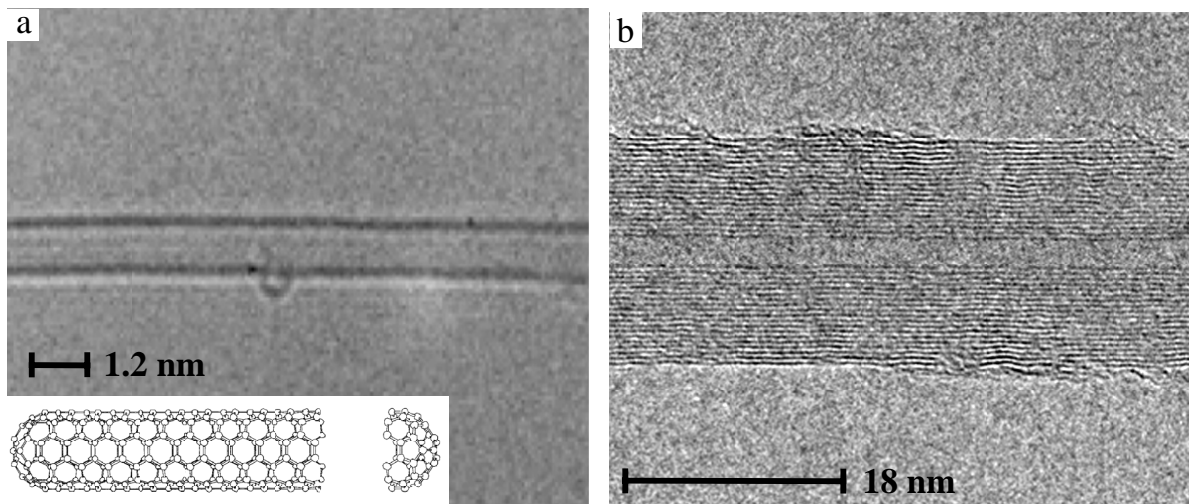


Figure 2.8: Transmission electron microscopy (TEM) images of a singlewall (a) and a multiwall (b) carbon nanotube. The inset shows one possible helicity of a singlewall nanotube.

was not solved. Using the arc discharge method yields a variety of tubes with different diameters, length and helicities. In addition, carbon polyhedra and amorphous carbon make up to 50% in weight of the raw arc product. Alternate production methods such as laser ablation [95] and catalytic decomposition of hydrocarbon gases by transition metal catalysts [96] have been found. Depending on the method used to generate the tubes and the exact conditions of the particular method their quality can vary⁴. The synthesis of large quantities of only one particular kind of particle remained a challenge and is not fully solved yet. A different way towards purer samples is the purification of the raw carbon deposit. Purification techniques use either oxidation (in gas phase or liquid phase) of the less crystalline particles or the dispersion of the wanted particles in solvents using surfactants followed by different mass separation methods [97–100].

The combination of interesting physical and chemical properties inherited from the parent in-plane graphite and a set of properties due to their small dimensions provides carbon nanotubes with a host of properties that are remarkable. Since this work is motivated by a possible application of carbon nanotubes as electron field emitters [101,102] in flat electron emission devices, we will limit the discussion on the emission properties of carbon nanotubes and the lithographic techniques for their patterning.

Patterning of Substrates with Carbon Nanotubes for Field Emission Applications

Field emission from metallic tips can be described by the Fowler-Nordheim equation [103]. The effective local electric field E_{loc} at an emitting tip determines the emission

⁴It is not surprising that results have not always been consistent from one research group to another. We tried for example to print catalyst precursors proposed by other groups. None of the different deposition experiments lead to the growth of carbon nanotubes.

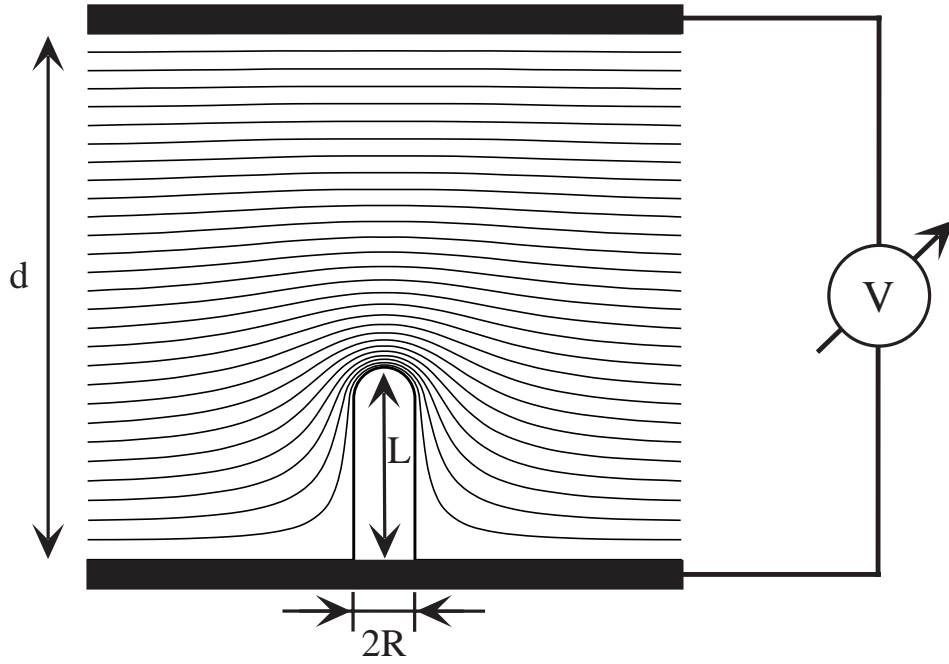


Figure 2.9: Cylindrical cross section of the electric field distribution for a closed metallic tube. The solid lines indicate lines of equipotential.

current density which is given by

$$j \propto \frac{E_{loc}^2}{\phi} e^{-A \frac{\phi^{1.5}}{E_{loc}}}, \quad (2.1)$$

where ϕ is the local work function, $A = 6.83 \cdot 10^9 \text{ VeV}^{-1.5} \text{ m}^{-1}$ and $E_{loc} = \beta V/d$. The field enhancing factor⁵ β is a measure of the increase of the average uniform field V/d between cathode and anode through the geometry of the tip. V is the voltage applied to the cathode separated by the distance d from the anode. It has been shown that it is very important to distinguish between the uniform applied field and the local field at the emission site [107, 108]. The local fields are always in the order of a few thousand $\text{V}\mu\text{m}^{-1}$, although the applied field ranges only between 1–50 $\text{V}\mu\text{m}^{-1}$.

Figure 2.9 shows that metallic tips effectively behave as sharp antennas and intensify the field at their tip apex. As shown by the equipotential lines, there is a considerable enhancement of the electric field at the tip. For a fixed length L the electric field in the proximity of the tip decreases as the tip diameter R increases, and for a fixed R the field increases with L .

The idea to using carbon nanotubes as cold electron sources looks attractive since they meet several requirements for such devices [101, 102, 109]: they exhibit a very high length-to-diameter ratio, are chemically and physically inert, support high electric

⁵Samples covered with singlewall carbon nanotubes can have values of β between 2'000 and 10'000 while samples with multiwall carbon nanotubes exhibit β values between 800 and 3'000 [104–107]. This is due to the fact that β depends on the diameter of the nanotubes.

currents, are patternable, and finally they can be produced by simple and inexpensive methods.

Basically, electron emission from carbon nanotubes can be used in two different ways. *Such emission devices can either consist of a continuous film* (for example, for large area flat emission devices) *or a patterned film* (for example, for flat panel displays) *of carbon nanotubes*. The production of continuous films is technically not very difficult and devices are commercially available. Despite the intensive research activity since the discovery of the carbon nanotubes in 1991, it was only in 1998 when the first reports on patterning of substrates with nanotubes were reported [110–112]. It turned out that patterning of substrates with carbon nanotubes for the electron field emission is a challenge for several reasons:

- The fabrication of high contrast patterns is required. Carbon emitters must be confined to precisely defined pixels and completely absent on adjacent regions.
- The contact resistance between carbon nanotubes and substrate should be as low as possible [113–115].
- A strong adhesion of the nanotubes on the substrate is a prerequisite for a stable emission of electrons.
- The patterned film must be capable of emitting current densities higher than $10 \mu\text{A}\mu\text{m}^{-2}$.
- The physical and chemical inertness of the patterns must allow the production of devices with a useful lifetime.

Patterning of substrates with carbon nanotubes can be achieved by three different approaches. The first method consists of the production and posttreatment (cleaning, shaping, chemical modification) of the nanotubes followed by a locally confined adsorption on the substrate. The substrate may consist of an electrode pattern modified with linker molecules which can bind to chemically preconditioned carbon nanotubes [111, 116]. The second method is based on the patterning of a substrate with a nanotube composite [112, 117]. In this approach the tubes are dispersed in a nonconducting polymer matrix which can be applied to a substrate. Some nanotubes are in contact with the conducting substrate, penetrate the polymer matrix and can therefore be used as electron sources. One of the main drawbacks of this device is the unspecific mechanical contact between the nanotubes and the substrate. Third, carbon nanotubes can be grown directly on substrates patterned with a catalyst using chemical vapor deposition of hydrocarbon-containing gases.

The realization of the patterned growth of tubes is promising. The central problem for a successful patterning is the choice of an appropriate combination of the substrate, the catalyst, and the method to apply the catalyst to the substrate.

First, the supporting *substrate* for the catalyst was found to play a key role in the type of nanotubes produced (for example, the number of walls, the diameter, and the degree of graphitization) [118, 119]. For a high-quality patterning, the substrate itself must be completely passive for any decomposition of the hydrocarbon gas. The morphology and chemistry of the surface of the substrate can then positively or negatively interact with the applied catalyst and in turn influence the growth of carbon nanotubes [120].

The second issue relates to the fact that the *catalyst* itself gives excellent control over the purity, quality, and dimensions of the nanotubes but also over their density, morphology, and orientation of the carbon nanotubes in the deposit. Basically, catalysts can bind to the substrate by transport through the vapor phase (for example, evaporation or sputtering), by impregnation with catalyst solutions, or by mechanical transfer. Depending on the method, the chemical composition and morphology of the catalyst can be quite different, resulting in completely different types of nanotubes and their orientation on the substrate [110, 120–126]. If necessary, additional treatment such as calcination, annealing, or reduction can be used to improve the selectivity of the catalyst before the deposition starts.

Third, the choice of the *technique to pattern* the substrate with the catalyst is important since not all techniques are compatible with all substrates and catalysts. Kong and coworkers used electron beam lithography to fabricate square-shaped holes in a poly(methylmethacrylate) (PMMA) film [110]. A drop of a methanolic solution of an iron catalyst was then deposited onto the pattern and vaporized before calcination and lift-off. In a later work they showed that substrates can be patterned with Fe films by electron beam evaporation through shadow masks [120]. We show here that μ CP can be used to print a catalyst precursor for the production of films of multiwall carbon nanotubes by catalytic decomposition of hydrocarbons. A similar approach was recently used by Cassell et al. to print a liquid-phase catalyst precursor material to direct the growth of singlewall carbon nanotubes bridging between towers of prestructured substrates [125].

It is important to note that the method of μ CP to pattern substrates with catalyst precursors for the growth of carbon nanotubes is not limited to devices for electron field emission but should be applicable for other systems where patterns of carbon nanotubes are required (for example, carbon nanotube field effect transistors [127, 128]).

Chapter 3

Electroless Deposition of Metals on Self-Assembled Monolayers

In this Chapter we show that selective electroless deposition (ELD) can be used as a tool for electrochemical nanostructuring. In a first step we bind Pd²⁺ ions to an aminothioliolate self-assembled monolayer (AT-SAM) on an Au(111) surface. Metallic Pd islands of monoatomic height are formed by chemical reduction and can in turn activate the ELD of Co. We study the growth of Co islands as a function of the aminothioliolate concentration in mixed amino-/alkanethioliolate SAMs and of the O₂ concentration in the deposition bath.

3.1 Introduction

From an electrochemist's point of view, assemblies of small aggregates – such as the Pd or Co/Pd islands that we have examined – form a micro- or even nanoelectrode array. Such electrodes have geometrical dimension smaller than the Nernst diffusion layer and consequently have important advantages pointed out earlier by Ewing et al. [129]. They can be used, for example, to study ultrafast electron-transfer reactions [130], to perform in vivo voltammetric measurements inside single cells [131], to observe changes in the conductivity of single ion channels [132], or to perform small-scale etching and lithography [133]. All these applications are mainly based on the fact that redox reaction kinetics scale inversely with the electrode radius, i.e. small currents can be sampled on a small area [20, 130, 134].

Metal island patterning by ELD requires a selective activation of an inactive surface by a catalyst [70]. Several methods of producing patterned catalysts are known, based on photolithographic techniques [135–138] or soft lithography [8]. The resolution of such sub-micrometer metallic features obtained by a selective ELD approach is often limited by the largest catalyst particle on the surface [139, 140].

Our approach is based on the properties of ω -functionalized alkanethiols. While the sulfur groups of these molecules selectively bind to different metal surfaces and

form strongly adsorbed, ordered monolayers, the other end group of the thiols can be tailored to control the interfacial properties [46, 48, 141]. A variety of metal ion ligands like pyridine, 2,2-bipyridine, amine, and ethylenediamine can be used as surface functionalities [135, 142, 143]. Metal ions such as Pd^{2+} can bind to these functional groups. The binding mechanism has been shown to be highly selective for different surface ligands [144]. Hence the ability to control the strength of the bond between the SAM and a catalyst precursor at the molecular level can offer control over the adhesion of the catalyst and then over metal structures deposited on the catalyst. We describe here a new method for selective ELD of only one monolayer Pd metal islands. The Pd^{2+} species from solution are bound by amine ligands to the organic surface. The reductant (dimethylamine-borane (DMAB)) then reduces Pd^{2+} to Pd. In a second step we focus on the ELD of nanometer-sized islands of Co onto these catalytic sites.

3.2 Experimental

Chemicals

Milli-Q water (Millipore Systems) was used for all experiments. All reagents were p.a. grade or better and were used as received. Ethanol, NaCl, Na_4EDTA , NaOH, NH_4Cl , dimethylamine-borane complex (DMAB, $(\text{CH}_3)_2\text{NHBH}_3$), decanethiol ($\text{CH}_3(\text{CH}_2)_9\text{SH}$), H_2SO_4 and HCl were all from Fluka. Na_2PdCl_4 and CoCl_2 were both from Aldrich Chemical Company. The aminothiols $\text{H}_2\text{N}(\text{CH}_2)_2\text{NHCO}(\text{CH}_2)_{10}\text{SH}$ was used as received from Prof. H. Vogel (Institut de Chimie Physique, École Polytechnique Fédérale de Lausanne). O_2 and N_2 (48 res. 50 grade from CarbaGas, Lausanne, CH) gases were purified by passage through H_2SO_4 and saturated with water by bubbling through water.

Solutions

Glassware was cleaned with Nochromix solution (Thomas Scientific, New York, NY), which reacts violently with many organic materials and should be handled with care. The electroless Co metallization bath was prepared immediately prior to use by mixing three parts of stock Co solution, two parts of stock solution of DMAB, and five parts of water. The Co stock solution was prepared by adjusting a solution of 1 g NH_4Cl , 0.6 g CoCl_2 , and 0.9 g Na_4EDTA in 100 mL water to pH=8 using a 2 M NaOH (aq) solution. The stock solution of reductant consisted of 1.7 g DMAB in 50 mL of water. Pd^{2+} catalyst solution was prepared of 10 mg Na_2PdCl_4 and 1.75 g NaCl in 50 mL water adjusting the solution with 37% HCl to pH=1. This yielded the desired $[\text{Pd}^{2+}]_{\text{tot}}$ of 0.7 mM and $[\text{Cl}^-]_{\text{tot}}$ of 0.7 M and showed the typical pale yellow color of dilute PdCl_4^{2-} solutions [145]. All solutions were used within 4 weeks. The pH of the electroless Co deposition bath measured over 24 hours at room temperature showed that the bath is stable at these conditions. Bubbling of clean N_2 through the electroless plating solution with simultaneous scratching of a pipette against the beaker wall started the bath, and a

Co layer deposited at the beaker wall was visible to the naked eye. The ELD was always accompanied by the formation of small hydrogen bubbles at the solid/liquid interface.

Substrate Preparation and Monolayer Formation

The gold samples were prepared by evaporation of 120–150 nm 99.99% Au (Advent, Halesworth, UK) on 570 K preheated cleaved mica in a 10^{-5} mbar vacuum and then annealed for several hours at ~ 600 K ($2 \cdot 10^{-6}$ mbar). Directly before starting the self-assembly, the Au films were flame-annealed at very dark red glow and cooled in ethanol. For the self-assembly, the samples were then quickly transferred into 20 μM ethanolic solutions of the aminothiols. The substrates were left immersed between 17 and 48 hours at ~ 325 K, thereafter several more days at 300 K. For the experiments with mixed monolayers, the samples were transferred into different mixtures of 20 μM ethanolic solution of the aminothiol and 20 μM ethanolic solution of decanethiol. These substrates were only left immersed 17 hours at ~ 325 K. All samples were rinsed with ethanol and used immediately.

Sample Preparation

The samples were dried in air and then mounted in a PCTFE STM cell, covered by a drop of the Pd^{2+} catalyst solution for two minutes, rinsed three times with water (or an aqueous solution containing 0.1 M HCl and 0.6 NaCl), and finally covered by the Co metallization bath. For XPS analysis the thiolate-covered substrates were rinsed with ethanol and then dipped into the Pd^{2+} catalyst solution for two minutes, rinsed with an aqueous solution containing 0.1 M HCl and 0.6 NaCl, and introduced via a fast entry lock into the vacuum system. All measurements were made at room temperature.

Instrumentation

The STM measurements were performed with a Besocke beetle type STM modified for in-situ electrochemical measurements [146, 147]. Additionally the microscope was insulated against vibration and electromagnetic fields by an acoustic cabin which at the same time serves as a Faraday cage. The microscope was suspended in the cabin by four rubber strings to suppress the vibrations of the building. All STM images are shown derivativized. The X-ray photoelectron spectra were collected in a VG ESCALAB 220. In order to minimize X-ray tube induced damage, the spectrometer transmission was maximized with lowest angular resolution and an overall energy resolution of 1.4 eV FWHM on the Au 4f peak at 84.0 eV binding energy. The X-ray twin anode that provides non-monochromatized $\text{MgK}\alpha$ (1253.6 eV) radiation was retracted and run with 70 W input power. For all spectra the Au 4f peak was set to 84.0 eV binding energy. The emission angles were 0° (normal emission) and 80° (grazing emission). UV absorption spectra of the Pd^{2+} solutions were obtained using a Shimadzu UV-260 spectrometer.

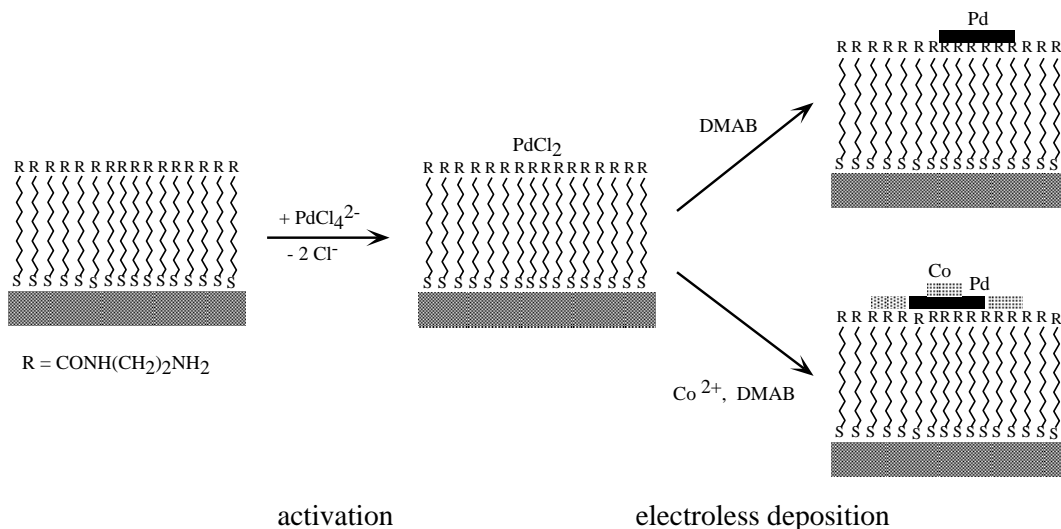
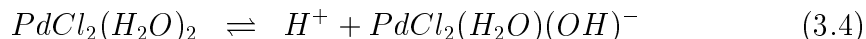
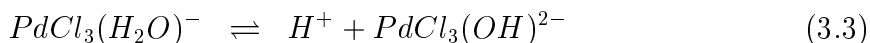
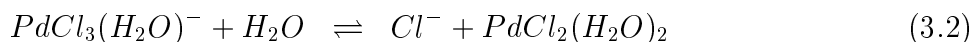
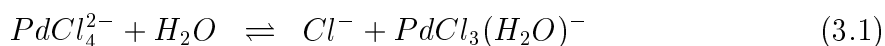


Figure 3.1: Schematic representation of the ELD of Pd islands and Co/Pd islands. Pd^{2+} binds to the amino groups on top of the thiolate layer. Dimethylamine-borane (DMAB) reduces Pd^{2+} and Co^{2+} to the respective metals.

3.3 Activation of SAMs with Pd^{2+} Catalyst

Pd^{2+} Catalyst Solution

Understanding of the Pd^{2+} activation is based on knowledge of the chemical composition of the activation bath. The chemistry of Pd^{2+} halogen complexes in aqueous solution is dominated by hydrolysis above $\text{pH} \sim 2$ [148–151] where hydroxo- and/or chloro-bridged Pd^{2+} oligomers precipitate. The mechanisms which dominate the chemistry in an aqueous solution of PdCl_4^{2-} are shown in Equations (3.1) to (3.4):



The Cl^- ligands are substituted one after the other by [152–155]. Deprotonation of the hydrolyzed species $\text{PdCl}_3(\text{H}_2\text{O})^-$ and $\text{PdCl}_2(\text{H}_2\text{O})_2$ is described by Eqs (3.3) and (3.4). The resulting hydroxo complexes easily lead to the formation of hydroxo- and/or chloro-bridged oligomers $[-\text{PdCl}(\text{OH})-]_x^y$ where $x > 1$ and $y \leq 0$ are integers [144, 148, 149, 151, 154, 156, 157].

Our purpose was to bind only one layer of Pd^{2+} ions to the amine-terminated surface (see Figure 3.1). This necessitates that the concentration of hydroxo- and/or chloro-bridged oligomers is kept as low as possible. For this reason we calculated from the reaction constants the required concentration of H^+ and Cl^- to have almost only PdCl_4^{2-} present in the solution [149, 151, 154, 156, 157]. In Figure 3.2 the normalized concentra-

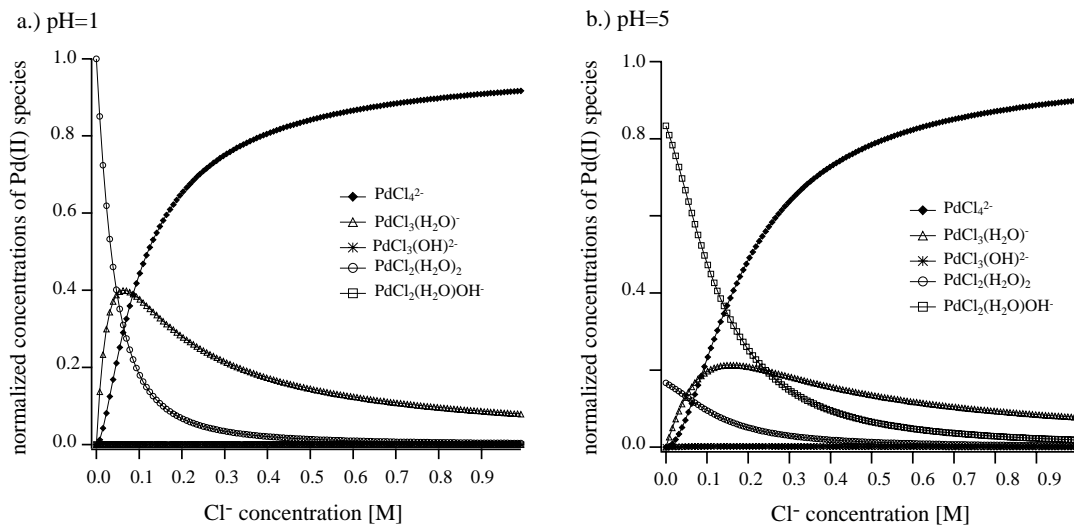


Figure 3.2: Normalized composition of the Pd^{2+} activation solution at (a) $\text{pH}=1$ and (b) $\text{pH}=5$ as a function of $[\text{Cl}^-]$. The aqueous solutions contain Na_2PdCl_4 , NaCl and HCl .

tions of the species are shown for $\text{pH}=1$ and 5 as a function of the Cl^- concentration. For our experiments we chose a Pd^{2+} solution at $\text{pH}=1$ with $[\text{Cl}^-]=0.7$ M. In this case the solution contains 86.6% PdCl_4^{2-} , 12.4% $\text{PdCl}_3(\text{H}_2\text{O})^-$, 0.9% $\text{PdCl}_2(\text{H}_2\text{O})_2$, $1.3 \cdot 10^{-5}\%$ $\text{PdCl}_3(\text{OH})^{2-}$, and $5 \cdot 10^{-4}\%$ $\text{PdCl}_2(\text{H}_2\text{O})(\text{OH})^-$ (calculated). A comparison of the corresponding UV spectra with spectra obtained by other groups [144, 152–155] provides further support that under these conditions PdCl_4^{2-} is indeed the majority species.

The choice of PdCl_4^{2-} as major component in the catalyst solution has another advantage. Compared to H_2O and OH^- , Cl^- is a labile (i.e. kinetically unstable) coordinator to Pd^{2+} sites and can be displaced by the surface amino ligands to covalently bind the Pd^{2+} to the SAM [158, 159].

Pd^{2+} Activation Experiments

Let us first focus on the chemical composition of Pd^{2+} activated AT-SAMs. An XPS analysis was performed to investigate the vertical position of Pd^{2+} relative to the monolayer. Au 4d and Pd 3d XP spectra are shown in Figure 3.3 for grazing (80°) and normal (0°) emission from a Pd^{2+} activated AT-SAM. The Pd 3d_{5/2} peak is clearly visible in grazing emission at 338.2 eV and corresponds to that of Pd^{2+} bound to N and/or Cl [144]. A component at 336 eV which should represent the oxo- or hydroxo-bridged Pd sites in the oligomers [144] is not found. In normal emission the Au signal is substantially increased while the Pd signal has disappeared. This can only be explained by a model in which the Pd^{2+} resides on top of the aminothiolate film [144]. A comparison of the survey spectra of pure and Pd^{2+} activated AT-SAM show that the activated samples are clean and not damaged during the treatment at $\text{pH}=1$. Furthermore it can be seen from the O 1s detail spectra that the untreated as well as the Pd^{2+} treated samples show only minute amounts of O_2 although they have been exposed to air for

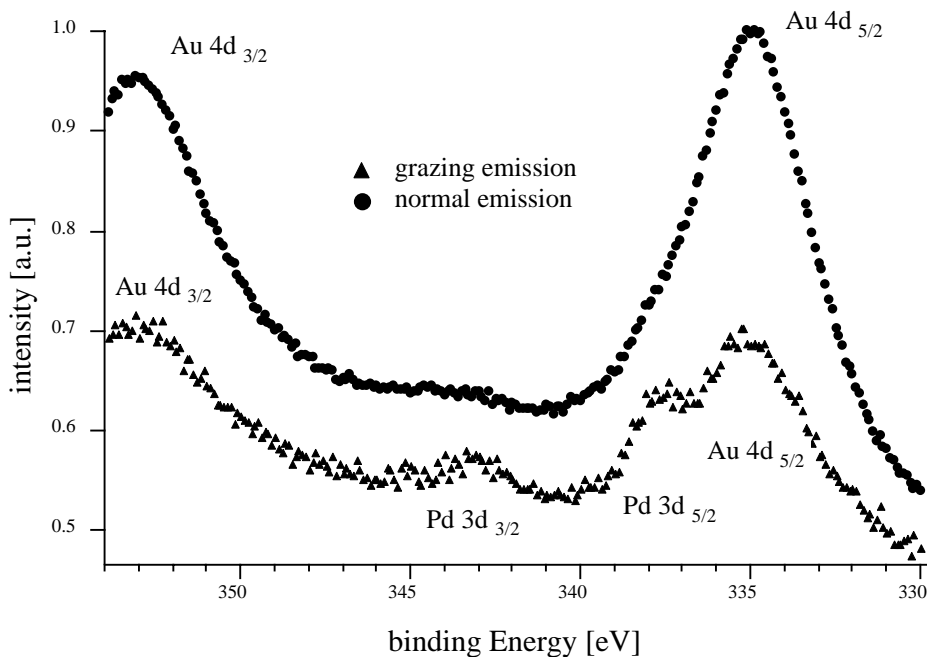


Figure 3.3: Normal and grazing emission XPS of the Au 4d and Pd 3d core level region of a Pd²⁺ activated AT-SAM. The increase of the ratio Pd 3d/Au 4f at grazing emission points towards Pd²⁺ on top of the AT-SAM. At normal emission the Pd 3d signal is too low to be resolved.

more than 30 s. As described elsewhere [147] for alkanethiolate films, we performed X-ray aging experiments for the AT-SAM. Intensity curves for the Au and Pd signal indicate a similar destruction of the AT-SAM with X-ray exposure time. For this reason exposure time was minimized to less than a few minutes.

By varying the time of contact between Pd²⁺ solution and AT-SAMs between 1 and 15 minutes, we found in STM measurements that the amount of unwanted Pd oligomers increases with activation time. These oligomers are bigger than 20–30 nm in diameter and more than 5–10 monolayers high. Nevertheless we always found flat areas of more than $2.3 \cdot 10^4$ nm² free of such oligomers. Rinsing of the Pd²⁺ activated samples with a solution of [Cl⁻]=0.7 M at pH=1 instead of water reduced further the number and size of the remaining Pd oligomers. Pd²⁺ activation times between 1 and 2 minutes were finally determined as best compromise for a sufficient activation without too many Pd oligomers. We note that careful rinsing should be sufficient to eliminate all excess Pd species which are not chemically bound to the surface.

Pd²⁺ Reduction Experiments

It is known that only metallic Pd can act as the catalyst for the ELD, but not Pd²⁺. This means that prior to the ELD of the metal (in our case Co) the Pd²⁺ species have to be reduced by the reductant (DMAB).

To estimate the size and the surface density of such Pd particles we performed in-

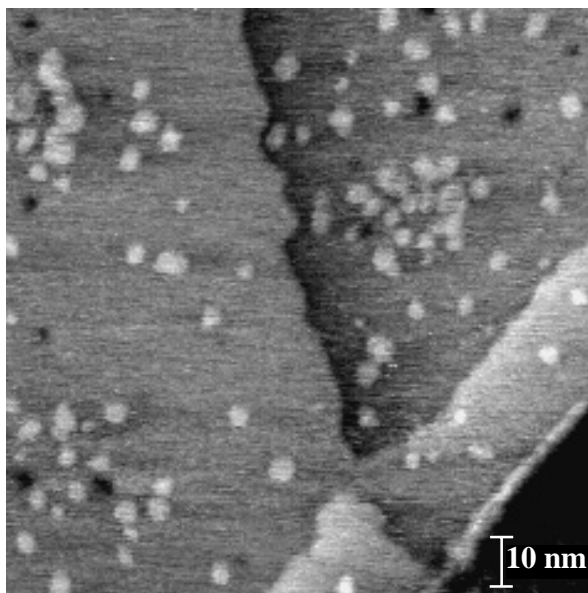


Figure 3.4: STM image of Pd islands (bright spots) on a Pd²⁺ activated AT-SAM electrode. The island height is one Pd monolayer. Areas of different gray shades are Au(111) terraces. The depressions (black), a few nm in diameter, one gold monolayer in depth, are typical for thiolate/gold interfaces. Bath: 50 mM DMAB. Tunneling parameters: I=1 nA, U=70 mV.

situ STM measurements. After the activation with Pd²⁺, the samples were immediately covered by a mixture of two parts of the DMAB stock solution and eight parts of water. A few minutes later the cell was mounted in the STM and measurements were started.

Images of the activated surfaces show that the metallic Pd particles¹ form islands that are homogeneously distributed on the surface, Figure 3.4. We find Pd islands of monoatomic height. The average diameter of the islands is between 1.5 and 6 nm (30-500 Pd atoms per island). Due to some variability during the Pd²⁺ activation (quality of rinsing with water, contact time with Pd²⁺ solution) the coverage of the surface by the islands varies between 1 and 4%. The reason for the low surface coverage of Pd islands has two origins: First, at pH=1 a non-negligible amount of amino groups will be protonated which reduces the capability to bind Pd²⁺. Second, the reduction of the Pd²⁺ species to Pd decreases the strength of the bond to the amino group and some Pd is probably lost into the electrolyte.

3.4 Electroless Deposition of Co

A prerequisite to understand the ELD of Co on Pd²⁺ activated AT-SAMs is the comprehension of the deposition of Co on bare Au electrodes and non-activated AT-SAMs. After presenting these experiments, we focus on Co deposition studies on Pd²⁺ acti-

¹It has been shown by Dressick et al. that Pd²⁺ particles in presence of DMAB are completely transformed to Pd [144].

vated AT-SAMs. Finally, we discuss the influence of aminothiolate concentration in mixed aminothiolate/alkanethiolate monolayers and show the dependence of the Co plating on the presence of O₂ in the deposition bath.

Co ELD on Bare Gold

To test the activity of the Co plating bath we performed an experiment on a gold wire. The gold wire was first cleaned in Nochromix solution, rinsed with water, and finally immersed in a Co plating bath. After 10–20 minutes the Co deposit is visible to the naked eye. The deposition can be accelerated either by bubbling N₂ through the bath or by increasing the bath temperature. These Co deposits –a few μm thick– can always be dissolved by both HNO₃ and HCl (both of pH=1) within a few minutes.

Co ELD on Non-Activated AT-SAMs

To test the passivating quality of our AT-SAMs we carried out in-situ STM measurements in the Co plating bath without having activated the AT-SAM with Pd²⁺ solution. Such samples show the typical features found for Au(111) electrodes covered with SAMs: flat terraces covered with pits of a few nm in size and one gold monolayer in depth. These depressions are vacancy islands in the topmost layer of the gold substrate formed during the self-assembling step [33,34]. We never found any clusters or small islands deposited on the non-activated SAMs. This means that our substrates are indeed covered by high density SAMs which are able to suppress the ELD of Co occurring on the bare gold substrate. It is important to note that for a Co deposition an activation with the Pd²⁺ solution is absolutely necessary. Finally, this proves –for the experiments described below– that we image Co and not any contaminations.

Co ELD on Pd²⁺ Activated AT-SAMs

After the activation with Pd²⁺ the solution was removed with a pipette. The samples were then carefully rinsed three times with water, and were immediately covered with the Co plating bath. A few minutes later the cell was mounted in the STM and measurements could start. During the induction time of 10–30 minutes the Faradaic tip current was too high to perform STM measurements [160,161]. After this period the islands already reached their final size of 2–10 nm diameter and one to two (in some rare cases three) monolayers height, Figure 3.5. Usually the islands are randomly distributed over the terraces and not attached to step edges. In rare cases islands are mainly deposited at step edges. It is very probable that such samples have a lower quality of the SAM. The coverage of the surface by the metallic islands varies between 2 and 20%², again depending on the sample. The variation in island size and surface

²The increased coverage of the surface –compared to SAMs covered only with Pd islands– is due to the fact that Co is deposited on top of the Pd islands and at their periphery, as can be seen in

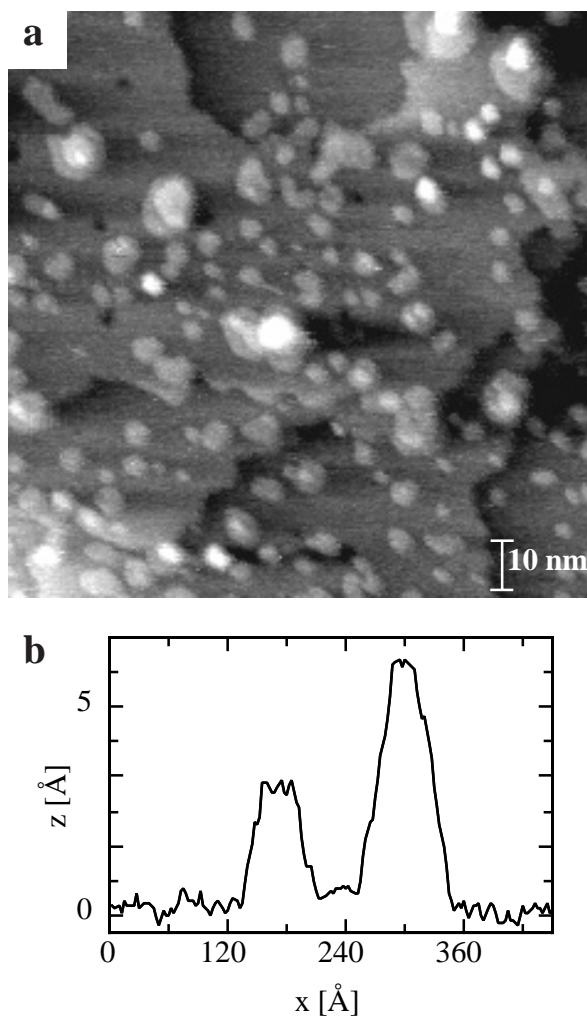


Figure 3.5: (a) STM image of Co/Pd islands on a Pd²⁺ activated AT-SAM electrode. Bath: 10 mM Co²⁺ + 50 mM DMAB. The brightest islands contain 3 monolayers. (b) Line scan through islands with one and two monolayers measured on an absolute height image. Tunneling parameters: I=0.6 nA, U=40 mV.

coverage is mainly attributed to the well known variability of the SAMs [147, 162, 163], the activation time, and the contact to air. STM measurements up to 24 hours later never showed any further growth of the islands. Even a strong increase of either Co²⁺ or DMAB concentration in the plating bath does not influence the island size.

In addition to the 1–3 monolayer high Co/Pd islands we found larger aggregates similar to that of the above-mentioned Pd oligomers (Figure 3.6). We are sure that these oligomers are covered with Co, because here again Pd²⁺ is easily reduced to Pd, albeit of unknown structure.

Upon increasing the tunneling current above 2 nA the islands can be moved over the surface, and even downward across steps. Sometimes they coalesce in the region close to the end of the scan lines. Such a mobility has never been found for Cu islands

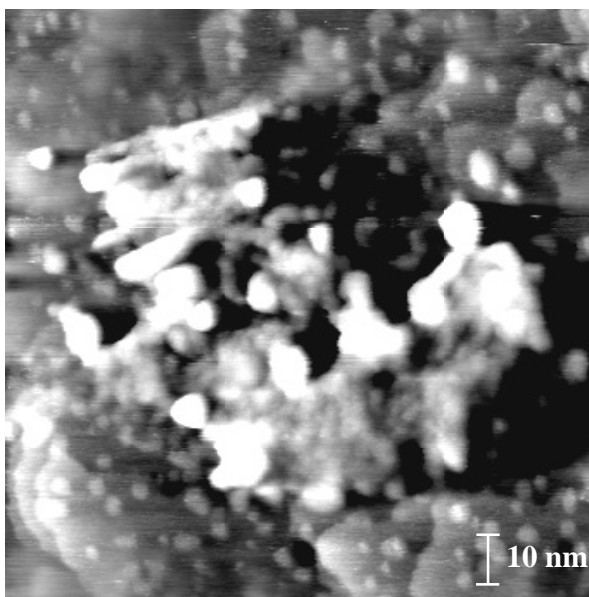


Figure 3.6: STM image of a hydroxo- and/or chloro-bridged oligomer covered by Co and of Co/Pd islands on a Pd^{2+} activated AT-SAM electrode. Bath: 10 mM Co^{2+} + 50 mM DMAB. Tunneling parameters: $I=1$ nA, $U=70$ mV.

electrodeposited on alkanethiolate SAMs, obviously since Cu penetrates into the SAM and attaches to the Au substrate [147, 164]. This gives us further support that the islands are located on top of the monolayer. However, the adhesion of the islands to the surface is strong enough that rinsing with water after the deposition does not remove the islands.

Influence of the Amine Surface Concentration in Mixed SAMs

Further proof that the Pd^{2+} species actually bind to the amine ligands is given in experiments where we changed the amino group concentration in the SAM. Freshly annealed Au(111) samples were transferred into ethanolic solutions containing different amounts of aminothiols and decanethiol. It is well known [35, 51, 55] that in this way the amino group concentration in the SAM can be varied. We changed the ratio aminothiol/alkanethiol in the solution between 2/1 and 1/100. Figure 3.7 shows a typical image of samples with low amine density. It is obvious that a decreased amine concentration leads to a lower Pd island density and as a consequence also to a lower Co/Pd island density. ELD of Co on Pd^{2+} activated pure decanethiol SAMs never succeeded since the Pd^{2+} species cannot bind to the monolayer and are thus completely washed away during the rinsing step. These facts strongly support our model of amine-bound Pd^{2+} species. Finally we notice a trend towards smaller islands for decreased amine concentrations (e.g. for aminothiol/alkanethiol = 1/100 the Co/Pd islands were only between 1 and 4 nm in diameter). A very similar shift of the size distribution of bound catalyst to smaller values was found by Brandow et al. [140] when they decreased the concentration

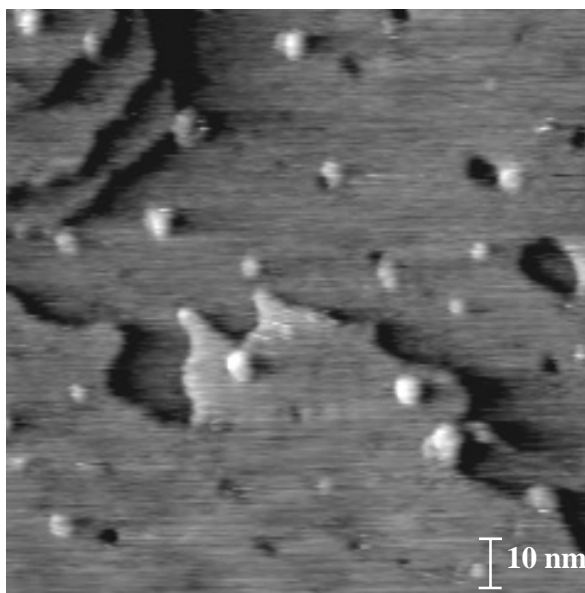


Figure 3.7: STM image of Co/Pd islands on a Pd²⁺ activated mixed aminothioliolate/alkanethiolate covered Au(111) electrode for a low aminothioliolate concentration. Bath: 10 mM Co²⁺ + 50 mM DMAB. The vacancies are typical for SAMs on Au(111). Tunneling parameters: I=0.8 nA, U=40 mV.

of surface functional groups capable of binding another Pd²⁺ catalyst.

Influence of the O₂ Concentration in the Plating Bath

For a better understanding of the Co growth step we performed experiments with plating baths containing less dissolved O₂ than a solution in contact with air. For this reason we bubbled clean N₂ through plating solutions during 15 minutes before use. After a sample was covered by the plating solution, the cell was kept in a N₂ box for an hour before it was mounted in the STM. STM imaging was carried out in the electrolyte in contact to air. Although a dispersion of the results was noticed, there is a clear trend towards islands with a bigger diameter, usually between 3 and 15 nm. A typical image at these conditions is shown in Figure 3.8. In one case we even found islands of 30 to 60 nm diameter with 10–20 monolayer height where the steps still could be resolved. Areas are often completely covered by three-dimensional Co deposits. The poor reproducibility is linked to the not completely controllable contact to air during the sample preparation (for example, the time for the transfer into the N₂ box).

On the other hand, we repeated the same procedure with a plating solution saturated with pure O₂ and kept under an O₂ atmosphere. For these conditions we noticed that the average size of the island is between 1 and 5 nm, which corresponds well to the values estimated for the pure Pd islands.

We conclude that the growth strongly depends on the O₂ concentration during the ELD. Hence, O₂ addition is a further control parameter to tune the size of the deposited

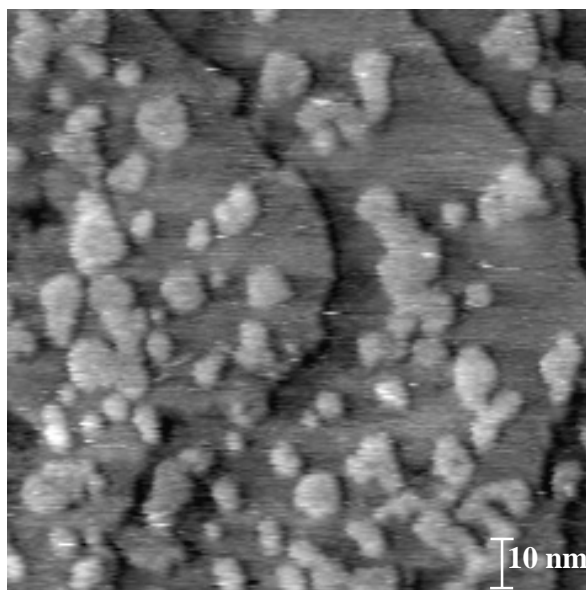


Figure 3.8: STM image of Co/Pd islands on a Pd²⁺ activated AT-SAM electrode in a bath saturated with N₂. Bath: 10 mM Co²⁺ + 50 mM DMAB. The increased island size is obvious from comparison with Figure 3.5 (O₂ saturated). Tunneling parameters: I=0.8 nA, U=40 mV.

islands. High O₂ concentrations can prevent Co deposition while decreased O₂ concentrations cause increased island sizes or even overgrowth of larger regions of the SAMs by a 3D Co deposit.

3.5 Discussion

Interactions between Pd²⁺ and Pd with AT-SAMs

We shall start the discussion with a look at the binding mechanism of the Pd²⁺ ions to the amino groups. PdCl₄²⁻ is the most convenient starting material for many complexes with N ligands and therefore a large collection of chemical and physical data exists [165,166]. Complexes are of the types [Pdam₄]²⁺, [Pdam₂X₂] and [PdamX₂]₂ with am = NH₃, amine, 1/2 diamine and X = Cl⁻, Br⁻, I⁻, SCN⁻, CN⁻. Adding the amine to a solution of [PdX₄]²⁻ under either neutral or acid conditions usually produces [Pdam₂X₂], hence, we expect a similar product when am = aminothiolate. In contrast [Pdam₄]²⁺ is more difficult to prepare [165].

Figure 3.9 shows 3 different conformations of the N-(2-aminoethyl)amide end group of the AT-SAM. Thermodynamics will favor the complex where Pd²⁺ is bound to four N atoms. In this geometry (Figure 3.9(c)) the chelation positively contributes, but Pd²⁺ would have to penetrate into the layer, which would be accompanied by a strong increase of steric and electrostatic repulsion between the neighboring Pd²⁺-aminothiolate entities. Taking into account kinetic arguments complex (a) will be more likely to be present at the surface than complex (b). When a PdCl₄²⁻ molecule arrives at the surface one Cl⁻

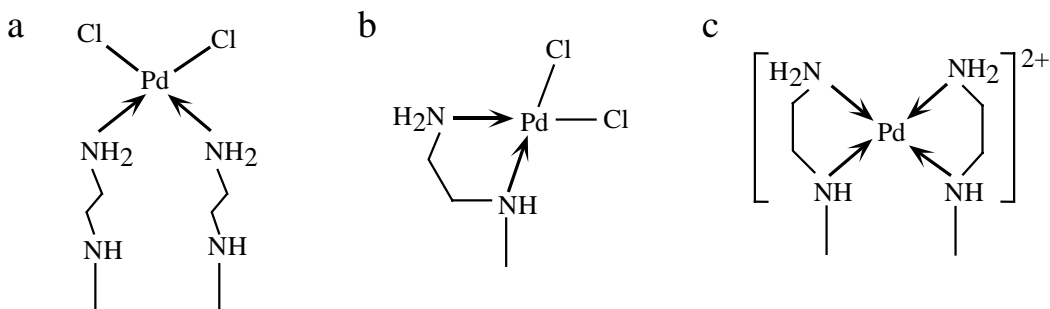


Figure 3.9: Representation of the possible configurations of the Pd^{2+} bonds with the amino end groups of the SAM.

is lost into the electrolyte while the Pd^{2+} complex forms a bond with an amino entity. Since several other amino groups from neighboring thiolates are very close to the Pd^{2+} complex, it is more likely that the Pd^{2+} binds to one of them than to penetrate into the monolayer and to bind to the second N group from the same thiolate.

Recent investigations of AT-SAMs by sum frequency generation (SFG) showed that the amino end groups are in all-trans-conformation when covered by aqueous solutions (with or without Pd^{2+}) [31]. Taking into account these results it is very likely that the conformation represented in Figure 3.9(a) are present at the surface. The two other conformations necessitate at least parts of the amino groups in cis-geometry which has not been observed by Epple et al..

For a better understanding of the island formation we focus now on the binding energies between Pd^{2+} and Pd with N species. First, we calculated approximately the Pd^{2+} -N binding energy from thermodynamical data [167] to be ~ 1.5 eV. Pd-N complexes could not be found in the literature (stable Pd complexes can only be formed with, for example, As, Sb or P containing ligands [165]). This fact can be explained by the ligand-field theory. The electron configuration of Pd is d^{10} and shows very unfavorable energetics compared to the Pd^{2+} configuration which is d^8 [158]. Therefore a Pd-N bond must be much weaker than the Pd^{2+} -N bond and thus the Pd species can diffuse over the surface of the SAM³. Calculating on the other hand the Pd-Pd bond energy in bulk metal, we found 3.9 eV for a macroscopic Pd solid [167]. Calculations with an effective medium code [169] estimated the bond energy for a Pd atom in a Pd(111) island containing 16 atoms to be ~ 3 eV. In both cases (microscopic and macroscopic) the Pd-Pd bond energy is twice as high as the Pd^{2+} -N binding energy. This favorable situation allows the formation of stable Pd islands.

We propose here a model where the Pd^{2+} entities are distributed homogeneously over the surface. They are then first reduced by the reductant to Pd atoms. During the

³There are mainly two reasons why the Pd^{2+} species do not penetrate into the SAM. First, there is no applied external potential which could force the penetration of the Pd^{2+} entities through the SAM as in the case of the electrodeposition of Cu [147,164,168]. Second, the alkane chains of thiols are very hydrophobic and the polar Pd^{2+} particles will not be dissolved in the SAM. Finally, the interaction of the amino groups with the Pd^{2+} particles is sufficient to inhibit their lost into the electrolyte.

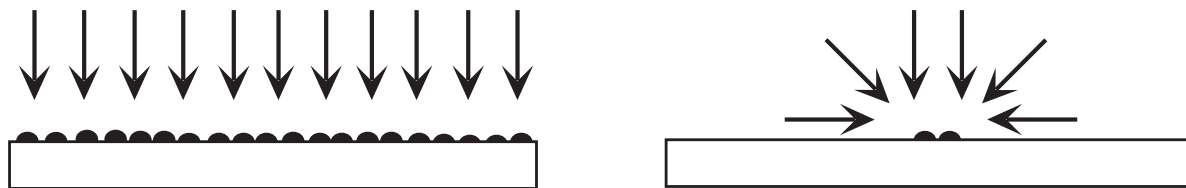
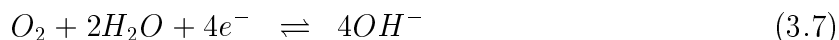


Figure 3.10: (a) Planar O_2 diffusion to a large activated area. (b) Radial diffusion to a small pattern of nuclei.

reduction the strength of the Pd-N bond is lowered and Pd atoms can diffuse over the surface. Nucleation and growth of the Pd atoms results in stable islands.

Inhibition of the Co Growth

Let us now concentrate on the discussion of the Co growth stop. To understand the growth inhibition it is necessary to consider the 3 main reaction current densities occurring at the islands: the oxidation of the reductant $j(\text{Red})$ (Eq. (3.5)), the reduction of the metal ion $j(M^{n+})$ (Eq. (3.6)), and the O_2 reduction $j(O_2)$ (Eq. (3.7)):



The following model considers electrocatalytic metal nuclei with a radius r on a dielectric substrate. At time $t=0$ the substrate is immersed in an unstirred alkaline solution containing a reducing agent (Red), complexed metal ions (M^{n+}) and dissolved O_2 . When the nuclei are small it is necessary to consider $j(O_2)$, since the radial diffusion flux of dissolved O_2 to small patterns is much larger than the planar O_2 diffusion to larger areas (Figure 3.10) [21].

Generally it can be stated that, at $t=0$, the catalyst is covered with O species (O_2 , OH). Since the open-circuit potential V_{oc} ⁴ of the covered catalyst is positive with respect to the redox potential of reaction (3.6) at $t=0$, reaction (3.5) and (3.7) will determine whether V_{oc} is shifted sufficiently negative to initiate metal deposition. For the following we assume that (3.5) and (3.6) are determined by kinetics, while (3.7) is determined by diffusion [21].

Considering a completely mass transport controlled O_2 -reduction at a microdisc [20], the current density of reaction (3.7) can be described by

$$j(O_2) \sim \sqrt{\frac{D}{\pi t}} + \frac{4D}{\pi r}, \quad (3.8)$$

⁴In ELD two or more reactions occur simultaneously at the electrode surface. Mixed potential theory assumes that the reactions proceed independently of each other ([170] and references therein). A steady state is obtained when all partial reactions proceed with the same rate, i.e. the sum of the current densities is zero. The potential of this steady state is called open potential V_{oc} .

where D is the diffusivity of O_2 in the bulk solution. For small r 's steady-state radial diffusion predominates over time-dependent planar diffusion. In conclusion $j(O_2)$ may become appreciably larger than $j(\text{Red})$ for small values of r . ELD can still start since the original metal catalyst particles have a large electrocatalytic activity for reaction (3.5). However, when the metal nuclei are covered by the electroless deposit, the latter cannot continue the autocatalytic growth due to the relatively increased contribution of reaction (3.7).

This purely classical model describes qualitatively well the behavior of the diffusional flux of the redox species to small electrodes and can explain the observed growth stop of the Co/Pd islands. However, we should not forget that for electrodes smaller than 10 nm a correct model must include effects of the finite dimension of redox molecules and the local diffusivity near the electrode surface [171].

We also compared $j(O_2)$ on Pd and Co [21, 172]. Both values are of the same order of magnitude and do not explain the growth stop of Co. If $j(O_2)_{Co}$ was much higher than $j(O_2)_{Pd}$, the following scenario would explain the growth inhibition: after the Pd island is completely covered with Co, $j(O_2)_{Co}$ would consume all electrons delivered by the reductant and the growth would cease.

Considering all these facts leads us to the conclusion that the growth stop is induced by an increased radial diffusion of O_2 to the nanometer-sized electrodes. Therefore, a very good control of the amount of O_2 in the plating bath is inevitable for any future work with this system.

3.6 Conclusions

Pd can be grown by ELD in nanometer-sized islands on AT-SAMs on Au(111) electrodes. The most likely place of the Pd is on top of the AT-SAM as proven by normal and grazing emission angle XPS, by the fact that they can be moved by slightly increasing the tunneling current and finally by the strong correlation with the amine surface concentration in mixed monolayers. The Pd island density can be varied over a large range by changing the amine concentration in mixed aminothioliolate/alkanethioliolate SAMs. On these Pd islands Co can be deposited via ELD. The size of the resulting Co/Pd islands can be controlled by the O_2 concentration in the Co plating bath. Processes causing the inhibition of the island growth are discussed.

Our concept to fabricate nanometer-sized islands of Co and Pd should be applicable to many magnetic and nonmagnetic metals. In combination with microcontact printing (see Chapter 2) to pattern AT-SAMs it should be possible to fabricate diverse metal cluster arrays. Patterning of nanometer-sized magnetic objects placed on an organic spacer would be interesting for a better understanding of the magnetism at small scales. The study of the magnetism as a function of size and geometry of nanostructures on top of a spacer would allow an interesting comparison with systems without spacers. In our case the thioliolate layer should help to minimize any electronic and magnetic interaction

between the substrate and magnetic objects on top of the spacer. It will also be possible to study the long range interaction between different magnetic aggregates.

Chapter 4

Patterned Electroless Deposition of Cu

An improved approach to pattern substrates with metals is described in this Chapter. The basic idea is to use the technique of microcontact printing (μ CP) to prepattern a substrate with a catalyst precursor. This catalytic pattern starts the electroless deposition (ELD) of Cu (or other metals) when it is immersed into an appropriate plating bath.

The experiments presented in this Chapter have been performed in the laboratory of Dr. B. Michel at IBM R uschlikon.

4.1 Introduction

As we have seen in the last Chapter ELD is a remarkable method to metallize substrates. It is proving increasingly useful in semiconductor and packaging technologies, for example. A major requirement prior to performing selective ELD is the seed (the placement and activation of the catalyst on the surface) and its selectivity: the catalyst must be confined to certain regions of the substrate and be completely absent from adjacent regions. This can be achieved either by selective deactivation of an active substrate or by selective activation of a nonreactive surface¹. Several approaches that seek to create catalyst patterns with high activity and contrast have been explored. They include photopatterning of pretreated substrates combined with the deposition of metal films [138, 173–175], selective modification of catalyst-binding monolayers [135, 137, 144], and μ CP of a catalyst onto substrates [176, 177].

The autocatalytic character of ELD renders this technique attractive to many fields of technology, but the catalysis associated with ELD and the absence of a directly mea-

¹The selective deactivation of an active surface is a difficult strategy since deactivation must be 100% efficient: a small number of defects give rise to an important deposition of metals on the passivated region. In contrast to the deactivation, selective activation is easier. These behaviors have their origin in the self-amplifying character of the autocatalytic nature of ELD.

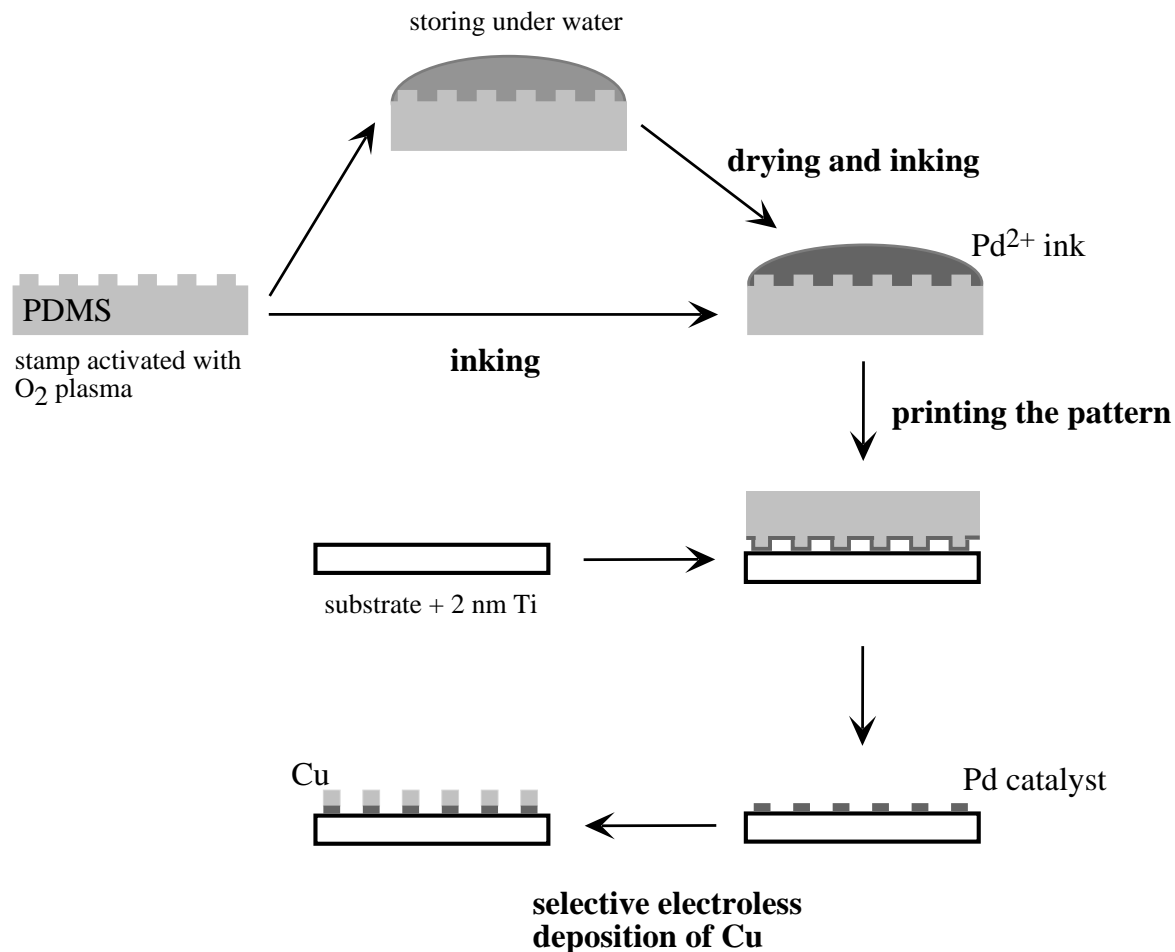


Figure 4.1: Procedure for selective electroless deposition of Cu by microcontact printing a Pd²⁺-based catalyst precursor onto a Ti-coated silicon wafer. A PDMS stamp is first hydrophilized with an O₂ plasma and stored in deionized water if not used immediately. The stamp is then inked with a solution of catalyst precursors in ethanol. Microcontact printing the Pd²⁺ complexes onto a freshly Ti-coated substrate immobilizes and activates the catalyst onto the substrate. Cu electroless deposition proceeds by immersion of the printed substrate in the Cu plating bath.

surable control, like a current to control or monitor this reaction, makes its application difficult as seen in Chapter 3. Many parameters can affect the ELD of metals, such as the density of the catalyst and its degree of activity on the surface, the adhesion of the deposit to the substrate, and the composition and conditions of the plating bath. Understanding the chemical reactions in ELD requires insight into the chemical and physical state of the catalyst interface, which can only be addressed using a restrictive scope of instrumentation [69]. Exploration of which parameters are significant and how they contribute to the observed effects can be cumbersome, in particular when ELD is sought to metallize only a subset of a substrate because contrast and accuracy of the metallized patterns are additional concerns.

In this Chapter we combine ELD (see Chapter 3) with μ CP [8, 59, 85–87] to obtain a

non-photolithographic technique for the selective deposition of metals on nonconducting substrates. Briefly, μ CP uses here a patterned and inked elastomeric stamp to print a catalyst precursor (a Pd^{2+} complex) as a pattern onto a substrate, Figure 4.1. A chemical reaction between the Pd^{2+} from the ink and Ti evaporated onto the substrate prior to the print creates the Pd^0 catalyst pattern. Deposition of Cu follows from the immersion of the printed substrate into a Cu plating bath. This application of μ CP is challenged by several interdependent parameters such as the appropriate surface chemistry of the stamp, the choice of the ink, the control over the transfer of the catalyst during printing, the activation of the catalyst, and the electroless plating of Cu in general. We suggest here one reliable method when μ CP provides the catalyst pattern for ELD. This method uses hydrophilization of poly(dimethyl)siloxane (PDMS) stamps and inking with the ethanol-soluble $[(\text{CH}_3-(\text{CH}_2)_{16}-\text{CN})_2\text{PdCl}_2]$ catalyst precursor. Printing this complex onto a thin Ti layer, which is evaporated onto SiO_2/Si , provides a high-level transfer of the Pd^{2+} complex from the stamp to the surface with simultaneous activation and fixation of the catalyst by reduction of Pd^{2+} to Pd^0 before immersion of the sample into the plating bath. Fabrication of high-resolution and high-contrast patterns of Cu is possible with this method.

4.2 Experimental

Stamps and Substrates

Unpatterned poly(dimethyl)siloxane (PDMS) stamps were prepared from Sylgard 184 (Dow Corning, Midland, MI), dispensed with an automatic mixer/dispenser (DOPAG MICRO-MIX E, Cham, CH), and cured for at least 12 h at 60 °C on a flat polystyrene surface (Petri dish, Falcon 1001 & 1013, Becton Dickinson Labware, NJ) [90]. Patterned stamps were prepared similarly to flat stamps but cured on masters prepared by contact photolithography using Novalac resist and fluoroalkylated with (1,1,2,2-tetrahydroperfluorodecyl)trichlorosilane (ABCR, Karlsruhe, D). Stamps with high-resolution features (<500 nm) were molded using commercially available copolymers and fluorinated masters prepared by electron beam (e-beam) lithography on a silicon-on-insulator (SOI) wafer [178]. Both types of stamps had a thickness of $\sim 4\text{--}5$ mm. We used an O_2 plasma treatment of the stamps (O_2 pressure ~ 0.8 mbar, load coil power ~ 100 W, 15 s; Technics Plasma 100E, Florence, KY) to render their surface hydrophilic prior to inking. Hydrophilized stamps were used immediately or stored in deionized water. Ti-covered substrates were prepared by e-beam evaporation of Ti (99.99%, Johnson Matthey) onto SiO_2/Si wafers (Siltronix, Neuchâtel, CH) and glass microscope slides at a pressure of $\sim 2 \times 10^{-7}$ mbar and a rate of ~ 0.01 nms^{-1} . All Ti substrates were used within 1 h after the evaporation of Ti to limit aging effects by oxidation and contamination of the Ti on subsequent printing and plating steps.

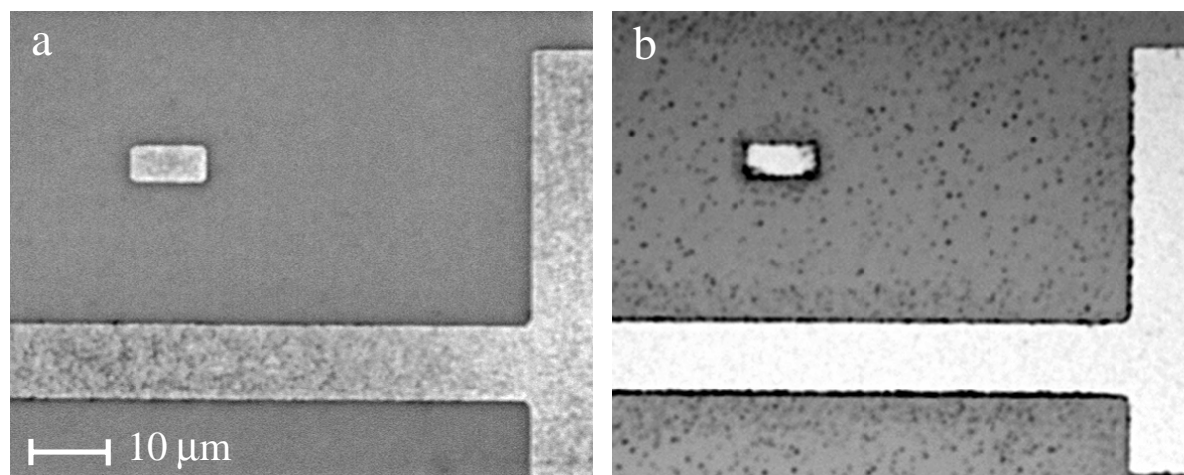


Figure 4.2: The optical micrographs show the Cu pattern when a filtered (a) and unfiltered (b) plating solution is used. For the unfiltered bath a plating fog is deposited between the Cu lines.

Inking and Printing

The ink was made of solutions of bis(octadecanenitrile)dichloro-palladium(II) $[(\text{CH}_3-(\text{CH}_2)_{16}-\text{CN})_2\text{PdCl}_2]$ in ethanol with concentrations ranging from 0.01–1.0 mM. All ink solutions were used within 6 h after their preparation to prevent oligomerization and evolution of the Pd^{2+} towards colloidal species (directly detectable by the change of color of the ink solution and by the precipitation of the colloids). The Pd^{2+} complex was synthesized as follows: 1.0 g (5.6 mmol) of PdCl_2 (Fluka) was dissolved in 6.0 g (22.6 mmol) of octadecanenitrile (Aldrich, recrystallized from 20 mL of ethanol) and stirred at 100 °C for 3 h. After cooling, 30 mL of pentane (Fluka) was added, and the residue was filtered and washed with cold pentane. The stearonitrile-substituted complex was separated from PdCl_2 and metallic Pd by extraction with toluene (Fluka). Removal of the solvent yielded 2.9 g (4.1 mmol, yield: 73%) of bis(octadecanenitrile)dichloro-palladium(II) as a yellow powder. $^1\text{H-NMR}$ (DMSO-d_6 , 400 MHz) was used to control the structure and purity of the complex, and proved that the synthesis was successful. Inking was achieved by covering a flat or patterned stamp with a 0.01–1.0 mM solution of the Pd^{2+} complex in ethanol for 60 s and drying the stamp for 10 s under a stream of N_2 . Inked stamps were used within ~ 15 s after their inking. Printing was done by placing stamps on substrates and removing them after a contact duration of 15 s. Each print used a new patterned stamp to prevent interference from the history of the stamps with the next print.

Electroless Deposition of Cu

Cu solutions were prepared by dissolving 3 g of $\text{CuSO}_4 \cdot 5\text{H}_2\text{O}$, 14 g of sodium potassium tartrate, and 2 g of NaOH in 100 mL of distilled water [179]. 100 μL of formaldehyde (37.2 w%, Fluka) was added to 10 mL of the Cu solution to supply the reducing agent

to the plating bath. Cu electroless plating baths were prepared immediately (~ 30 min) prior to plating samples or series of samples. Printed samples were immersed in the Cu plating bath for 30–120 s at room temperature. The duration of plating was kept constant for a series of experiments. Plating was stopped by removing the sample from the bath and rinsing it with distilled water. Occasionally, small (~ 100 nm) Cu particles developed or deposited from the bath onto nonprinted areas of the sample and appeared in the optical microscope as a diffuse background², as shown in Figure 4.2. This problem was strongly suppressed by filtration of the bath before plating with a $0.22 \mu\text{m}$ pore filter (Millipore). Mechanical stirring and air bubbling were not used but can reduce plating fog of this type as well [180]. The Ti film between the Cu structures could be removed within a few seconds, if desired, by dissolution in 1% HF or other strong acids.

Instrumentation

Contact angles of water with substrates were determined with a Krüss (Hamburg, D) contact angle goniometer equipped with a motorized pipette (Matrix Technology, Nashua, NH). Advancing and receding angles were measured at three or more locations on each sample. Roughness measurements were performed with a commercial Nanoscope III AFM (Digital Instruments, Santa Barbara, CA) operated under ambient conditions in tapping mode. Optical inspection of the samples was carried out in reflection with a Leica Polyvar SC microscope equipped with a charge-coupled camera (3-CCD Donpisha, Sony) and a high-resolution (768×512 pixels) frame grabber to digitize images (Image-Pro Plus, Version 1.3, Media Cybernetics). High-resolution patterns of plated Cu were examined using a Hitachi S-4000 scanning electron microscope (SEM). X-ray photoemission spectroscopy (XPS) spectra were acquired on a Sigma Probe VG Scientific spectrometer operating at a base pressure of $<10^{-9}$ mbar and equipped with a monochromatized AlK_α source ($E = 1486.6$ eV). The X-ray spot was focused to $100 \mu\text{m}$ to perform a series of XPS measurements at several locations on the same sample. The analyzer had an angle of 45° to the sample, and samples were mounted on a multisample holder stage for examination under identical conditions. Spectra are referenced to the C 1s peak at 285 eV. For all samples, survey spectra were acquired first with a pass energy of 80 eV, and high-resolution spectra for the various elements investigated were acquired in the same sequence for all samples with a pass energy of 40 eV. The comparison of the peak of Si 2p or Ti 2p acquired first and last for each sample indicated no noticeable damages on the surface of the sample during the measurements. XPS on PDMS stamps was done with a flood gun ($\sim 1 \mu\text{A}$ emission current) and partial pressure of Ar of $\sim 5 \times 10^{-8}$ mbar for charge compensation of these insulating samples.

²These particles are called *plating fog* and are caused by the instability of the electroless plating solution.

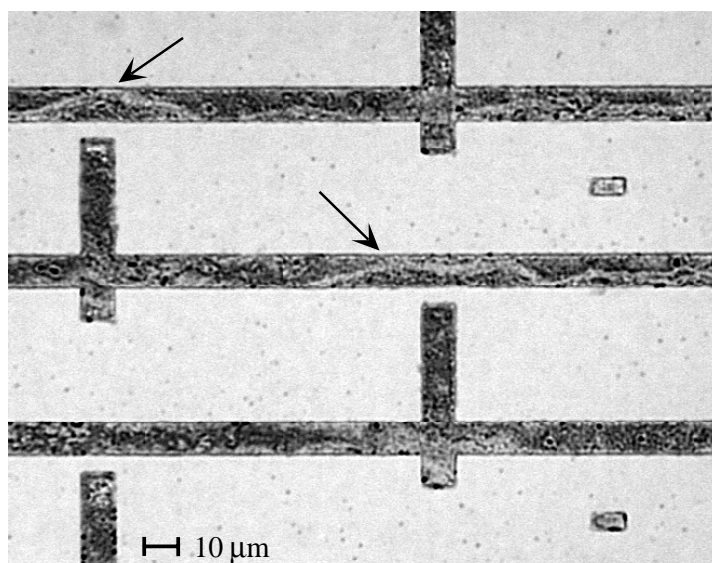


Figure 4.3: The optical micrograph show the Cu pattern when an aqueous ink solution is used. The inhomogeneities in thickness of the Cu deposit (see arrows) are due to possible drying effects of the ink when the stamp is dried under a stream of N_2 .

4.3 The Catalytic Ink

We synthesized a series of bis(alkanenitrile)dichloro-palladium(II) complexes as catalytic precursors for the ELD of Cu because (i) these complexes are simple to prepare and easily reduced to Pd^0 , (ii) Pd^0 is an excellent catalyst for ELD of Cu, (iii) these Pd^{2+} catalytic precursors are soluble in ethanol, (iv) long alkyl chains on the nitrile ligands considerably improve the stability of the Pd^{2+} complexes in the ink against the formation of colloidal species, and (v) molecular catalyst precursors may be printed at higher resolution than colloidal species [140]. Interestingly, increasing the length of the alkyl part of both nitrile ligands did not improve the affinity between hydrophobic PDMS stamps and the catalyst precursor in the ink (see Chapters 2 and 5). We consequently used hydrophilic PDMS stamps and $[(CH_3-(CH_2)_{16}-CN)_2PdCl_2]$ for all experiments because this complex is more stable in ethanol than its shorter analogs.

A large variety of other Pd complexes was tested as catalyst precursor for the ELD of Cu. The majority of them were either insoluble (in sufficient concentrations) or unstable in ethanol. Some of the stable ethanolic inks could be used to print but resulted in no or only minor deposition of Cu. Many of these catalysts were soluble and stable in water, however. Printing them on substrates always resulted in Cu structures decorated with drying traces³: during the final drying of the stamp the water film starts to form droplets and the catalyst precursor is left in higher concentration where these droplets dry out and in lower concentration on the remaining of the pattern [181]. This inhomogeneous

³This is probably due to two contributions. Water exhibits a decreased wetting of the hydrophilic surface of the stamp compared to ethanol and has in addition a lower vapor pressure which is bad for a homogeneous drying.

pattern is then transferred to the substrate and is reproduced by a low quality Cu deposit. Cu grows faster on regions with a high catalyst density and the resulting Cu features are not uniform in thickness, as shown in Figure 4.3.

4.4 Printing the Catalyst onto Ti Films

Transferring the catalytic precursor from the stamp after inking and drying to the substrate is the next step. This too, is critical for obtaining adhesive and high-quality deposits. Deposition of a catalyst for ELD usually follows the immersion of a preconditioned substrate into a solution of Pd particles (see Chapters 2 and 3). The preconditioning step can be simple, but it may also consist of a long series of dips and rinses resulting in a homogeneous fixation of the catalyst particles on the surface to be plated. Here, we seek to use μ CP to pattern the catalyst such that the scope of possible pretreatment of the substrate before printing is less lavish compared to more conventional and proprietary approaches. Derivatization of surfaces carrying silanol ($-\text{SiOH}$) groups with ω -functionalized alkylsilanes proved useful in previous work for printing colloidal Pd onto the surface of oxides [176]. In our case, SiO_2/Si was selected as a substrate because it has important technological applications, it is available pure and clean, it is neither conductive nor active for ELD, it is compatible with silane-coupling chemistry, and a variety of analytical techniques can readily be performed on wafers. Microcontact printing the Pd^{2+} complex onto Si wafers cleaned with strong chemical oxidants, or sonicated with detergents and ethanol, or as received from manufacturers did not seem to lead to homogeneous ELD of Cu. Neither conventional pretreatment of the substrate with SnCl_2 , nor proprietary vendor treatments, nor etch-induced roughening of the substrates, nor silanization of the substrates were satisfactory for our study.

Ti was evaporated onto the wafers as an alternative to wet chemical treatments or cleaning. Evaporation of metals such as Ti on substrates is a well-defined and controllable method to derivatize a substrate. Ti, like Cr, is often used as an adhesion promoter for metals on oxides. Partially oxidized Ti can reduce Pd^{2+} , and we hypothesized that it could bind Pd^{2+} during printing and reduce it to its metallic state [182]. Figure 4.4 reveals that the quality of the Cu deposits is optimal and similar when at least 2 nm of Ti have been evaporated onto the SiO_2/Si wafers⁴. Interestingly, the quality of the deposits increases with the thickness of evaporated Ti despite equivalent inking, printing, and plating conditions for all experiments in Figure 4.4. This indicates that more active Pd is present on surfaces coated with more than 2 nm Ti because ELD of Cu represents a very sensitive diagnostic of how much catalyst is available and how active it is on the surface.

⁴The optical microscope images shown here do not reveal the color of the Cu deposit. The color of the Cu deposit, however, is an important criterion for its quality: Cu plated on thin Ti films (<1 nm) has a dark “nonmetallic” color. For a Ti layer thicker than 2 nm, the Cu metal deposits have a bright, reddish color corresponding to thicker and partially oxidized Cu.

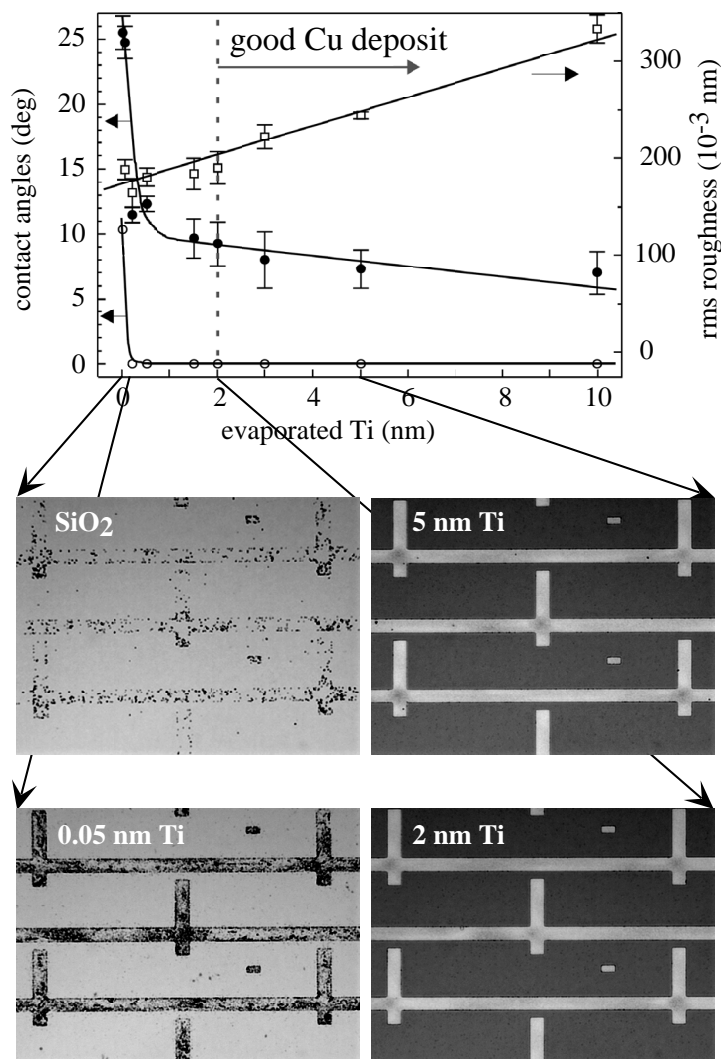


Figure 4.4: Dependence on roughness, contact angle, and thickness of a Ti layer evaporated onto a SiO₂/Si wafer of the electroless deposition of Cu that followed microcontact printing a 0.5 mM Pd²⁺ catalytic precursor onto the Ti surface. The roughness (open squares) of the Ti layer and its advancing (solid circles) and receding (open circles) contact angles with water are reported in the graph as a function of the Ti thickness. The optical microscope images show the quality of the electroless Cu deposits for several particular thicknesses of Ti. The roughness and wettability of the evaporated Ti layer do not correlate with the quality of the Cu electroless deposit, but rather 2 nm is the critical thickness of Ti necessary for good Cu deposits.

The roughness of a substrate can be an extremely important factor in influencing the quantity and the adhesion of a catalyst transferred to a substrate in ELD methods. Substrates are often roughened and etched prior to their derivatization with a catalyst for this reason. However, AFM investigation of the roughness of the substrates as a function of the Ti thickness suggests no evident correlation between the quality of the Cu deposits and the roughness of the modified substrates. Changes in this roughness

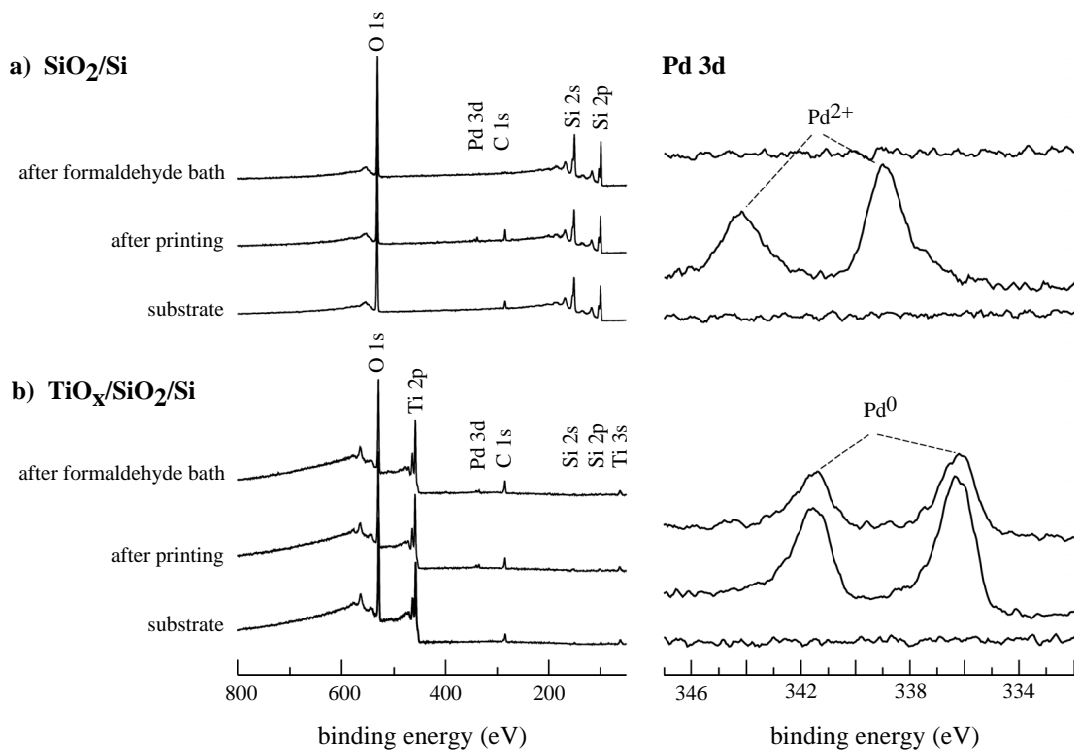


Figure 4.5: XPS survey and high-resolution spectra of the Pd 3d region of (a) SiO_2/Si substrates and (b) 2.5 nm of Ti evaporated on the SiO_2/Si substrates before and after microcontact printing a Pd^{2+} catalytic precursor and after immersion of the printed samples in an electroless Cu plating bath containing only formaldehyde but no Cu. The action of the Ti layer evaporated prior to printing the Pd^{2+} catalyst precursor is dual: it reduces Pd^{2+} metallic Pd during printing, and prevents Pd from being washed off the surface during the immersion of the printed sample in the formaldehyde bath.

seem marginal and the quality of the Cu deposits is independent of this roughness for Ti films thicker than 2 nm. Similar to the roughening of substrates, changing their wettability can strongly influence their ability to interact productively or negatively with a catalyst from a solution (see below). Substrates coated with only a few angstroms of Ti have an excellent wettability by water but lead to Cu deposits of mediocre quality. For this reason, the wetting properties of the substrates are not the determinant factor for obtaining high-quality Cu, but Ti seems to play the role of a reactant during the printing of the Pd^{2+} complex to the surface. We reproduced the results presented in Figure 4.4 in a single operation by evaporating Ti on a SiO_2/Si wafer with a gradient of thickness from 0 nm up to ~ 5 nm. This indicated that changes in the Cu quality are not induced by uncontrolled printing conditions or by aging effects of the plating bath or the Ti substrates. The adhesion of the Cu structures was measured by a standard scotch tape test and followed the correlation between the quality of the Cu deposit and the thickness of Ti on the substrate: Cu is not removed by peeling off the scotch tape when more than 2 nm of Ti is present on the surface.

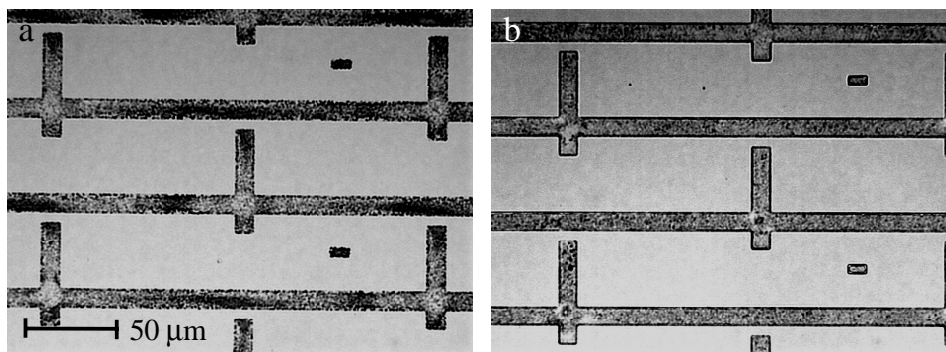


Figure 4.6: The optical micrographs show a dark brown and incomplete pattern of Cu when the catalyst precursor is printed on substrates modified with a (a) dodecyltriethoxysilane- and (b) 3-aminopropyltrimethoxy SAM.

XPS experiments presented in Figure 4.5 indicate that Ti provides two simultaneous advantages for μ CP of a Pd^{2+} catalyst onto a surface: Ti fixes and reduces Pd^{2+} , whereas printing Pd^{2+} on the native oxide of a Si wafer does not change its oxidation state (II) [183]. Figure 4.5(b) illustrates how Ti acts on the printed Pd. An equivalent amount of Pd^{2+} appears to transfer from the stamp to SiO_2/Si and Ti on SiO_2/Si but the Pd^{2+} is reduced to Pd^0 when Ti is present on the substrate and is not washed away after the substrate is immersed in a bath containing only formaldehyde but no Cu. This reduction is consistent with the standard electrochemical potentials of partially oxidized Ti and Pd^{2+} , but it also implies that fully oxidized Ti should lose its ability to coordinate and reduce Pd^{2+} [182]. This was confirmed (i) by a complete oxidation of Ti evaporated on SiO_2/Si in an O_2 plasma after which the surface behaved similarly to SiO_2/Si and (ii) by the observation that exposure of Ti-coated substrates to ambient air for more than a few hours reduced the benefits of the Ti evaporation considerably. In the absence of Ti, a weak Cu deposition occurs in the plating bath due to the Pd^{2+} catalyst remaining on the oxide surface. The Pd^{2+} is reduced first by formaldehyde in the bath before Cu plating can start.

Several other approaches exist to place and fix a Pd catalyst on a surface. The majority of these techniques uses direct deposition of colloidal Pd and Sn species from solution on preconditioned substrates [64, 66, 71, 184–187]. Activation of the catalyst on the surface can then proceed by reaction with hydrofluoroboric acids to liberate Pd atoms or clusters from the colloids. The fraction of the catalysts present in an oxidized state may additionally be reduced by the reducing agents in the plating baths. We tried several of these approaches to μ CP catalytic patterns for ELD but always found low-quality Cu structures with poor resolution.

Other interesting pretreatments involve silanization of substrates for the fixation of Pd complexes [144, 176]. To examine if this could be an alternative for the evaporation of Ti, we prepared a series of silanized samples, as shown in Figure 4.6. In changing the tail group, we produced SAMs with different surface chemistries. Printing on CH_3 -terminated SAMs resulted in little deposition of dark brown Cu (in good agreement

with our experiments in Chapter 3), Figure 4.6(a). Increasing the chain length of these silanes –which increased the ordering of the chains in the SAM and thus decreased the surface free energy by exhibiting more CH_3 groups at the surface– decreased the amount of plated Cu. Printing on samples covered with SAMs of higher free surface energy (for example, NH_2 -terminated) showed a similar behavior, Figure 4.6(b). We suggest that there is only a weak interaction between the surfaces of the modified SAMs and the catalyst precursor: an important part of the catalyst is washed away when immersed in the Cu plating solution. Consequently, the catalyst precursor cannot be bound in sufficient amounts and strength to such modified SAMs during the printing.

Taking into account these results we favored the evaporation of Ti in this work as it is a simple and reliable technique and may be more generally applicable to the fixation and activation of a large variety of catalytic precursors. Moreover, Ti can easily be etched selectively .

4.5 The Role of the Stamp

We observed that changing the inking time of the stamp from a few seconds to 10 minutes does not affect the quality of the Cu deposit, indicating that the density and distribution of the catalyst precursor on the stamp surface remain comparable in either case. Three phenomena may account for this observation: (i) the stamp may be limited in its ability to incorporate the Pd^{2+} complex at its surface, (ii) the overall transfer may be limited by the printing time, or (iii) the reaction between Pd complexes and Ti on the surface is optimal and reaches completion. Changing printing times from 1 s to several minutes did not have obvious effects on the quality of the Cu patterns. Immersion of Ti-coated substrates in a solution of the Pd^{2+} catalyst resulted in Cu deposits of slightly higher quality (denser and smaller Cu grains). This suggests that the stamp represents the limiting factor for printing the Pd^{2+} on the surface.

Figure 4.7 corresponds to the investigation using XPS of the amount of Pd^{2+} that can be inked onto the surface of a hydrophilized stamp and transferred by printing onto a Ti-coated substrate. Several stamps were prepared for the three different steps investigated in Figure 4.7, exposed to ultrahigh vacuum conditions, and analyzed under the same conditions. The principal components of the PDMS stamps after O_2 plasma treatment are O_2 , carbon, and silicon. The presence of an important peak of carbon at 285 eV denotes the presence of methyl groups on or near the surface of the siloxane polymer. This suggests that “restructuring” of the oxidized air-polymer interface occurred after the plasma treatment and before the XPS experiments or that combustion of these groups by the O_2 plasma remains confined to a very thin surface layer [84,89,91]. Inking the stamp with a 0.5 mM solution of the Pd^{2+} in ethanol for 30 s provides an observable quantity of catalyst precursors. The broadening of the Pd 3d region is due to a slight charging of the sample during data acquisition. Taking this charging into account, the species found on the stamp could always be attributed to Pd^{2+} . Apparently no Pd^{2+}

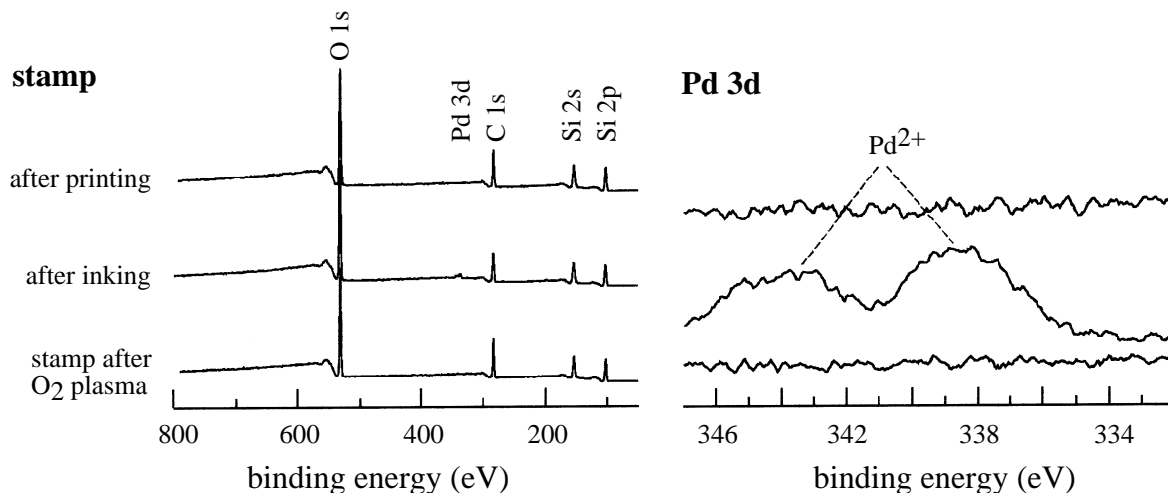


Figure 4.7: After inking, the catalytic precursor remains in the (+II) oxidation state and apparently transfers entirely from the stamp to the substrate after printing.

remains on the stamp after printing. The XPS results in Figure 4.7 are qualitative in nature but demonstrate that it is possible to ink a hydrophilic PDMS stamp with the Pd²⁺ complex and that its transfer during printing appears to be complete. The quantity of Pd²⁺ on the inked stamp was variable but could never be increased noticeably by increasing the duration of the plasma oxidation, the concentration of the complex in the ink, or the duration of inking. This reinforces the idea that the stamp is limited in its ability to capture the complex during inking. Two coinciding factors contribute to this limit. First, the solubility of the Pd²⁺ compound in the PDMS stamp is poor. In contrast to μ CP alkanethiols on gold and Fe³⁺ on SiO₂/Si (see Chapter 5), no multiple printing is possible without reinking the stamp. No reserve of Pd²⁺ exists in the bulk of the stamp, which could progressively release Pd by diffusion. Second, the affinity between nonhydrophilized PDMS stamps and the Pd complex is very low: not enough Pd²⁺ for good ELD of Cu could be transferred when using a nonhydrophilized stamp. The hydrophilic layer on the plasma-treated stamp provides a small reservoir for the catalytic precursor. The depth of this hydrophilic layer cannot be increased noticeably with a treatment such as an O₂ plasma because the plasma apparently forms a self-passivating silicate layer on the surface of the stamp [89,91].

4.6 High-Resolution Patterning

The resolution and accuracy of Cu patterns produced by ELD and μ CP, in addition to the quality, homogeneity, and adhesion to the substrate of Cu deposits, are important criteria to evaluate the virtues of this technique. The SEM image in Figure 4.8(a) demonstrates that microcontact printing of the Pd²⁺ catalyst precursor can lead to Cu structures with a line width of 170 nm when high-resolution stamps provide the

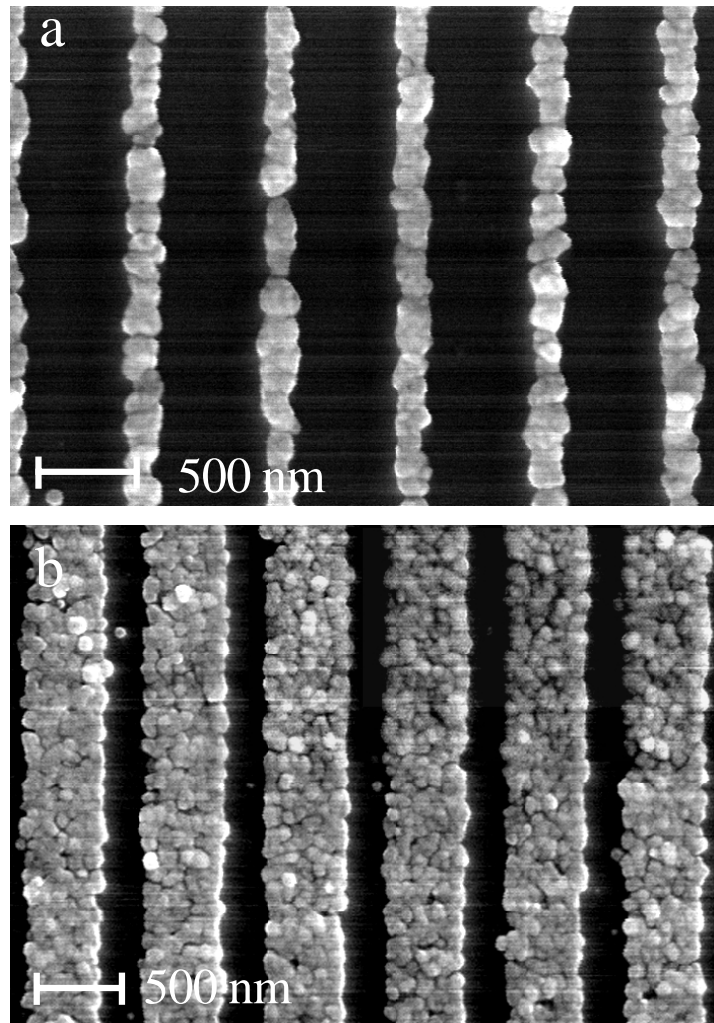


Figure 4.8: Scanning electron microscope images of electroless Cu deposits at an early stage over a high-resolution microcontact print of $[(\text{CH}_3-(\text{CH}_2)_{16}-\text{CN})_2\text{PdCl}_2]$ onto a Ti-coated SiO_2/Si wafer. In both cases, the Cu lines match with accuracy and contrast the (A) 170 nm and (B) 500 nm wide lines that were present on the stamps used here.

pattern [178]. The size of the Cu grains is between 80 and 120 nm in width and thickness. The very high contrast indicates that no catalyst has diffused away from the zones of print and that ELD of Cu remained confined to the catalytic areas of the substrate. We found in general that optimization of the concentration of the Pd^{2+} complex in the ink and of the duration of the print was less important than when printing eicosanethiol on gold, suggesting that the Pd ink had little diffusion on the substrate during printing. Cu grains of 170 nm seem to be continuously connected and form the lines in these samples. It is equally possible to form 170 nm nonplated gaps with high resolution and contrast, Figure 4.8(b). There, the distribution of the Cu grains in the 500 nm lines suggest that the catalyst pattern underneath is homogeneous. The thickness of the Cu structures in both images is ~ 100 nm. It is difficult in these experiments, however, to deconvolute the influence of the plating conditions (strength, stirring, temperature, and

stability of the bath) on the highest achievable resolution of μ CP for Cu ELD, but the particle grain size of Cu can range, in the limit, between 5 and 200 nm for deposits on activated surfaces [69]. In choosing an appropriate Cu bath, a minimal line width of about 30–50 nm may be achievable.

4.7 Conclusions

Microcontact printing a catalyst onto a substrate to initiate selective ELD of Cu is a challenge because it requires that this contact patterning technique be used in a markedly different way than for microcontact printing alkanethiols on gold. This raises such questions as, what is the surface chemistry for the chemically relatively inert PDMS stamps in the former case? How can one compose the catalytic ink for ELD? How can one attach the catalyst firmly to the substrate during the printing step, and what is its catalytic state? ELD of Cu itself contributes to some of these challenges by being a technique that is difficult to understand in detail. Hidber et al. boldly opened the exploratory route paved with these questions [176, 177]. Our use of microcontact printing combined with ELD of metals extends the work of these authors to a different paradigm. We relied on surface chemistry to control the operations necessary for good printing of a catalyst and satisfactory electroless plating. The catalyst used here is a molecular complex and can be inked with stamp-compatible solvents such as ethanol onto a hydrophilic stamp. The stamp is not yet permanently hydrophilic and the ink only contains a catalyst precursor, which can be reduced to a catalytic active state and fixed to the substrate during the printing on a Ti-coated surface. Surface chemistry here again ensures that ELD of Cu proves satisfactory in terms of the amount plated on the surface and the resolution and contrast of the Cu pattern on the surface.

Our method has great potential for many different applications where a patterned catalyst is needed, but will require detailed characterization. One of the most important pending issues will be to elaborate an alternative to the Ti evaporation for substrate activation based on wet chemistry. Chemical control over the surface composition of the stamps should help to achieve better inking schemes with other catalyst precursors. Optimization of the plating conditions will be equally important to improve the quality of plated patterns. Finally, these issues all together should lead to adhesive, homogeneous and conductive Cu ELD patterns. Printing high-resolution patterns of catalysts with our method will be important to evaluate the accuracy and contrast characteristics of this technique and will be important for future technological applications.

Chapter 5

Patterned Growth of Carbon Nanotubes

Regarding the recently investigated types of catalysts for the catalytic growth of carbon nanotubes makes it obvious that microcontact printing (μ CP) of catalyst precursors (see Chapter 4) could be a very simple way to pattern substrates with carbon nanotubes. The current chapter elucidates some important aspects when μ CP is used to pattern silicon substrates with catalysts followed by the growth of carbon nanotubes on the activated regions.

5.1 Introduction

The enormous increase of portable electronic devices (personal computers, telecommunication systems, etc.) in everyday life increased the demand to display information in a convenient way. Up to now, backlit active-matrix liquid-crystal displays (LCD's) are most commonly used. The performance of this type of display is far from being ideal. LCD's suffer from a bad viewing angle, relatively high power consumption due to a bad optical efficiency, and high production cost.

One possible future display technology is based on the field emission of electrons (see Chapter 2). The working principle of the so-called field emission displays (FED's) is based on the fact that each pixel has its own electron source, allowing a flat geometry of the device. To obtain a stable electron emission each pixel consists of several hundreds of emitters. The failure of a few of them is not critical for the operation of the screen. FED's can deliver high brightness images with a large viewing angle at low power consumption and over a wide temperature range.

As mentioned in Chapter 2 carbon nanotubes are very efficient electron field emitters. In this Chapter we combine pyrolysis of acetylene with μ CP to produce samples patterned with films of multiwall carbon nanotubes. μ CP is used to transfer a Fe^{3+} containing gel-like catalyst precursor from a hydrophilized elastomeric stamp to a substrate, Figure 5.1. The catalytic pattern activates the growth of multiwall carbon nanotubes

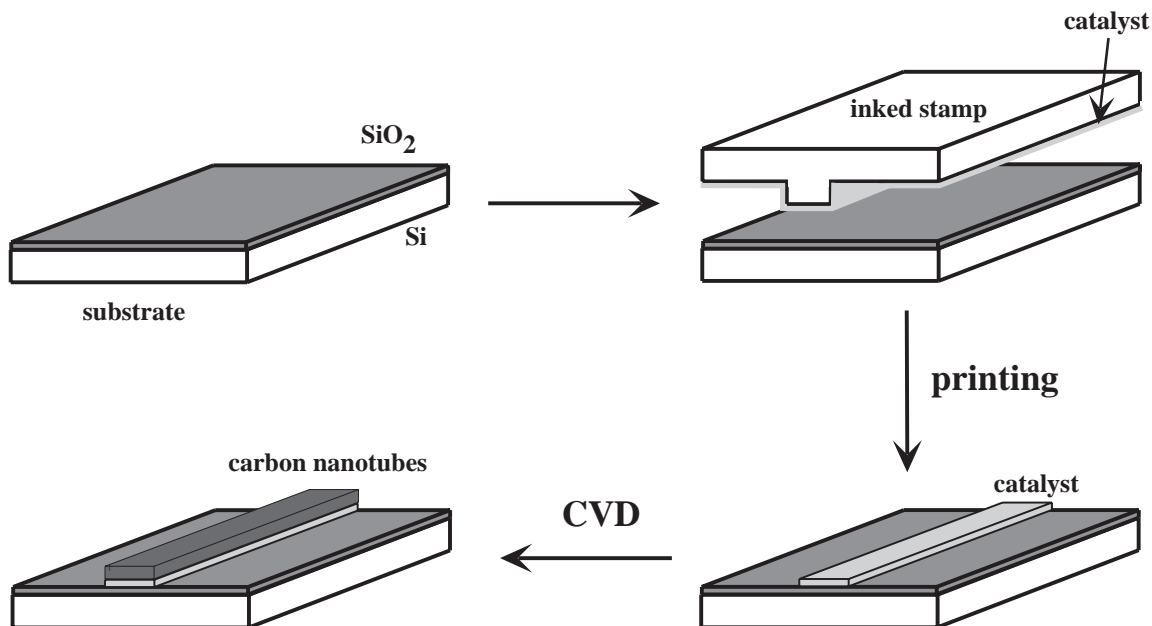


Figure 5.1: Procedure for the patterned growth of carbon nanotubes by microcontact printing a Fe^{3+} -based catalyst precursor onto silicon wafers. The stamp is inked with an ethanolic solution of Fe^{3+} first and then printed onto the substrate. The growth of carbon nanotubes proceeds by the catalytic decomposition of acetylene.

using chemical vapor deposition (CVD) of acetylene (C_2H_2). Our results show that the choice of the catalyst is of outmost importance. Most of the aqueous and ethanolic Fe^{3+} inks used give rise to drying effects on the stamp surface, which leads to an island formation of the catalyst within the pattern (see Chapter 4). To avoid these shortcomings we developed a catalyst precursor which has better performances on the stamp and as catalyst on the substrate. A simple aging of an ethanolic Fe^{3+} ink results in a polymerized gel-like catalyst precursor which can be printed homogeneously with an excellent contrast to the substrate. Changing the concentration of the catalyst in the ink solution allows one to tune the density of the nanotubes from single randomly oriented nanotubes to densely packed arrays of nanotubes which are oriented perpendicular to the substrate. The electron field emission properties of patterned samples are measured locally with a scanning anode field emission microscope. The emission images reproduce the grown pattern nicely and show that films of a medium density of nanotubes give rise to the highest emitter density within the features.

5.2 Experimental

Materials and Substrates

All chemicals were of purris. p.a. quality from Fluka except for the ferric acetylacetonate (Aldrich). Absolute ethanol was used as received; water was produced with a Milli-Q

Millipore purification unit. SiO₂/Si wafers (Meiningen Wafer GmbH, Meiningen, D) were used as received. All gases had a purity of at least 99.99% (Carbagas, Lausanne, CH).

Patterned poly(dimethyl)siloxane (PDMS) stamps were prepared from Sylgard 184 (Dow Corning, Midland, MI) and cured for at least 12 h at 60 °C on masters prepared by photolithography using Novalac resist and fluorinated with a monolayer of (1,1,2,2,-tetrahydroperfluorodecyl)trichlorosilane (ABCR, Karlsruhe, D) [90]. Stamps had a thickness of 4–5 mm. We used an O₂ plasma treatment of the stamps (O₂ pressure ~1 mbar load coil power ~100 W, 15 s; Technics Plasma 100E, Florence, KY) to render their surface hydrophilic prior to inking. Hydrophilized stamps were stored under water before use.

Inking and Printing

Wet inking involved placing a drop of an aqueous or ethanolic (absolute ethanol) solution containing 10 to 100 mM catalyst onto a hydrophilized stamp for 15 s. Fe(NO₃)₃·9H₂O, FeCl₃, FeCl₃·6H₂O, Ni(NO₃)₂·6H₂O, Co(NO₃)₂·6H₂O, ferrocene, or ferric acetylacetonate were used as catalyst precursors. Inks used within 2 h are referred to as “fresh” in the text while “aged” inks have been prepared more than 12 h before use. The stamp was then dried for 10 s under a continuous stream of N₂. Printing was done by placing the stamps on substrates. The time of conformal contact between stamp and substrate was 3 s. For each print we used a newly patterned stamp to prevent interference from the history of the stamp with the next print. Temperature and humidity were kept constant during the preparation and printing.

Deposition of Multiwall Carbon Nanotubes

The deposition of multiwall carbon nanotubes was carried out in a horizontal flow reactor (Figure 5.2) at a reaction temperature of typically 720 °C. The samples were mounted in the tube reactor and the system was purged with 1000 mLmin⁻¹ N₂ for 15 min before a mixture of 15 mLmin⁻¹ acetylene and 1000 mLmin⁻¹ N₂ was introduced at atmospheric pressure for 30 min. Finally the system was purged again with 1000 mLmin⁻¹ N₂ for 10 min. For experiments with other pure and mixed gases (Ar, NH₃, H₂) the total flow was kept constant.

Instrumentation

The nanotube deposits were examined using a Jeol 6300 F scanning electron microscope (SEM) operated at 5 kV. High-resolution transmission (TEM) electron micrographs were taken with a Philips CM 300 microscope operated at 300 kV. Optical inspection of the samples and stamps was carried out using an Olympus BX50 microscope. UV-VIS absorption spectra of solutions were obtained using a Shimadzu UV-260 spectrometer.

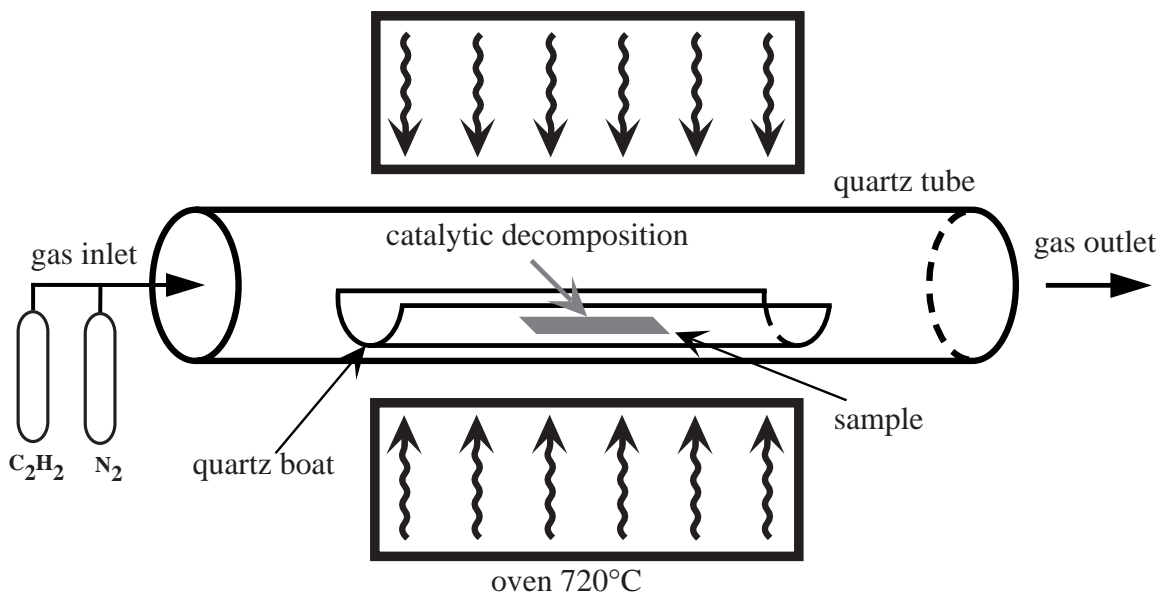


Figure 5.2: Experimental setup for the production of carbon nanotubes by catalytic decomposition of acetylene.

X-ray photoemission spectroscopy (XPS) spectra were acquired on a Perkin-Elmer Phi-5500 spectrometer operating at a base pressure of $<10^{-9}$ mbar and equipped with a monochromatized AlK_α source ($E = 1486.6$ eV). The analyzer had an angle of 45° to the sample, and samples were mounted on a multisample holder stage for examination under identical conditions. Spectra are calibrated to the C 1s peak at 285 eV. For all samples, survey spectra were acquired first with a pass energy of 90 eV, and high-resolution spectra for C 1s, O 1s, N 1s, and Fe 3p investigated were acquired in the same sequence for all samples with a pass energy of 24 eV. XPS on PDMS stamps was done with a flood gun for charge compensation of these insulating samples. For the emission experiments a scanning system was mounted in a vacuum chamber working at a pressure of $\sim 5 \times 10^{-7}$ mbar. A tip with a radius of $2\text{--}5$ μm was scanned over the surfaces with a stepping motor at a constant height of $3\text{--}6$ μm above the surface. The tip-sample bias (typically 100 V) was held constant and the current was recorded every 3 μm with a Keithley 237 source-measure unit.

5.3 Patterned Growth of Multiwall Carbon Nanotubes

Figures 5.3(a) to (d) show a typical pattern of nanotubes for a sample printed with an 40 mM Fe^{3+} ethanolic solution (aged). It is obvious that nanotubes can be patterned over large areas with a homogeneous density. The major requirement of selectivity of the printing step is fulfilled: the nanotubes are confined to the printed regions and completely absent between the structures. A slight broadening ($\sim 1\text{--}2$ μm) of the structures

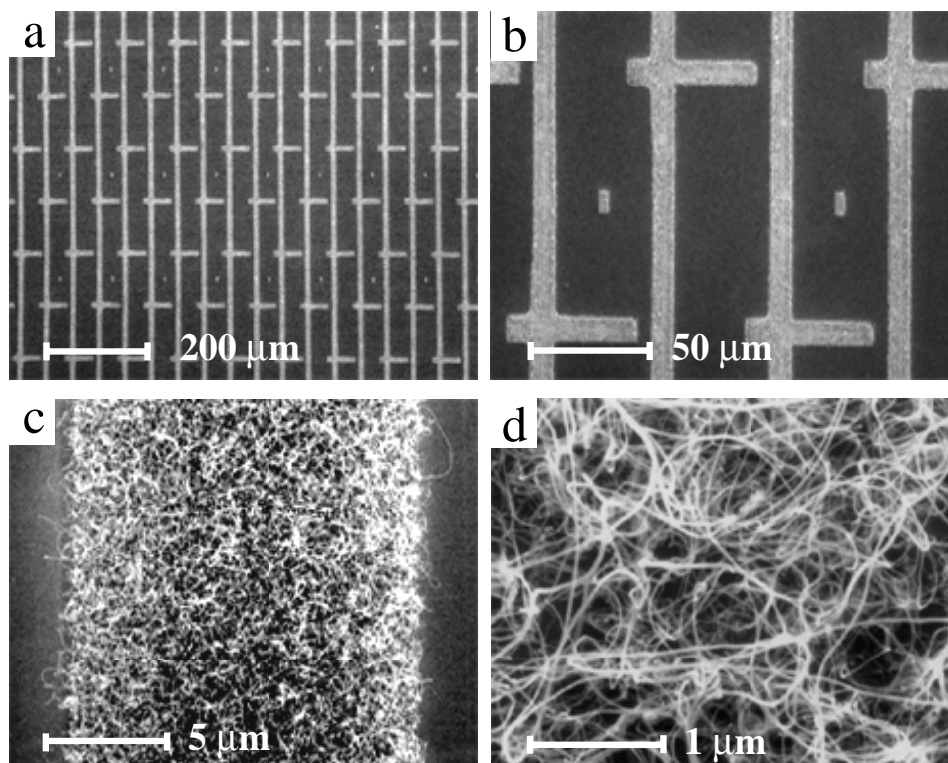


Figure 5.3: Scanning electron microscope images of a surface patterned with carbon nanotubes showing the homogeneity and selectivity of the method to printing a Fe^{3+} catalyst precursor for the decomposition of acetylene.

occurred after the deposition since some nanotubes stand partially out of the structures. The proportion of nanotubes in the deposit is very high, reaching almost 100%. Other carbon allotropes were almost completely suppressed in the film. This is surprising since multiwall carbon nanotubes produced by catalytic decomposition of hydrocarbons usually are present in much lower proportions [118,188]. In the following we will discuss in detail the contributions of the single fabrication parameters on the quality of the resulting patterns of carbon nanotubes.

5.4 The Catalytic Ink

As seen in Chapter 4 inking a PDMS stamp with catalyst precursors for μCP is a challenge. First, the number of useful solvents is restricted to water and ethanol; other organic solvents often interfere with the chemical and topological integrity of the stamp (toluene, acetone, acetonitrile, hexane, etc) which leads to a swelling of the PDMS surface and finally to the breakdown of the homogeneous conformal contact between substrate and stamp. Second, the catalyst precursor must be soluble in the solvent in sufficient concentrations and be stable for more than a few hours. The third issue is related to the affinity of the catalyst to the stamp surface. We have seen in Chapters 2 and 4 that hydrophilization of the PDMS surface using an O_2 plasma [89,91] is an imper-

	Solvent	Color of Ink	Morphology of the Pattern of Nanotubes
Fe(NO ₃) ₃ ·9H ₂ O	H ₂ O	yellow	islands
	EtOH	dark reddish-brown	homogeneous pattern
FeCl ₃ ·6H ₂ O	H ₂ O	yellow	islands
	EtOH	yellow	islands
FeCl ₃	H ₂ O	yellow	islands
	EtOH	yellow	islands and diffuse background

Table 5.1: Influence of different catalyst precursors (40 mM aged for at least 12 hours before use) and solvents on the morphology of the patterns.

ative step for printing catalysts. All our attempts to print catalysts with hydrophobic PDMS stamps failed. Fourth, the stamp must be loaded with catalyst homogeneously over the complete surface. For this reason the removal of excess ink (by drying the stamp under a stream of N₂ or by spincoating) after the impregnation with catalyst should not allow the formation of drying traces or the crystallization of the catalyst. Finally, the transfer of the catalyst precursor to the substrate must be sufficient and homogeneous.

In order to evaluate the best catalytic ink, we performed a series of experiments with different transition metal salts. Table 5.1 reveals the catalyst precursors printed on SiO₂/Si wafers followed by our standard CVD deposition. As stressed out in Figure 5.4, the assembly of these catalysts gives rise to three phenomena: (a) Fe(NO₃)₃·9H₂O dissolved in ethanol is the only catalyst which results in a homogeneous film of carbon nanotubes, Figure 5.4(a). (b) All other metal salts dissolved in water or ethanol (except ethanolic FeCl₃) give rise to patterns consisting of islands with a high density of carbon nanotubes, surrounded by a film of lower density, Figure 5.4(b). In this case, however, the carbon nanotubes are strictly confined to the lines of the pattern and absent from the adjacent regions. (c) SEM images of samples activated with ethanolic FeCl₃ show substrates completely covered with a diffuse background which consists of small particles of amorphous carbon and some carbon nanotubes, Figure 5.4(c). Based on these results, we now discuss the processes involved in the ink, during inking, drying, and printing.

5.4.1 Aqueous Inks

When water is used as solvent we observe a yellow solution for all catalysts which does not change within several days. UV-VIS spectra (200 to 900 nm wavelength) of the inks in function of their age confirmed this behavior. The absence of a change towards a dark reddish-brown color indicates that there is no major formation of Fe³⁺ oxo/hydroxo-polymers¹ which is typical for the hydrolysis of Fe³⁺ [189, 190]. Printing these catalyst precursors leads to islands or droplets within the printed pattern. Since

¹The nature of the formation of such polymers is a polycondensation reaction. The terms polymerization and polycondensation are both used in literature.

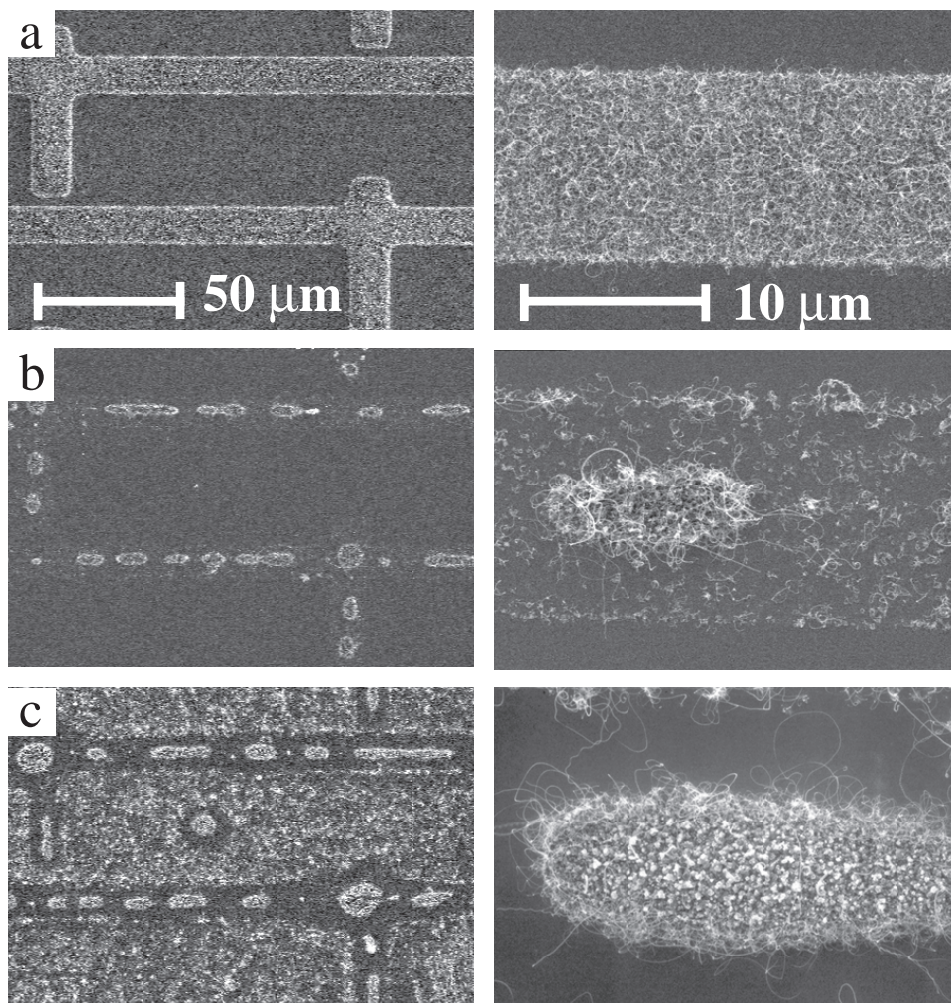


Figure 5.4: Scanning electron microscope images of a surface patterned with carbon nanotubes for 3 different ethanolic inks (all 40 mM inks were aged for at least 12 hours): (a) $\text{Fe}(\text{NO}_3)_3 \cdot 9\text{H}_2\text{O}$, (b) $\text{FeCl}_3 \cdot 6\text{H}_2\text{O}$, (c) FeCl_3 . The images show that the catalyst precursor has to be chosen carefully and that only catalyst (a) leads to a homogeneous pattern of carbon nanotubes.

we form these islands already on the stamp surface after drying but before printing (Figure 5.5), we conclude that they arise from an insufficient wetting of the stamp surface by the ink and/or a slow evaporation of the ink which leads to the formation of droplets. During the final drying of the stamp the water film starts to form droplets and the catalyst precursor is left in high concentration where these droplets dry out and in lower concentration on the rest of the pattern (see Chapter 4) [181]. This inhomogeneous pattern is then printed to the surface and finally leads to the phenomenon observed in Figure 5.4(b).

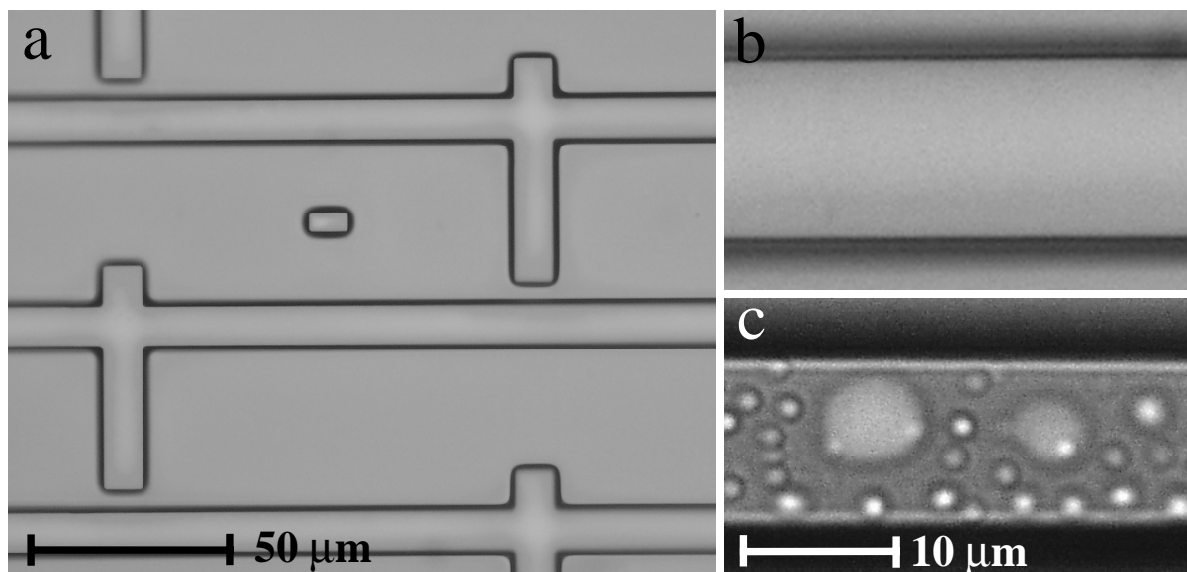


Figure 5.5: Optical images revealing the surface of patterned stamps after an O_2 plasma activation (a), after inking (and drying) with an ethanolic 40 mM $Fe(NO_3)_3 \cdot 9H_2O$ ink (b), and after inking (and drying) with an aqueous 40 mM $Fe(NO_3)_3 \cdot 9H_2O$ ink (c). The islands are formed on the stamp surface during the drying under N_2 . Other inks which lead to island formation are listed in table 5.1.

5.4.2 Ethanolic Inks

In order to suppress island formation during the drying, we performed experiments using ethanol as solvent. Ethanol has a higher vapor pressure than water and allows in addition a better wetting of the hydrophilic stamp surface. We expected that it dries without leaving any drying traces on the stamp. The choice of the three catalysts given in Table 5.1 allows to check two different important parameters without affecting the rest of the ink: the influence of crystal water and the type of ligands of the transition metal salt.

Influence of Crystal Water

The difference of the carbon deposit after printing with either nonhydrated or hexahydrated ethanolic $FeCl_3$ is substantial². Printing the hydrated chloride complex results in the formation of islands while printing the nonhydrated catalyst produces in addition a diffuse background over the entire sample surface (compare Figures 5.4(b) and (c)). Both catalyst solutions are yellow when prepared and do not change their color during weeks. This was confirmed by UV-VIS measurements which reveal the same time-independent spectrum for both catalysts. Regarding the stability of the solutions we assume that there is again no major hydrolysis for both chloride catalysts. For nonhydrated $FeCl_3$ dissolved in ethanol this is in agreement with earlier results which

²If $FeCl_3$ is dissolved in absolute ethanol Fe^{3+} ions are complexed by 6 Cl^- . Dissolving $FeCl_3 \cdot 6H_2O$ in ethanol, however, leads to Fe^{3+} with H_2O and Cl^- as ligands.

proved that FeCl_3 is in its monomeric state [191]. Optical images of the printed patterns of the two catalysts show the same image: the lines are decorated with islands but regions between the lines are completely free of material. We believe that in the case of the hydrated catalyst the crystal water gives rise to some hydrolysis during the drying of the stamp [181]. Evaporating the ethanol increases the relative amount of water in the ink and forces the formation of bigger Fe^{3+} oxo/hydroxo-aggregates which –printed to the substrate– might be too large to diffuse on the surface during the 15 min of annealing at 720 °C. For the nonhydrated catalyst the polymerization during the drying is strongly suppressed and the monomers or small aggregates can diffuse on the surface and produce the observed background.

Influence of Ligands

Catalysts with different ligands cause a completely different pattern of carbon nanotubes. Replacing the chloride ligands with nitrate ligands leads to a solution which turns from reddish-brown to dark reddish-brown within 12 hours. It is known that this change of color is due to the hydrolysis of Fe^{3+} [189, 190]. The nitrate ligands from $\text{Fe}(\text{NO}_3)_3 \cdot 9\text{H}_2\text{O}$ are completely lost and hexaaquo complexes are formed. They readily undergo polycondensation reactions and a gel-like polymer is produced³. In turn, the nitrate-containing ink can be printed homogeneously on the substrate and catalyzes the growth of a high-quality patterned film of multiwall carbon nanotubes, as shown in Figure 5.4(a).

Increasing the amount of water in the ethanolic nitrate ink (these inks showed a dark brown precipitate after a few hours) was accompanied by the occurrence of island formation on the stamp during printing. In fact, the UV-VIS spectrum does only change little on adding some extra water, which indicates that the island formation in this case is mainly due to a drying effect and/or a change of the wetting behavior caused by the extra water and not due to a dramatic change of the chemistry of the catalyst.

Since $\text{Fe}(\text{NO}_3)_3 \cdot 9\text{H}_2\text{O}$ dissolved in ethanol is the only catalyst resulting in homogeneous patterns we always used this type of ink for the following experiments.

Influence of Aging

The change of the color of the nitrate catalyst in ethanol to dark reddish-brown occurs in a few hours. However, the time needed to obtain a stable solution as well as the final degree of hydrolysis strongly depends on the ambient temperature and humidity, which should be kept constant. Printing freshly prepared nitrate catalysts resulted always in the formation of inhomogeneous patterns, as shown in Figure 5.6. We suppose that the degree of polymerization of freshly prepared catalyst precursor solutions is too low. As a consequence a bad wetting of the stamp by the ink and/or an insufficient drying behavior of the ink on the stamp leads to the formation of inhomogeneous patterns.

³In solutions containing Cl^- instead of NO_3^{2-} , Fe^{3+} is coordinated by H_2O and Cl^- and we suppose that the presence of Cl^- inhibits a successful polycondensation.

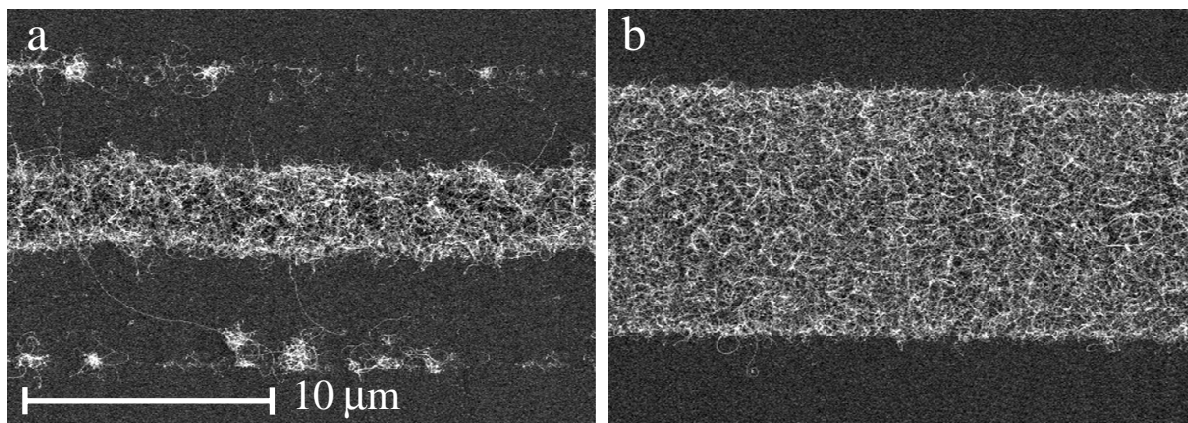


Figure 5.6: SEM images of the features covering the pattern after the deposition when printed (a) with a fresh and (b) with an aged 40 mM $\text{Fe}(\text{NO}_3)_3 \cdot 9\text{H}_2\text{O}$ ethanolic ink.

Multiple Printing

We observed that successful printing without reinking the stamp can be repeated up to 4 times, indicating that the quantity of catalyst on the stamp is high. Semi-quantitative XPS measurements of the amount of Fe^{3+} on the stamp before and after printing confirmed this fact and showed that only a part of the catalyst is transferred to the substrate during each print. This is in contrast with the Pd^{2+} catalyst used for the ELD of Cu (see Chapter 4), where printing can be executed only once. These results are a further indication that our Fe^{3+} catalyst is present in a polymerized gel-like form on the stamp. Two additional factors support this interpretation. First, the solubility of Fe^{3+} compounds in the PDMS stamp is poor. No reserve of Fe^{3+} exists in the bulk of the stamp, which could progressively release catalyst by diffusion. Second, the affinity between hydrophobic stamps and Fe^{3+} is very low: printing Fe^{3+} with hydrophobic stamps always failed. The hydrophilic layer on the plasma-treated stamp provides only a small reservoir for the catalyst and cannot be increased by a longer O_2 plasma treatment [89,91].

The fact that stamps can be loaded with important amounts of the Fe^{3+} catalysts can be used to contact-ink patterned stamps from preinked flat stamps [192]. In this case a flat stamp is inked first before a second patterned stamp is brought into contact to pick up the catalyst. This inking process gives another possibility to control the amount of catalyst to be printed since during contact inking less than 50% of the material is transferred from the flat stamp to the patterned one. Contact inking is therefore very suitable to print low density patterns of catalysts without changing the chemistry of the ink solution (the degree of hydrolysis of Fe^{3+} depends on the concentration of the dissolved metal salt).

Influence of N_2 Annealing

XPS experiments of the printed catalyst before and after 15 min of annealing in N_2 indicate several interesting facts. The N 1s peak at 407 eV from the nitrate ligands is

found before the annealing but completely disappears during the heating at 720 °C. At this temperature the nitrate ligands are fully evaporated from the catalytic material. No change in the Fe 3p peak at 710.8 eV from Fe³⁺ typical for Fe³⁺ oxides could be observed after the annealing. The appearance of a small shoulder at 530 eV in the region of the O 1s peak indicates the formation of Fe-O-Fe bonds during the heating which can be attributed to Fe₂O₃ [193,194]. Taking into account these results, we propose the following process: the printed catalyst consists of a gel-like material of partially hydrolyzed Fe³⁺ nitrate, during the heating the nitrate ligands are evaporated, and Fe₂O₃ is formed.

Summary

In light of all these experimental results (influence of crystal water, ligands, aging, etc.) we conclude that the success of using an aged ethanolic solution of Fe(NO₃)₃·9H₂O for μCP is based on the following ⁴: the nitrate ligands allow the hydrolysis of Fe³⁺ with the crystal water, the limited amount of crystal water stops the polymerization after a few hours, the polymers are large but still soluble in ethanol, drying of the catalyst on the stamp is improved because the gel-like catalyst [190,195] forms a porous but uniform film, and finally most of the crystal water is incorporated in the polymer during the hydrolysis and cannot induce an island formation during the drying step.

5.5 Morphology of the Carbon Nanotubes

The investigation of methods to pattern substrates with carbon nanotubes was motivated by the strong interest in their physical properties and possible applications (for example, as cold electron emitters) [101,102,104,196,197]. So far, several groups have shown different methods for the patterning of substrates with catalysts. It turned out that these methods are successful in producing homogeneous patterns of different types of carbon nanotubes (singlewall, multiwall, and fibers) depending on the catalyst and the deposition parameters [110,120,125,126,198]. However, none of these methods was able to vary the density of the carbon nanotubes within the deposited structures in a controlled way. This is a serious drawback since the emission properties of arrays of field emitters strongly depend on their local density.

⁴In addition to Fe(NO₃)₃·9H₂O we tried to use Co(NO₃)₂·6H₂O and Ni(NO₃)₂·6H₂O as catalyst precursors. UV-VIS measurements and observation of the color showed that no aging occurs for Co²⁺ and Ni²⁺. Therefore, it is not surprising that these catalysts dissolved in water and ethanol formed islands on the stamp upon drying. We tried to print ferrocene and ferric acetylacetonate dissolved in ethanol using either hydrophobic or hydrophilic stamps. We never succeeded in any deposition of carbon on samples patterned with these catalyst precursors which is probably due to the fact that the ligand exchange with H₂O is inhibited and hence also the polycondensation.

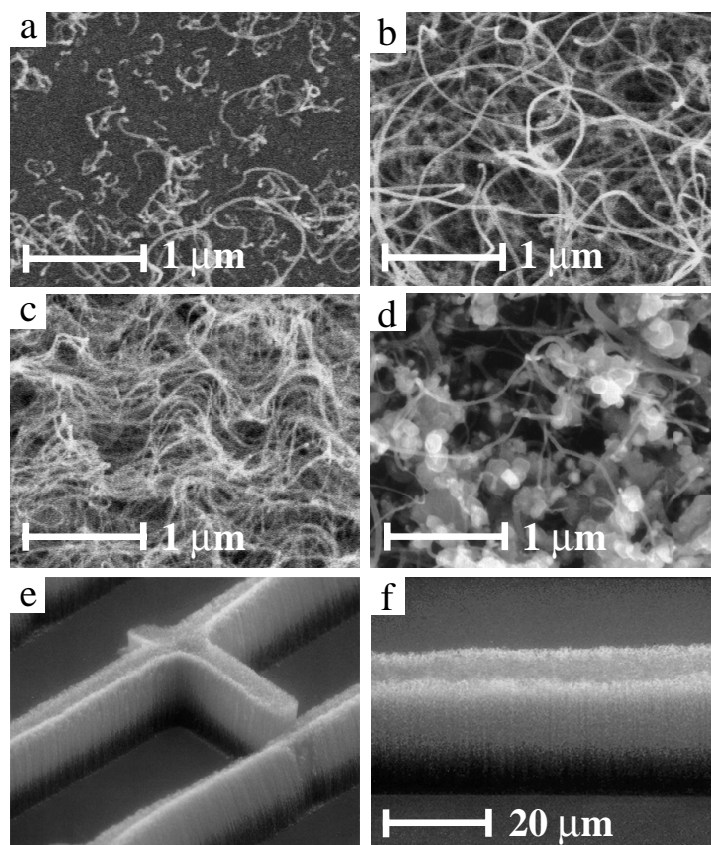


Figure 5.7: Dependence of the patterned film of carbon nanotubes on the concentration of the printed catalyst (dissolved in ethanol and aged): (a) 10 mM, (b) 25 mM, (c) 40 mM, (d) 70 mM, and (e), (f) 50 mM $\text{Fe}(\text{NO}_3)_3 \cdot 9\text{H}_2\text{O}$. Images (e) and (f) show structures of aligned nanotubes grown perpendicular to the surface.

Influence of the Ink Concentration

One of the advantages of microcontact printing catalysts is in fact the possibility to tune the density of the carbon nanotubes in the printed pattern. This can easily be achieved by changing the density of the catalyst in the ink solution. Figure 5.7 shows the influence of the catalyst concentration on the topography of the deposited film.

Increasing the concentration from 10–40 mM is accompanied by a similar increase of the density of the deposited nanotubes, Figures 5.7(a) to (c). For low concentrations (10 mM) only a few single nanotubes are randomly distributed over the printed zones. Increasing the concentration of the catalyst to 20–40 mM is accompanied by the formation of a film of entangled nanotubes. Finally, using a concentration around 50 mM results in arrays of nanotubes aligned perpendicularly to the surface (see Figures 5.7(e) and (f)), similar to aligned assemblies of nanotubes found by other groups [120–123,198,199]. The side walls are flat and no tubes are branching away. High-magnification SEM images reveal that the top of the “towers” are smooth without protruding nanotubes. The transition from an entangled film obtained by using a low ink concentration to a well aligned film of carbon nanotubes for high ink concentrations is due to a change of the

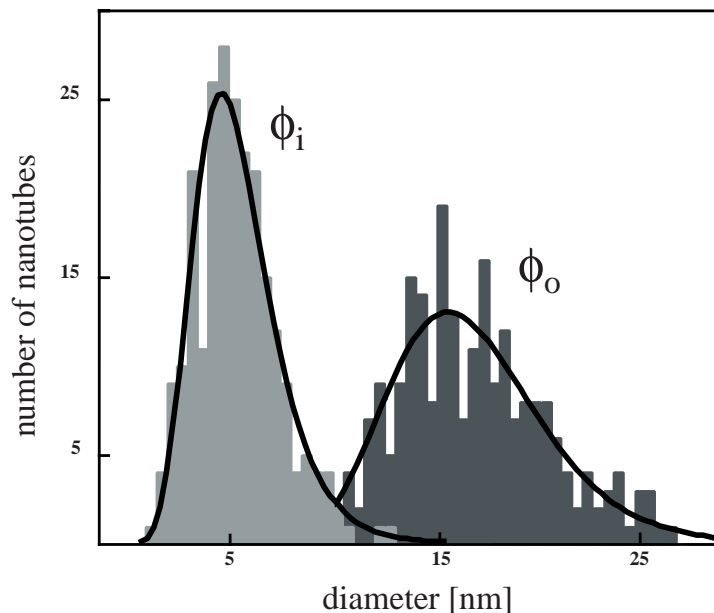


Figure 5.8: The size distributions of the inner and outer diameter (Φ_i , Φ_o) of the multiwall carbon nanotubes do not show any dependence either on the ink concentration or the annealing time of the catalyst precursor. Plotted lines are log-normal fits of the data and should help as guide for the eyes. Typically the diameters of 400 tubes are evaluated for the size distributions.

nucleation density of the catalyst particles. If the nucleation density is low, nanotubes have a large volume where they can grow and a strongly entangled film is formed. For high nucleation densities the situation is different. Nanotubes grow from the nucleation centers and are forced to extend along the direction normal to the substrate because neighboring nanotubes force them to grow in one direction. As the tubes lengthen, they interact with their neighbors via van der Waals forces to form bundles. The attractive force is such that even the outermost nanotubes are held to the tower without branching away.

For concentrations higher than about 60 mM, the growth of nanotubes is almost inhibited and the pattern is decorated by particles of carbon, Figure 5.7(d). This result stresses the importance of the catalyst concentration: printing too much catalyst leads to the growth of carbon grains instead of nanotubes. We believe that this is due to a too large nucleation density on the substrate. In this case acetylene is decomposed at so many centers that the deposited carbon nuclei coalesce and form grains. We should keep in mind that there is a threshold density –given by the outer diameter of the carbon nanotubes– which determines the maximal number of tubes per surface area. If the nucleation density of carbon is higher than this threshold, a carbon film will be formed.

To evaluate the influence of the ink concentration on the inner and outer diameter (Φ_i , Φ_o) of the multiwall carbon nanotubes, we determined the diameters for samples printed with inks of different concentrations from TEM measurements. Printing concentrations of 15, 30, and 45 mM results in tubes with an inner diameter Φ_i of ~ 5.3 nm and an outer diameter Φ_o of ~ 15.4 nm. An obvious trend towards larger Φ_i for higher

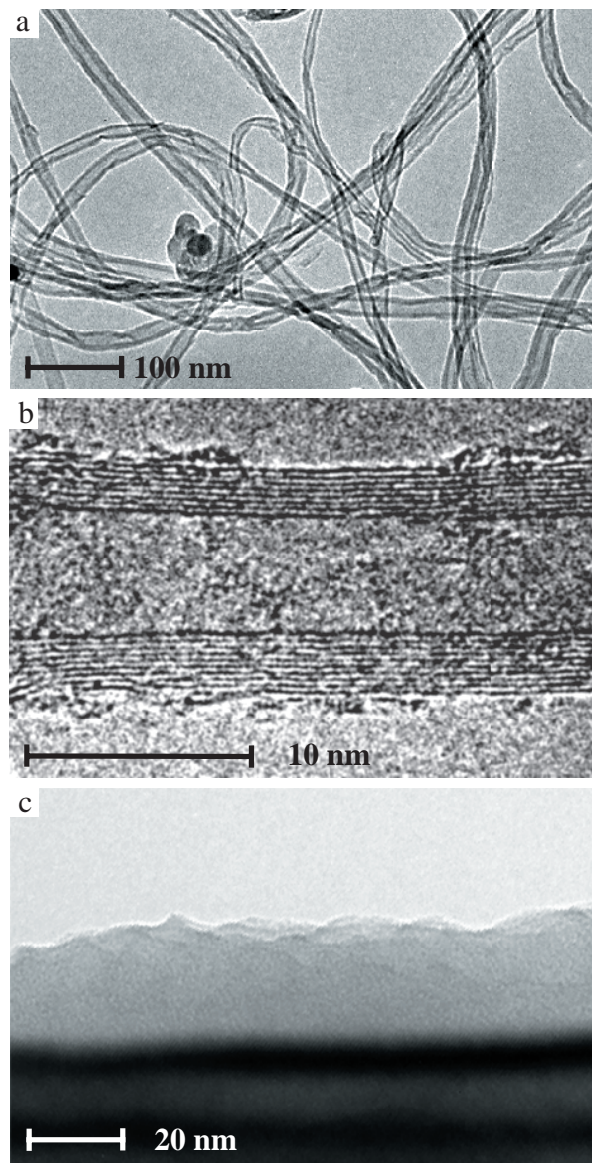


Figure 5.9: Transmission electron microscopy images showing (a) the structure of the deposited film of multiwall carbon nanotubes (without any purification) and (b) an individual multiwall nanotube. (c) TEM image of the cross-section through a printed and annealed film of catalyst at the border of a thin substrate revealing the amorphous nature of the catalyst.

concentrations is absent. The histogram in Figure 5.8 shows a typical size distribution of the diameters. The maxima of the Φ_i distributions for all three ink concentrations is located within ± 0.5 nm around 5.3 nm while the values of Φ_o are spread ± 3.2 nm around 15.4 nm. We attribute the larger variation of Φ_o to slightly different amounts of acetylene arriving at different positions in our reactor and not to an effect from the catalyst.

Quality of the Multiwall Carbon Nanotubes

Figures 5.9(a) and (b) show TEM images of the structure of the carbon nanotubes. They reveal the typical structure of multiwall carbon nanotubes produced by catalytic decomposition: well-graphitized walls, aligned with the tube axis, covered with some amorphous carbon, and some defects. These images show the high selectivity of the deposition process: the catalytic decomposition of acetylene over the catalytic pattern leads almost exclusively to the growth of carbon nanotubes. Most of the other methods to produce carbon nanotubes are followed by time consuming purification procedures.

Influence of N₂ Annealing Time

To examine the influence of the N₂ annealing time –which could change the size and topography of the catalyst– on the carbon nanotubes, we measured their diameters for samples printed with 40 mM ink but annealed for 0, 15 and 30 minutes under N₂. The results reveal that the annealing time at 720 °C has no influence on the diameters. Φ_i and Φ_o for all three annealing times exhibit size distributions which are very similar to the one shown in Figure 5.8. TEM measurements of the printed ink at the border of a thin sample⁵, presented in Figure 5.9(c), show that the annealed ink forms a compact amorphous film with a surface roughness of a few nanometers. Particles cannot be resolved in this material. Hence, such particles must be smaller than 1 nm or absent. The annealing of the printed catalysts (gel-like polymer containing Fe³⁺ oxo/hydroxo-species and ethanol) is probably fast and leads for all samples to a similar topography of the catalytic film, independent of the annealing time. We conclude from these results that there is no correlation between catalyst particles –which we could not find in the printed catalyst– and the diameters of the nanotubes.

Influence of Substrate

The choice of an appropriate substrate is critical. Besides printing on the native oxide of silicon wafers, we printed on quartz, HOPG, and nanoporous silicon. Glass shows the same behavior as silicon wafers and could easily be patterned with nanotubes. In contrast, printing on HOPG results in patterns decorated with islands of amorphous carbon decorated with very few nanotubes, as shown in Figure 5.10. Apparently, the surface free energy and chemical nature of the HOPG surface has an important influence on the behavior of the catalyst. It is not clear so far if the failure of a homogeneous patterning occurs during the printing or annealing. This point needs further investigation. Printing on nanoporous silicon is not successful neither. The effective surface which is in contact with the stamp during the printing step is much smaller than on a

⁵The printed ink was characterized by mounting a thin cleaved sample on a TEM grid with the electron beam at an angle of 45° incidence to the substrate surface. Measurements were performed at the edge of the substrate surface. The method used here is described in reference [200].

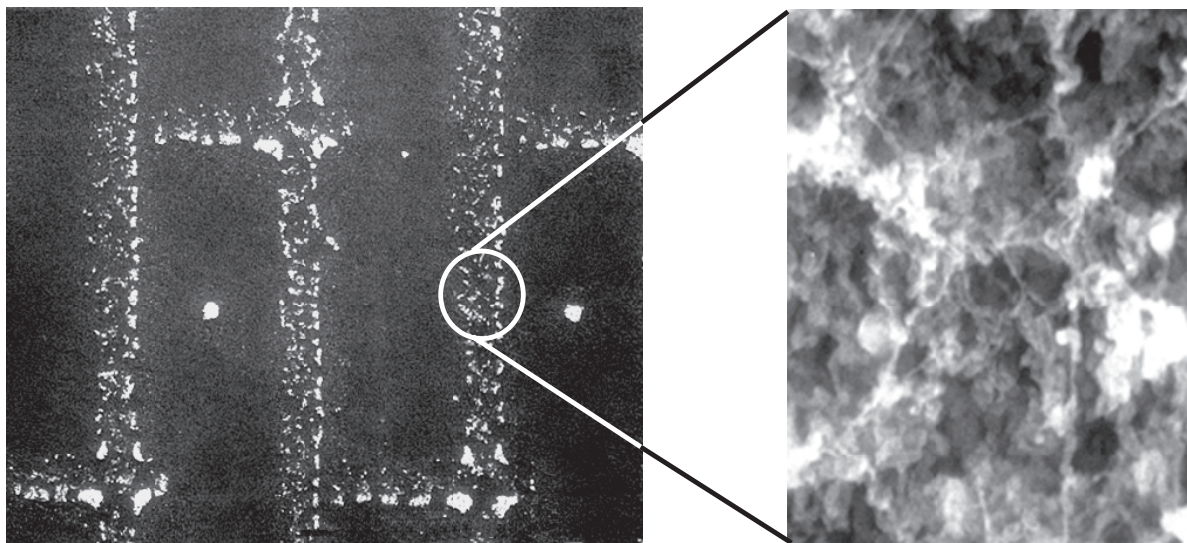


Figure 5.10: The SEM images reveal the morphology of an amorphous carbon deposit when HOPG is used as the substrate. On the amorphous islands some carbon nanotubes can still be found.

flat surface. In turn, very little catalyst is transferred to the substrate, and finally only a few nanotubes can be found after the deposition with acetylene.

Influence of the Deposition Parameters

In order to obtain an estimate of the importance of the different deposition parameters on the morphology of the carbon nanotubes, a series of different depositions were carried out: no strong influence on the temperature was visible by SEM in the region between 650 °C and 800 °C. The multiwall carbon nanotubes always show a similar morphology. Decreasing the deposition temperature to 620 °C resulted in an inhibition of the growth of the nanotubes. Apparently the minimal temperature for the production of nanotubes is around 630 °C for our deposition system. Increasing the temperature to more than 800 °C is accompanied by an increased deposition of particles of amorphous carbon within the film and on the walls of the nanotubes.

Figure 5.11 shows the influence of the deposition atmosphere on the morphology of the carbon nanotubes. Using Ar or a 10/90 v% mixture of NH₃ and N₂ as carrier gas changes the morphology of the carbon nanotubes: the deposited films are more entangled, the length of uncurved regions of the nanotubes decreases, and a larger amount of amorphous particles is found. Reduction of the printed catalyst precursor (Fe³⁺) in H₂ before the standard deposition is started leads to a similar appearance. All these different gas treatments result in tubes of slightly smaller dimensions ($\Phi_i \sim 3.2$ nm and $\Phi_o \sim 11.6$ nm) compared to the tubes produced in a standard deposition with pure N₂. We think that this is due to a different behavior of the printed ink during the annealing in the various gases. Nevertheless, the best quality of the carbon nanotubes is obtained when N₂ without NH₃ is used as carrier gas and when the catalyst is not

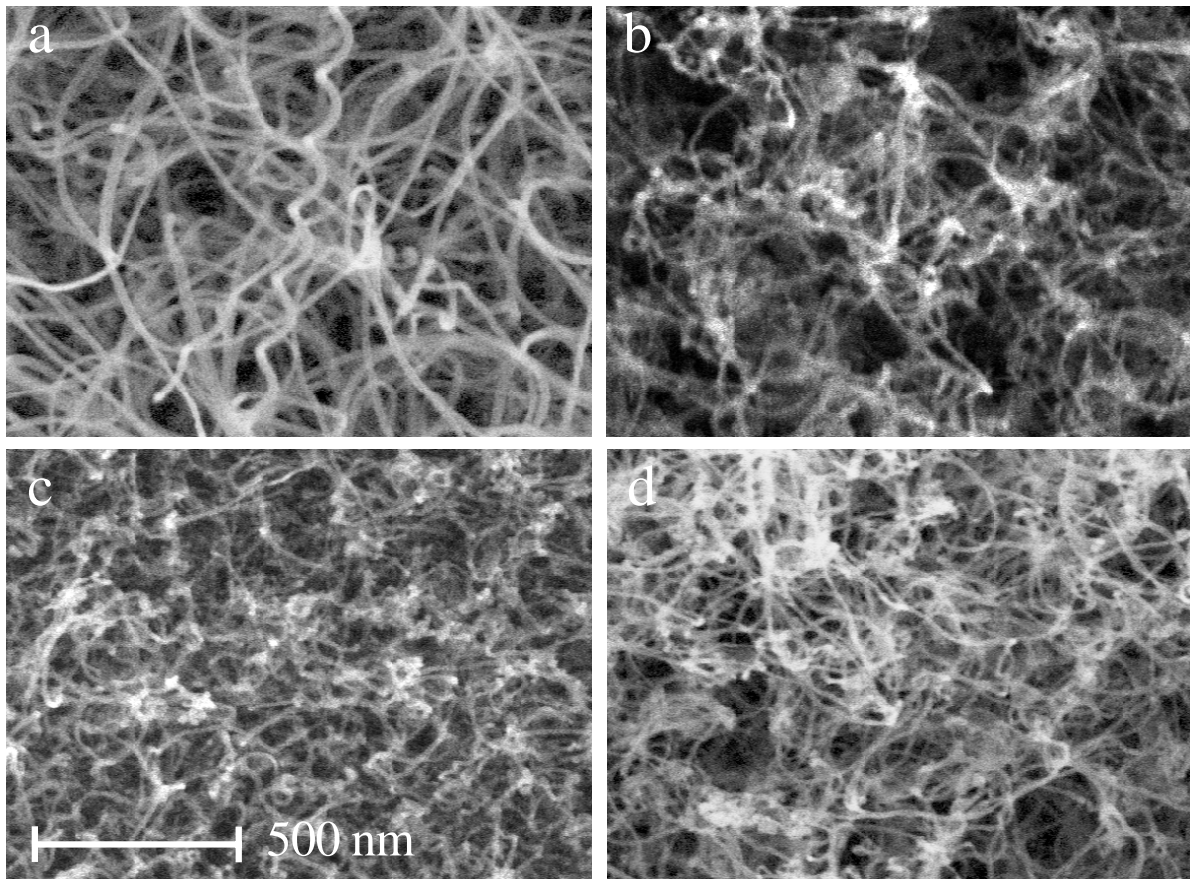


Figure 5.11: Influence of the deposition atmosphere on the morphology of the carbon nanotubes. The carrier gases used were (a) N_2 (standard deposition), (b) Ar, and (c) a 10/90 v% mixture of NH_3 and N_2 . Sample (d) was pretreated with a 10/90 v% mixture of H_2 and N_2 for 15 min before a standard deposition was carried out.

reduced in H_2 . We have not examined the influence of the other gases in detail for this reason. Taking into account these results emphasizes that the deposition parameters appear to have a weaker impact on the final film than the composition of the ink.

5.6 Electron Emission Properties of Patterned Substrates

Substrates patterned with carbon nanotubes might be used as cold electron sources for flat panel devices [101, 102, 106]. Measuring their local field emission of electrons should reproduce the pattern of nanotubes and gives a good test of the selectivity of the emission process: electrons should only be emitted from areas covered with nanotubes. Therefore, a scanning anode field emission microscope was used to measure the local emission properties of the samples. A tip with a radius of $\sim 3 \mu m$ was scanned over the sample at constant height with a constant applied voltage of typically 100 V. The

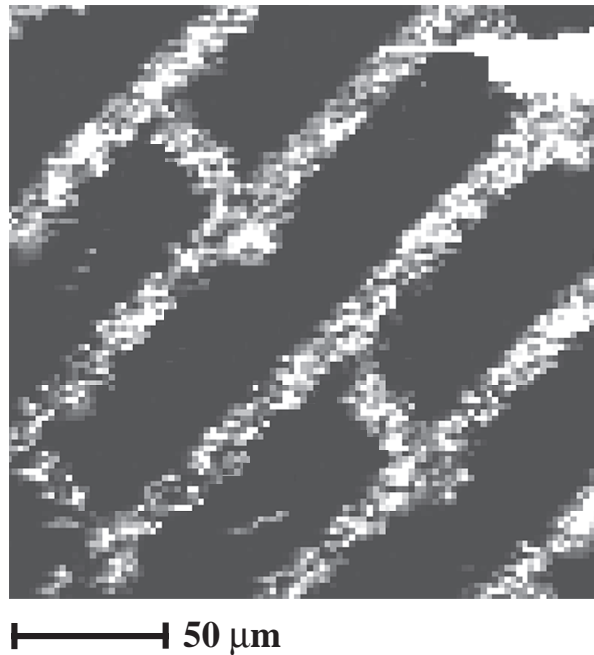


Figure 5.12: Emission image of a patterned substrate recorded with a tip scanned over the surface at a height of 5×10^{-6} m and an applied tip-sample voltage of 100 V. The intensity scale varies from no current for black pixels to maximal 10^{-2} mA/pixel for bright pixels.

resulting field emission current (up to $10 \mu\text{A}/\text{pixel}$) was acquired every $3 \mu\text{m}$ [201].

Figure 5.12 shows the emission image of a sample printed with a 20 mM concentration which corresponds to a rather low density of carbon nanotubes, similar to the one shown in Figure 5.7(b). The image nicely reproduces the lines of the printed pattern and emission of adjacent regions is strongly suppressed. Line widths are broadened ($\sim 15 \mu\text{m}$) because the emission image is a convolution of tip apex, tip-sample distance, and the height of the deposited nanotubes. In the upper right corner a bright spot appeared because one or more nanotubes branched out of the film and touched the tip during scanning.

Field emission scans on patterns of low (Figure 5.7(a)) and high (Figure 5.7(c)) density films show a decreased and rather inhomogeneous emission pattern [201]. The poor emission of high density films can be explained by an electrostatic screening provoked by neighboring nanotubes. The high density of carbon nanotubes lowers the potential drop into the film, the local electric field at the emission sites decrease, and finally the electron emission is reduced. The remaining emission is due to some tubes branching out of the pattern. Low density films give rise to a poor emission for a different reason. In this case, the nanotubes are short, bent, and not protruding out of the pattern. Only a few of them are suited for field emission. Thus the morphology of the films is indeed of crucial importance and we conclude that films of medium density of high aspect ratio tubes show optimal local field emission performance.

In addition to the local emission measurements integrated field emission over $\sim 1 \text{ cm}^2$

was investigated using a phosphor screen. The macroscopic emission of patterned samples does not reveal a significant dependence on the density of the carbon nanotubes in the films. All samples start to emit at low fields ($2\text{--}3\text{ V}\mu\text{m}^{-1}$) but the emission sites are randomly distributed over the whole surface. Emission is dominated by a small number of very strong sites while emitters with a lower field amplification factor β are not detected. This is due to the fact that the number of observed emitters depends on the size of the measured area. A macroscopic area ($\sim 1\text{ cm}^2$) will always include some very strong emitting sites ($\beta\sim 1000$), whereas a microscopic window ($\sim 10^4\ \mu\text{m}^2$) reveal many low emitting sites ($\beta\sim 100\text{--}200$) when no strong emitters are present in this particular window.

The comparison of the local and integrated emission data show that traditional I/V measurements with large area anodes are not sufficient for a proper characterization of the field emission properties of patterned samples. When our samples are measured with a large area anode, the emitters with the highest β dominate the emission. Since they represent a very small fraction of all emitters, the emission is inhomogeneous and the current densities are low. When local emission measurements are performed, the low β emitters can be recorded and much higher current densities are observed. Lars et al. found out that local current densities can be a factor 10^5 higher than the corresponding values measured by integrated methods [201].

These results show the importance to fabricate samples with an improved monodispersity of the β values. A careful control of density and morphology (and hence the β values) of the films is inevitable to obtain homogeneous high emission currents over large anodes.

5.7 Conclusions

What is the advantage to using μCP of catalysts for the patterning of substrates with carbon nanotubes by catalytic decomposition of hydrocarbons? Our results suggest that printing a gel-like polymerized catalyst is an enticing alternative to the usual lithographic techniques: the growth process leads to a carbon deposit consisting of almost 100% of multiwall carbon nanotubes, the contrast achieved is excellent and the density of nanotubes within the pattern can be tuned. PDMS, the elastomeric material used in soft lithography is fully compatible with many other wet catalysts, is cheap and can be scaled up to large areas. The choice of wet catalysts opens the possibility to investigate a new class of customer designed catalysts which give a better control over the inner and outer diameter of the nanotubes, the density of the nanotubes in the film, and their orientation on the substrate.

Chapter 6

Conclusions and Outlook

The deposition of Pd and Co nanoislands on aminothioliolate self-assembled monolayers (AT-SAMs) by electroless deposition (ELD) has been investigated by electrochemical scanning tunneling microscopy (STM). Size and density of the islands on top of the SAM can be tuned over a wide range by changing the concentration of the aminothioliolates in mixed amino-/alkanethioliolate SAMs and the concentration of O₂ in the plating solution respectively.

The results obtained represent a valuable base for the ongoing research in this field. There remain, however, some points which should be considered for future work. STM measurements always showed oligomers present on the surface. If, for example, one wants to study the magnetic properties of nanoislands in function of their size and density, the formation of oligomers must be suppressed. This might be achieved by a direct binding of metal ions to modified SAMs without an activation with a catalyst precursor. In the case that this approach fails a decreased number and size of oligomers might be achieved by simply filtering the Pd²⁺ catalyst solution or by using a different catalyst which does not tend to form oligomers.

The possibility of increasing the size and density of the islands towards a complete monolayer is necessary for a better understanding of the diffusion phenomena encountered when using small electrodes. Under careful control of the oxygen concentration in the plating bath it should be possible to observe the transition from the radial diffusion regime of oxygen (with growth inhibition) to planar diffusion (without growth inhibition). Increasing the island size and density might also be possible by repeating the deposition (with or without catalyst) several times.

The use of AT-SAMs for the fabrication of surfaces patterned with microscopic islands is problematic. AT-SAMs should not be exposed to air since the reactivity of the end groups (for example with CO₂) can cause a damage to the monolayers [202]. It would be of great advantage to use other modified SAMs which are stable in air and show an increased strength of the ligands for the metal ions. One might even find a ligand which is known to form stable complexes with the ionic *and* metallic oxidation state of the transition metal. The possibility to have a stronger and better defined interaction between the surface of the SAM and the metal particles would be interesting

for the understanding of the island formation and might change their density and size.

Having solved at least some of the above mentioned problems an object of investigation could concern the patterning of nanoislands into artificially defined patterns. Microcontact printing (μ CP) could be used to print patterns of functionalized thiolates (or alkanethiolates). In a next step, the regions between the printed regions must be filled with alkanethiolates (or functionalized thiolates) before metallic islands can be deposited.

The results presented in the second part of the work are remarkable. The comparatively simple technique of μ CP was used to pattern different substrates with catalysts with feature sizes down to ~ 170 nm. Catalyst patterns produced in this way then started different chemical reactions, in our work shown on the basis of two examples; the ELD of Cu and the growth of carbon nanotubes through pyrolysis of acetylene. It can be expected that similar routes to pattern catalysts could be interesting for other reactions in chemistry and biochemistry when patterns are required.

One of the most important requirements for a technological application of the two mentioned examples is the adhesion of the deposit (Cu and carbon nanotubes) on the substrate. This problem has been successfully solved for the ELD of Cu, but remains a challenge for the application of carbon nanotubes. By measuring the local field emission properties Larsson et al. found that increasing the emission current can lead to a complete destruction of the emitting film [203]. Since the currents through the nanotubes are not high enough to evaporate them we suppose that the breakdown occurs at the interface between substrate/catalyst and/or between catalyst/nanotube. Future work will have to find ways to improve the adhesion by a pretreatment of the substrate (to improve the interaction between substrate and catalyst), and/or a posttreatment of the deposited films (to increase the interaction between nanotubes and catalyst, and substrate respectively), or by the development of a new catalyst material.

Although there is an increasing number of examples where soft lithography (SL) has demonstrated its power, it cannot be expected to replace photolithography which will continue as the dominant technology in microfabrication of semiconductor devices and many other systems for the near future. There are, however, applications that take advantage (or require) the properties of these soft techniques. The fact that SL is less developed than the conventional photo-, electron-, or ion-beam lithography offers more opportunities for unexpected innovations. The rising success of SL indicates that it has the potential to become an important addition to the field of micro- and nanofabrication. A combination of high-precision writing of masters with low cost replication of these masters seems to provide the most practical protocol for manufacturing: high-resolution, high-cost fabrication techniques can be used to make masters; these structures can then be replicated in a low cost process to other materials such as PDMS.

Bibliography

- [1] G. Wallraff and W. Hinsberg, Chem. Rev. **99**, 1801 (1999).
- [2] D. Eigler and E. Schweizer, Nature **344**, 524 (1990).
- [3] G. Binnig, H. Rohrer, C. Gerber, and E. Weibel, Phys. Rev. Lett. **49**, 57 (1982).
- [4] A. Ulman, *An Introduction to Ultrathin Organic Films. From Langmuir-Blodgett to Self-Assembly* (Academic Press, San Diego, CA, 1991).
- [5] H. Brune, Surface Science Reports **31**, 173 (1998).
- [6] H. Kroto *et al.*, Nature **381**, 162 (1985).
- [7] S. Iijima, Nature **354**, 56 (1991).
- [8] Y. Xia and G. Whitesides, Angew. Chem. Int. Ed. **37**, 551 (1998).
- [9] A. Yazdani *et al.*, Science **265**, 1767 (1997).
- [10] L. Kouwenhoven and C. Marcus, Physics World **6**, 35 (1998).
- [11] U. Simon, Adv. Mater. **17**, 1487 (1998).
- [12] G. Prinz, Science **282**, 1660 (1998).
- [13] D. Klein *et al.*, Nature **389**, 699 (1997).
- [14] S. Chou, Proc. of the IEEE **85**, 652 (1997).
- [15] D. Carroll *et al.*, Phys. Rev. Lett. **81**, 2332 (1999).
- [16] K. Liu, M. Burghard, S. Roth, and P. Bernier, Appl. Phys. Lett. **75**, 2494 (1999).
- [17] M. Bockrath *et al.*, Nature **397**, 598 (1999).
- [18] K. Tsukagoshi, B. Alphenaar, and H. Ago, Nature **401**, 572 (1999).
- [19] A. Morpurgo, J. Kong, C. Marcus, and H. Dai, Science **286**, 263 (1999).
- [20] M. Fleischmann, F. Lasserre, J. Robinson, and D. Swan, J. Electroanal. Chem. **177**, 97 (1984).

- [21] J. Jacobs and J. Rikken, *J. Electrochem. Soc.* **135**, 2822 (1988).
- [22] A. Bard, *Electroanalytical Chemistry* (Marcel Dekker, New York, NY, 1984).
- [23] J. Sagiv, *J. Am. Chem. Soc.* **102**, 92 (1980).
- [24] R. Nuzzo and D. Allara, *J. Am. Chem. Soc.* **105**, 4481 (1983).
- [25] C. Bain *et al.*, *J. Am. Chem. Soc.* **111**, 321 (1989).
- [26] M. Porter, T. Bright, D. Allara, and C. Chidsey, *J. Am. Chem. Soc.* **109**, 3559 (1987).
- [27] G. Whitesides and P. Laibinis, *Langmuir* **6**, 787 (1990).
- [28] C. Duschl *et al.*, *Biophys. J.* **67**, 1229 (1994).
- [29] R. Nuzzo, L. Dubois, and D. Allara, *J. Am. Chem. Soc.* **112**, 558 (1990).
- [30] P. Fenter, A. Eberhardt, K. Liang, and P. Eisenberger, *J. Chem. Phys.* **106**, 1600 (1997).
- [31] M. Epple, *Second Harmonic and Sum Frequency Spectroscopy of Thin Films and Monomolecular Layers* (Ecole Polytechnique Fédérale de Lausanne, Lausanne, CH, 1999).
- [32] L. Dubois, B. Zegarski, and R. Nuzzo, *J. Phys. Chem.* **98**, 678 (1993).
- [33] C. Schönenberger, J. Sondag-Huethorst, J. Jorritsma, and L. Fokkink, *Langmuir* **10**, 611 (1994).
- [34] J.-P. Bucher, L. Santesson, and K. Kern, *Langmuir* **10**, 979 (1994).
- [35] E. Delamarche, B. Michel, H. Biebuyck, and C. Gerber, *Adv. Mater.* **8**, 719 (1996).
- [36] D. Lavrich, S. Wetterer, S. Bernasek, and G. Scoles, *J. Phys. Chem. B* **102**, 3456 (1998).
- [37] J. van Alsten, *Langmuir* **15**, 7605 (1999).
- [38] H. Häussling, H. Ringsdorf, F.-J. Schmitt, and W. Knoll, *Langmuir* **7**, 1837 (1991).
- [39] H. Häussling, H. Ringsdorf, and W. Knoll, *Thin Solid Films* **210**, 815 (1992).
- [40] L. Scheibler *et al.*, *Angew. Chem. Int. Ed.* **38**, 696 (1999).
- [41] E. Delamarche *et al.*, *Science* **276**, 779 (1997).
- [42] Y.-S. Shon, K. Kelly, N. Halas, and T. Lee, *Langmuir* **15**, 5329 (1999).

- [43] M. Brust, P. Blass, and A. Bard, *Langmuir* **13**, 5602 (1997).
- [44] R. Jordan *et al.*, *J. Am. Chem. Soc.* **121**, 1016 (1999).
- [45] L. Dubois and R. Nuzzo, *Annu. Rev. Phys. Chem.* **43**, 437 (1992).
- [46] R. Nuzzo, B. Zegarski, and H. Dubois, *J. Am. Chem. Soc.* **109**, 733 (1987).
- [47] C. Bain, H. Biebuyck, and G. Whitesides, *Langmuir* **5**, 723 (1989).
- [48] M. Bryant, *J. Am. Chem. Soc.* **113**, 8284 (1991).
- [49] H. Finklea and D. Hanshew, *J. Am. Chem. Soc.* **114**, 3173 (1992).
- [50] G. Poirier and E. Pylant, *Science* **272**, 1145 (1996).
- [51] C. Bain, J. Evall, and G. Whitesides, *J. Am. Chem. Soc.* **111**, 7155 (1989).
- [52] C. Chidsey and D. Loiacono, *Langmuir* **6**, 682 (1990).
- [53] C. Bain and G. Whitesides, *Science* **240**, 62 (1988).
- [54] C. Bain and G. Whitesides, *J. Am. Chem. Soc.* **110**, 6560 (1988).
- [55] T. Takami, E. Delamarche, B. Michel, and C. Gerber, *Langmuir* **11**, 3876 (1995).
- [56] M. Tarlov, D. Burgess, and G. Gillen, *J. Am. Chem. Soc.* **115**, 5305 (1993).
- [57] J. Sondag-Huethorst, H. van Helleputte, and L. Fokkink, *Appl. Phys. Lett.* **64**, 285 (1994).
- [58] K. Berggren *et al.*, *Science* **269**, 1255 (1995).
- [59] A. Kumar and G. Whitesides, *Appl. Phys. Lett.* **63**, 2002 (1993).
- [60] A. Kumar, H. Biebuyck, and G. Whitesides, *Langmuir* **10**, 1498 (1994).
- [61] N. Larsen, H. Biebuyck, E. Delamarche, and B. Michel, *J. Am. Chem. Soc.* **119**, 3017 (1997).
- [62] A. Brenner and G. Riddell, *J. Res. Nat'l Bur. Std.* **37**, 31 (1946).
- [63] A. Brenner and G. Riddell, *J. Res. Nat'l Bur. Std.* **39**, 385 (1947).
- [64] C. Shipley, *Plating Surf. Finish.* **71**, 92 (1984).
- [65] M. Paunovic, *Proc. Electroless Deposition of Metals and Alloys* **88**, 3 (1988).
- [66] G. Mallory and J. Hajdu, *Electroless Plating: Fundamentals and Applications* (American Electroplaters and Surface Finishers Society, Orlando, FL, 1990).

- [67] A. Molenaar, Proc. Electroless Deposition of Metals and Alloys **88**, 37 (1988).
- [68] H. Gerischer, , and C. Tobias, *Advances in Electrochemical Science and Engineering* (VCH, Weinheim, D, 1994).
- [69] C. Weber, *In-Situ Scanning Tunneling Microscopy Study of Morphological and Mechanistic Aspects of Electroless Copper Deposition* (The Pennsylvania State University, University Park, PA, 1998).
- [70] A. van der Putten and J. W. de Bakker, J. Electrochem. Soc. **140**, 2229 (1993).
- [71] T. Osaka, H. Rakematsu, and K. Hikei, J. Electrochem. Soc. **127**, 1021 (1980).
- [72] P.-L. Pai and C. Ting, IEEE Electron Device Letters **10**, 423 (1989).
- [73] C. Mak, MRS Bull. **8**, 55 (1994).
- [74] J. Patterson *et al.*, Applied Surface Science **91**, 124 (1995).
- [75] C.-K. Hu, R. Rosenberg, and K. Lee, Appl. Phys. Lett. **74**, 2945 (1999).
- [76] Y. Xia *et al.*, Science **273**, 347 (1996).
- [77] E. Kim, Y. Xia, and G. Whitesides, Nature **376**, 581 (1995).
- [78] E. Kim, Y. Xia, and G. Whitesides, J. Am. Chem. Soc. **118**, 7155 (1996).
- [79] M. Zhao, Y. Xia, and G. Whitesides, Adv. Mater. **8**, 837 (1996).
- [80] E. Kim, Y. Xia, X.-M. Zhao, and G. Whitesides, Adv. Mater. **9**, 651 (1997).
- [81] R. Jackman, D. Duffy, O. Cherniavskaya, and G. Whitesides, Langmuir **15**, 2973 (1999).
- [82] M. Madou, *Fundamentals of Microfabrication* (CRC Press, Boca Raton, FL, 1997).
- [83] H. Biebuyck, N. Larsen, E. Delamarche, and B. Michel, IBM J. Res. Develop. **41**, 159 (1997).
- [84] E. Delamarche *et al.*, J. Phys. Chem. B **102**, 3324 (1998).
- [85] H. Biebuyck and G. Whitesides, Langmuir **10**, 2790 (1994).
- [86] N. Jeon *et al.*, Langmuir **11**, 3024 (1995).
- [87] A. Bernard *et al.*, Langmuir **14**, 2225 (1998).
- [88] G. Ferguson, M. Chaudhury, G. Sigal, and G. Whitesides, Science **253**, 776 (1991).
- [89] M. Chaudhury and G. Whitesides, Science **255**, 1230 (1992).

- [90] E. Delamarche, H. Schmid, B. Michel, and H. Biebuyck, *Adv. Mater.* **9**, 741 (1997).
- [91] M. Chaudhury and G. Whitesides, *Langmuir* **7**, 1013 (1991).
- [92] G. Ferguson, M. Chaudhury, H. Biebuyck, and G. Whitesides, *Macromolecules* **26**, 5870 (1993).
- [93] P. Ajayan and T. Ebbesen, *Rep. Prog. Phys.* **60**, 1025 (1997).
- [94] S. Iijima and T. Ichihashi, *Nature* **363**, 603 (1993).
- [95] A. Thess *et al.*, *Science* **273**, 483 (1996).
- [96] M. Endo *et al.*, *J. Phys. Chem. Solids* **54**, 1841 (1993).
- [97] T. Ebbesen, P. Ajayan, H. Hiura, and K. Tanigaki, *Nature* **367**, 519 (1994).
- [98] S. Tsang, Y. Chen, P. Harris, and M. Green, *Nature* **372**, 159 (1994).
- [99] J.-M. Bonard *et al.*, *Adv. Mater.* **9**, 827 (1997).
- [100] G. Duesberg *et al.*, *Chem. Commun.* **3**, 453 (1998).
- [101] W. de Heer, A. Châtelain, and D. Ugarte, *Science* **270**, 1179 (1995).
- [102] A. Rinzler *et al.*, *Science* **269**, 1550 (1995).
- [103] R. Fowler and L. Nordheim, *Proc. Roy. Soc. Lond. Ser. A* **119**, 173 (1928).
- [104] J.-M. Bonard *et al.*, *Appl. Phys. Lett.* **73**, 918 (1998).
- [105] J.-M. Bonard *et al.*, *Ultramicroscopy* **73**, 7 (1998).
- [106] J.-M. Bonard *et al.*, *Appl. Phys. A* **69**, 245 (1999).
- [107] O. Gröning, *Field Emission Properties of Carbon Thin Films and Carbon Nanotubes* (Université de Fribourg, Fribourg, CH, 1999).
- [108] A. Maiti, C. Brabec, C. Roland, and J. Bernholc, *Phys. Rev. B* **52**, 14850 (1995).
- [109] I. Brodie and C. Spindt, *Advances in Electronics and Electron Physics* **83**, 6 (1992).
- [110] J. Kong *et al.*, *Nature* **395**, 878 (1998).
- [111] M. Burghard *et al.*, *Adv. Mater.* **10**, 584 (1998).
- [112] Q. Wang *et al.*, *Appl. Phys. Lett.* **72**, 2912 (1998).
- [113] H. Soh *et al.*, *Appl. Phys. Lett.* **75**, 627 (1999).

- [114] J. Tersoff, *Appl. Phys. Lett.* **74**, 2122 (1999).
- [115] M. Burghard *et al.*, *Synthetic Metals* **103**, 2540 (1999).
- [116] J. Liu *et al.*, *Chem. Phys. Lett.* **303**, 125 (1999).
- [117] W. Choi *et al.*, *Appl. Phys. Lett.* **75**, 3129 (1999).
- [118] K. Hernadi *et al.*, *Catalysis Lett.* **48**, 229 (1997).
- [119] J. Kong, A. Cassell, and H. Dai, *Chem. Phys. Lett.* **292**, 567 (1998).
- [120] S. Fan *et al.*, *Science* **283**, 512 (1999).
- [121] W. Li *et al.*, *Science* **274**, 1701 (1996).
- [122] M. Terrones *et al.*, *Nature* **388**, 52 (1997).
- [123] Z. Ren *et al.*, *Science* **282**, 1105 (1998).
- [124] O. Küttel, O. Gröning, C. Emmenegger, and L. Schlapbach, *Appl. Phys. Lett.* **73**, 2113 (1998).
- [125] A. Cassell *et al.*, *J. Am. Chem. Soc.* **121**, 7975 (1999).
- [126] X. Xu and G. Brandes, *Appl. Phys. Lett.* **74**, 2549 (1999).
- [127] S. Tans, A. Verschueren, and C. Dekker, *Nature* **393**, 49 (1998).
- [128] R. Martel *et al.*, *Appl. Phys. Lett.* **73**, 2447 (1998).
- [129] A. Ewing, M. Dayton, and R. Wightman, *Anal. Chem.* **53**, 1842 (1981).
- [130] R. Penner, M. Heben, T. Longin, and N. Lewis, *Science* **250**, 1118 (1990).
- [131] A. Ewing, R. Wightman, and M. Dayton, *Brain Res.* **249**, 361 (1982).
- [132] F. Conti and E. Neher, *Nature* **285**, 140 (1980).
- [133] D. Craston, S. Lin, and A. Bard, *J. Electrochem. Soc.* **135**, 785 (1988).
- [134] A. Bard and L. Faulkner, *Electrochemical Methods: Fundamentals and Applications* (John Wiley and Sons, New York, NY, 1980).
- [135] W. Dressick, C. Dulcey, J. Georger, and J. Calvert, *Chem. Mater.* **5**, 148 (1993).
- [136] T. Vargo, J. Gardella, J. Calvert, and M. Chen, *Science* **262**, 1711 (1993).
- [137] S. Potochnik, P. Pehrsson, D. Hsu, and J. Calvert, *Langmuir* **11**, 1841 (1995).
- [138] M.-S. Chen *et al.*, *J. Electrochem. Soc.* **146**, 1421 (1999).

- [139] C. Marrian *et al.*, Appl. Phys. Lett. **64**, 390 (1994).
- [140] S. Brandow *et al.*, J. Electrochem. Soc. **142**, 2233 (1995).
- [141] N. Camillone, C. Chidsey, G. Liu, and G. Scoles, J. Phys. Chem. **98**, 4234 (1993).
- [142] J. Calvert *et al.*, J. Vac. Sci. Technol. B **12**, 3884 (1994).
- [143] J. Calvert, J. Vac. Sci. Technol. B **11**, 2155 (1993).
- [144] W. Dressick *et al.*, J. Electrochem. Soc. **141**, 210 (1994).
- [145] A. van der Putten, J. de Bakker, and L. Fokkink, J. Electrochem. Soc. **139**, 3475 (1992).
- [146] S. Gilbert, O. Cavalleri, and K. Kern, J. Phys. Chem. **100**, 12123 (1996).
- [147] O. Cavalleri *et al.*, Z. Phys. Chem. **208**, 107 (1999).
- [148] I. Wyatt, Chem. Weekbl. **62**, 310 (1966).
- [149] V. Kazakova and B. Ptitsyn, Russ. J. Inorg. Chem. **12**, 323 (1967).
- [150] B. Nabivanets and L. Kalabina, Russ. J. Inorg. Chem. **15**, 818 (1970).
- [151] B. Nabivanets and L. Kalabina, Sov. Prog. Chem **41**, 81 (1975).
- [152] L. Elding, Inorg. Chim. Acta **6**, 683 (1972).
- [153] L. Elding and L. Olssen, J. Phys. Chem. **82**, 69 (1978).
- [154] P. Bekker and W. Robb, J. Inorg. Nucl. Chem. **37**, 829 (1975).
- [155] M. Vargaftik, V. Igoshin, and Y. Syrkin, Izv. Akad. Nauk SSSR, Ser. Khim. **6**, 1426 (1972).
- [156] J. Rund, Inorg. Chem. **9**, 1211 (1970).
- [157] P. Maitlis, *The Organic Chemistry of Palladium: I. Metal Complexes* (Academic Press, New York, NY, 1971).
- [158] J. Huheey, *Inorganic Chemistry: Principles of Structure and Reactivity* (Harper Row, New York, NY, 1983).
- [159] S. Brandow *et al.*, J. Electrochem. Soc. **144**, 3425 (1997).
- [160] S. Haruyama and I. Ohno, Proc. Electrochem. Depos. Thin Films **93**, 70 (1993).
- [161] C. Weber, H. Pickering, and K. Weil, J. Electrochem. Soc. **144**, 2364 (1997).
- [162] J. Sondag-Huethorst and L. Fokkink, Langmuir **11**, 4823 (1995).

- [163] N. Camillone, T. Leung, and G. Scoles, *Surf. Sci.* **373**, 333 (1997).
- [164] O. Cavalleri, *Ordering and Electrodeposition at the Alkanethiol/Au(111) interface* (Ecole Polytechnique Fédérale de Lausanne, Lausanne, CH, 1997).
- [165] S. Livingston, *Comprehensive Inorganic Chemistry* (Pergamon Press, Oxford, UK, 1973).
- [166] C. Baes and R. Mesmer, *The Hydrolysis of Cations* (Wiley-Interscience, New York, NY, 1976).
- [167] C. Mortimer, *Rev. Inorg. Chem.* **6**, 233 (1984).
- [168] H. Hagenström, M. Schneeweiss, and D. Kolb, *Langmuir* **15**, 7802 (1999).
- [169] P. Stoltze, *Condens. Mater.* **6**, 9495 (1994).
- [170] P. Bindra and J. Roldan, *J. Electrochem. Soc.* **132**, 2581 (1985).
- [171] R. Morris, D. Franta, and H. White, *J. Phys. Chem.* **91**, 3559 (1987).
- [172] R. Meruva and M. Meyerhoff, *Anal. Chem.* **68**, 2022 (1996).
- [173] E. O'Sullivan *et al.*, *IBM J. Res. Develop.* **42**, 607 (1998).
- [174] Y. Shacham-Diamand, *J. Micromech. Microeng.* **1**, 66 (1991).
- [175] J. Cho, H. Kang, S. Wong, and Y. Shacham-Diamond, *MRS Bull.* **6**, 31 (1993).
- [176] P. Hidber, W. Helbig, E. Kim, and G. Whitesides, *Langmuir* **12**, 1375 (1996).
- [177] P. Hidber, P. Nealey, W. Helbig, and G. Whitesides, *Langmuir* **12**, 5209 (1996).
- [178] H. Schmid and B. Michel, submitted to *Macromolecules*.
- [179] H. Niino and A. Yabe, *Appl. Phys. Lett.* **60**, 2697 (1993).
- [180] S. Sugihara, A. Iwasawa, K. Onose, and J. Yamaki, *J. Appl. Electrochem.* **26**, 63 (1996).
- [181] C. Brinker and G. Scherer, *Sol-Gel Science* (Academic Press, San Diego, CA, 1996).
- [182] A. Bard, R. Parson, and J. Jordan, *Standard Potentials in Aqueous Solution* (IUPAC, New York, NY, 1985).
- [183] M. Charbonnier, M. Alami, and M. Romand, *J. Appl. Electrochem.* **28**, 449 (1998).
- [184] R. Cohen and K. West, *J. Electrochem. Soc.* **120**, 502 (1973).

- [185] N. Feldstein, M. Schlesinger, and N. Hedgecock, *J. Electrochem. Soc.* **121**, 738 (1974).
- [186] J. Horkans, J. Kim, C. McGrath, and L. Romankiw, *J. Electrochem. Soc.* **134**, 300 (1987).
- [187] J. Kim, S. Wen, D. Jung, and R. Johnson, *IBM J. Res. Develop.* **28**, 697 (1984).
- [188] H. Dai *et al.*, *Chem. Phys. Lett.* **260**, 471 (1996).
- [189] R. Cornell and U. Schwertmann, *The Iron Oxides* (VCH, Weinheim, D, 1996).
- [190] C. Flynn, *Chem. Rev.* **84**, 31 (1984).
- [191] A. Vertes, I. Nagy-Czakó, and K. Burger, *J. Phys. Chem.* **82**, 1469 (1978).
- [192] L. Libioulle *et al.*, *Langmuir* **15**, 300 (1999).
- [193] L. Armelao *et al.*, *J. Mater. Chem.* **5**, 79 (1995).
- [194] A. Al-Bawab, S. Friberg, J. Sjöblom, and G. Farrington, *Phys. Chem. Glasses* **39**, 122 (1998).
- [195] D. Dzombak and F. Morel, *Surface Complexation Modeling* (Wiley & Sons, New York, NY, 1990).
- [196] P. Collins and A. Zettl, *Appl. Phys. Lett.* **69**, 1969 (1996).
- [197] G. Che, B. Lakshmi, E. Fisher, and C. Martin, *Nature* **393**, 346 (1998).
- [198] Z. Ren *et al.*, *Appl. Phys. Lett.* **75**, 1086 (1999).
- [199] J. Li, C. Papadopoulos, J. Xu, and M. Moskovits, *Appl. Phys. Lett.* **75**, 367 (1999).
- [200] J.-M. Bonard, J.-D. Ganière, F. Morier-Genoud, and M. Achtenhagen, *Semicond. Sci. Technol.* **11**, 410 (1996).
- [201] L.-O. Nilsson *et al.*, submitted to *Appl. Phys. Lett.*
- [202] V. Dérue *et al.*, *Thin Solid Films* **306**, 1 (1997).
- [203] L.-O. Nilsson, personal communication.

List of Publications

1. *Electroless Deposition of Metal Nanoislands on Aminothiolate-Functionalized Au(111) Electrodes.*
H. Kind, A.M. Bittner, O. Cavalleri, T. Greber and K. Kern
J. Phys. Chem. B **102**, 7582 (1998).
2. *Temperature-Promoted Electrodeposition on Thiolate-Modified Electrodes.*
O. Cavalleri, H. Kind, A.M. Bittner, and K. Kern
Langmuir **14**, 7292 (1998).
3. *Copper Electrodeposition on Alkanethiolate Covered Gold Electrodes.*
O. Cavalleri, A.M. Bittner, H. Kind, and K. Kern
Z. Phys. Chem. **208**, 107 (1999).
4. *Patterned Electroless Deposition of Copper by Microcontact Printing Palladium(II) Complexes on Titanium-Covered Surfaces.*
H. Kind, M. Geissler, H. Biebuyck, H. Schmid, B. Michel, K. Kern, and E. Delamarche
submitted to Langmuir.
5. *Method for Printing a Catalyst on Substrates for Electroless Deposition.*
H. Biebuyck, E. Delamarche, M. Geissler, H. Kind, and B. Michel
US Patent, filed 18.6.1999.
6. *Patterned Films of Nanotubes using Microcontact Printing of Catalysts.*
H. Kind, J.-M. Bonard, C. Emmenegger, L.-O. Nilsson, K. Hernadi, E. Maillard-Schaller, L. Schlapbach, L. Forró, and K. Kern
Adv. Mater. **15**, 1285 (1999).
7. *Printing Gel-Like Catalysts for the Directed Growth of Multiwall Carbon Nanotubes.*
H. Kind, J.-M. Bonard, K. Hernadi, L.-O. Nilsson, L. Schlapbach, L. Forró, and K. Kern
submitted to J. Phys. Chem. B.

8. *Field Emission From Patterned Carbon Nanotube Thin Films.*
L.-O. Nilsson, O. Gröning, C. Emmenegger, O. Küttel, E. Maillard-Schaller, L. Schlapbach, H. Kind, J.-M. Bonard, and K. Kern
submitted to Appl. Phys. Lett.

Curriculum Vitae

Name: Hannes Kind

Date of Birth: Mai 20, 1970

Nationality: Swiss

1985–1990 High School at the Kantonsschule Schaffhausen, Switzerland

1991–1996 Studies in physics at the University of Fribourg, Switzerland

Oct 1995–May 1996 Diploma thesis in the group of Prof. Dr. L. Schlapbach at the Laboratory for Solid State Physics of the University of Fribourg: “Raman-Spectroscopy on C₆₀, CVD-Diamond, and Plasma-Treated Polymers”

1997–2000 Research and teaching assistant in the group of Prof. Dr. K. Kern at the Institute for Experimental Physics of the Swiss Federal Institute of Technology in Lausanne

March 1998–Sept 1998 Joint research studies with the group of Dr. B. Michel at the IBM Research Laboratory in Rüschlikon, Switzerland

2000 PhD thesis: “Patterning of Surfaces by Locally Catalyzed Chemical Reactions”

Merci

J'aimerais remercier en premier lieu le professeur Klaus Kern pour m'avoir donné l'opportunité de réaliser ce travail en m'accueillant dans son groupe et pour son soutien pendant cette période.

Ensuite j'aimerais remercier tous ceux qui, au cours de ces trois années, ont contribué au succès de ce travail:

Ornella Cavalleri pour l'introduction au projet et son aide pendant les premiers mois,

Alexander Bittner, pour ses idées, ses conseils et son aide au STM,

tous les membres de l'équipe IBM: André Bernard, Hans Biebuyck, Alexander Bietsch, Emmanuel Delamarche, Matthias Geissler, Bruno Michel et Heinz Schmid pour la collaboration stimulante et amicale,

Jean-Marc Bonard, pour son soutien énorme, son aide pour toutes sortes de travaux et finalement pour les discussions motivantes,

Klara Hernadi, Lars-Ola Nilsson et Christophe Emmenegger pour toutes les activités concernant les nanotubes,

tous les membres des ateliers de mécanique et d'électronique pour la précieuse collaboration ainsi que Claire-Lise Bandelier et Françoise Jenny,

Lukas Bürgi, Jens Weckesser pour les activités hors institut

et finalement Monika Bauer pour toutes une série d'autres choses.